Abstract

Title of dissertation: MAGNETORHEOLOGICAL FLUIDS AND APPLICATIONS TO ADAPTIVE LANDING GEAR FOR A LIGHTWEIGHT HELICOPTER

Louise Aminata Ahuré-Powell, Doctor of Philosophy, 2014

Dissertation directed by: Professor Norman M. Wereley

Department of Aerospace Engineering

During hard landing or crash events of a helicopter there are impact loads that can be injurious to crew and other occupants as well as damaging to the helicopter structure. Landing gear systems are the first in line to protect crew and passengers from detrimental crash loads. The main focus of this research is to improve landing gear systems of a lightweight helicopter.

Magnetorheological fluids (MRFs) provide potential solutions to several engineering challenges in a broad range of applications. One application that has been considered recently is the use of magnetorheological (MR) dampers in helicopter landing gear systems. In such application, the adaptive landing gear systems have to continuously adjust their stroking load in response to various operating conditions. In order to support this rotorcraft application, there is a necessity to validate that MRFs are qualified for landing gear applications.

First, MRF composites, synthesized utilizing three hydraulic oils certified for use in landing gear systems, two average diameters of spherical magnetic particles, and a lecithin surfactant, are formulated to investigate their performance for potential use in a helicopter

landing gear. The magnetorheology of these MR fluids is characterized through a range of tests, including (a) magnetorheology (yield stress and viscosity) as a function of magnetic field, (b) sedimentation analysis using an inductance-based sensor, (c) cycling of a small-scale MR damper undergoing sinusoidal excitations (at 2.5 and 5 Hz), and (d) impact testing of an MR damper for a range of magnetic field strengths and velocities using a free-flight drop tower facility. The performance of these MR fluids was analyzed, and their behavior was compared to standard commercial MR fluids. Based on this range of tests used to characterize the MR fluids synthesized, it was shown that it is feasible to utilize certified landing gear hydraulic oils as the carrier fluids to make suitable MR fluids.

Another objective of this research is to satisfy the requirement of a helicopter landing gear damper to enable adaptive shock mitigation performance over a desired sink rate range. It was intended to maintain a constant stroking force of 17 793 N (4000 lb_f) over a sink rate range of 1.8-7.9 m/s (6-26 ft/s), which is a substantial increase of the high-end of the sink rate range from 3.7 m/s (12 ft/s), in prior related work, to 7.9 m/s (26 ft/s). To achieve this increase in the high-end of the sink rate range, a spiral wave spring-assisted passive valve MR landing gear damper was developed. Drop tests were first conducted using a single MR landing gear damper. In order to maintain the peak stroking load constant over the desired sink rate range, a bang-bang current control algorithm was formulated using a force feedback signal. The controlled stroking loads were experimentally evaluated using a single drop damper test setup. To emulate the landing gear system of a lightweight helicopter, an iron bird drop test apparatus with four spiral wave spring-assisted relief valves MR landing gear dampers, was fabricated and successfully tested. The effectiveness of the proposed adaptive MR landing gear damper was theoretically and experimentally verified. The bang-bang current control algorithm successfully regulated the

stroking load at 4000 lb_f over a sink rate range of 6-22 ft/s in the iron bird tests, which significantly exceeds the sink rate range of the previous study (6-12 ft/s). The effectiveness of the proposed adaptive MR landing gear damper with a spiral wave spring-assisted passive valve is theoretically and experimentally verified.

MAGNETORHEOLOGICAL FLUIDS AND APPLICATIONS TO ADAPTIVE LANDING GEAR FOR A LIGHTWEIGHT HELICOPTER

by

Louise A. Ahuré-Powell

Dissertation submitted to the Faculty of the Graduate School of the
University of Maryland, College Park in partial fulfillment
of the requirements for the degree of
Doctor of Philosophy
2014

Advisory Committee:
Professor Norman M. Wereley, Chair/Advisor
Professor Amr Baz (Dean's Representative)
Professor Inderjit Chopra
Professor Sung Lee
Professor James Baeder

Dedication

This dissertation is dedicated to my mother, Fatou, who has been my biggest support system throughout this journey. Her early personal struggles in life, as a victim of a bad car accident, affected her physically and emotionally. However, after more than two dozen surgeries and years of therapy, my mom can walk without crutches and has willingly worked every day to support me and help me finish my studies. Her determination to see me succeed is beyond means. Without her continued support and encouragements, I could not have completed this work. Her will to recover and determination to achieve her dreams have been my inspiration through life to always follow my dreams and be whoever I want to be through hard work and dedication.

Acknowledgements

First and foremost, I would like to sincerely thank my advisor, Dr. Norman M. Wereley, who, over the course of my time at the University of Maryland, has been a great source of encouragements and guidance. Dr. Wereley has served as The Best Advisor and mentor I have ever had, and his support is truly appreciated. Dr. Wereley first hired me as research assistant under the Master's program and gave me countless words of advice, which have and will always stay with me. He easily convinced me to pursue a Doctoral degree, and I am truthfully appreciative of his trust in me. Even during a time when I did not believe in myself, Dr. Wereley still did. I am truthfully grateful to Dr. Wereley for giving me the opportunity to pursue my graduate studies under his great leadership and for helping me build my confidence to complete my dissertation. Dr. Wereley's tremendous knowledge, patience, instruction, and support have allowed me to have a solid foundation to accomplish my research studies at the University of Maryland. I am candidly thankful for his teaching, and for always keeping a great atmosphere in the Core Lab. I would not be where I am today if it were not for all of his help, so I thank him so much for everything.

I would also like to thank my distinguished Ph.D. committee members for their support and great feedback that significantly contributed towards this work. Dr. Amr Baz, Dr. Inderjit Chopra, Dr. Sung Lee, and Dr. James Baeder have each challenged me to work hard, and patiently encouraged me through my academic pursuits and completion of my Doctoral degree. I thank them for all their help, advice, and assistance during my time at the University of Maryland.

I would like to extend my gratitude to John Ulicny for his great support and work in preparing the MR fluids used in the research on MRFs employing substitution of nonmagnetic for magnetic particles.

Further, I would like to acknowledge the Aviation Applied Technology Directorate, particularly Jin Woodhouse, for partially funding this Ph.D. work. I would also like to extend my deepest gratitude to The Boeing Company for the continuous financial support of my research work. I am especially thankful and grateful to Akif Bolukbasi and Terrence Birchette for their invaluable support and guidance throughout the Boeing-funded project that contributed towards most of my dissertation work. I want to thank Terrence for his insights and guidance throughout the design and testing of the landing gear dampers and iron bird apparatus.

I would like to thank Dr. Young-Tai Choi and Dr. Wei Hu, for their constant help, guidance, patience, support, and encouragements. I am indebted to them for their valuable assistance on a countless number of occasions, and for being directly involved through extensive testing help and in making this research possible. I also thank Dr. Na for allowing me to use his instruments in Dr. Flatau's lab, and I am appreciative of the help of Michael "Mike" Perna and Howard "Howie" Grossenbacher who manufactured all of the parts for the landing gear dampers.

I would like to particularly thank Grum Ngatu for helping me adjust when I just started working in the lab and for helping me so much on the work of MR fluids and dampers in my earlier years at the University of Maryland. Also, I would like thank Harinder Singh for being such a great friend and giving me great advice and significant help throughout the time I spent working on my Ph.D. dissertation and preparing for my defense.

I would also like to thank all of my past and present colleagues and friends from the office who made me want to come to work each day. They made work so much more enjoyable

and kept a great and friendly atmosphere while I was finishing up my dissertation. I send my special thanks to Ben Woods, Nick Wilson, Robert Vocke, Min Mao, Ryan Robinson, Andrew Becnal, Erica Hocking, Steve Sherman, and Tom Pillsbury for their great help in the lab and during practice exams. Also, thanks to John for his friendship and delicious cupcakes and to Brian, Pablo, Richard, and Lei "Romy" for their friendships. I would also like to thank other officemates, Lina Castano, David Mayo, and Jürgen Rauleder for their great friendships and support. I would also like to thank my friend Juanita for her encouragements, support, love, and prayers, as well as Djamie and Aicha for their support and friendships. I would like to thank and send a prayer to Jenna Catherine for being such a great friend and for caring so much about all of us in the lab. You are truly missed but never forgotten.

I would also like to thank my brother, Ismael, for his well appreciated prayers and words of wisdom, and my son, Maximus, for being a good child and allowing me to get some work done at home. I am also grateful to my family in Cote d'Ivoire (my grandmother, Nanou, my aunts, Awa, Nina, and Ramata) and in France (my aunt, Habibata) for their encouragements, love, prayers, and weekly phone calls to check on my well being. I would like to thank my husband, Sean, for his assistance, enthusiasm, and encouragement throughout this process. Finally, I would like to extend my utmost gratefulness to His Excellency Alassane Ouattara and his wife, Mrs. Dominique Ouattara, for their remarkable support and encouragements towards the completion of my dissertation.

Thank you to all of you who contributed to the person I have grown into, on a personal and a professional level, and I thank God for always being by my side. I earn strength through my faith in God, and I pray that He continues to guide me.

Table of Contents

List of Figures

List of Tables

Nomenclature

A	Cross-sectional area of the sensing coil wire
A_1	Cross-sectional area of the MR annular gap
A_{mr}	Flow area of the MR valve
A_{open}	Flow area of the opened relief valve orifice
A_p	Piston area of the MR landing gear damper
A_{relief}	Cross-sectional area of the center orifice
B	Magnetic field density
C_c	Contraction coefficient
C_d	Discharge coefficient
C_{po}	Post-yield damping
C_{pr}	Pre-yield damping
C_v	Velocity coefficient
D	Mean conventional spring coil diameter
D_h	Hydraulic diameter
D_m	Mean diameter
D_p	MR damper piston diameter
E	Modulus of elasticity
F	Measured MR damper force
F_d	Desired damper force
F_m	Actual damper force measured at each damper top position
F_{MR}	Damper ON-state force due to MR fluid effect

$F_{passive}$	Damper OFF-state passive force
F_s	Constant peak stroking load
F_{sp}	Spring force due to the gas pressure
F_{s0}	Pre-compressed spring force
F_t	Total damper force
F_y	MR yield force
G	Modulus of elasticity of spring material in shear
H	Magnetic field strength
$H_{max_{att.}}$	Estimated maximum attainable magnetic field strength
K	Multiple wave factor
$K_{en.or}$	Minor loss factors in the center orifice passage due to sudden entrance
K_{entry}	Minor loss factors in the MR valve due to sudden entrance
K_{exit}	Minor loss factors in the MR valve due to sudden exit
$K_{ex.or}$	Minor loss factors in the center orifice passage due to sudden exit
$K_{tot.or}$	Total minor loss coefficient in the center orifice passage
K_1	Minor loss coefficient in the MR annular gap
L	Inductance
L_a	Total MR valve active length
L_{a_1}	Active MR valve length associated with one coil winding
L_c	Length of one magnetic coil winding
L_o	Total center orifice of the relief valve length
L_1	MR annular gap length
M	Mass of the seal

N	Number of waves per turn
P_i	Initial gas pressure
Q_{mr}	Flow rate passing through the MR valve
Q_p	Total flow rate passing through the piston
Q_{relief}	Flow rate passing through the relief valve
Q_{total}	Total flow rate
$\bar{R}$	Ratio of viscous effects and the sum of minor loss effects
Re	Reynolds number
S	MR Damper stroke
V	Average velocity of the flow passing through the MR valve gap
V_{d_o}	MR fluid velocity in the center orifice passage
V_{d_1}	MR fluid velocity in the MR annular gap
$V_{eq,sink}$	Equivalent sink rate
V_p	MR landing gear damper piston velocity
V_{po}	Initial condition: impact velocity
V_{2i}	Initial gas volume
W	Energy dissipated by the landing gear damper
Z	Spring number of turns
b	Radial width of material
c	Damping of the spring
d	Diameter of spring wire
d_o	Center orifice of the passive valve diameter
d_1	MR valve gap diameter

f	Darcy friction factor
f_{or}	Darcy friction factor across the relief valve
f_1	Darcy friction factor across the MR valve
g	Gravitational acceleration
h_{drop}	Initial drop height
i	Control current input
i_m	Control current inputs at each damper position
k	Stiffness of the spring
k_{coil}	Conventional coil spring stiffness
l	Sensing coil length
l_2	Length of chamber #2
m	Number of MR landing gear dampers
n	Number of turns per coil winding
n_s	Number of conventional spring active coils
t	Time
t_s	Spring material thickness
t_d	Duration of the impact event
v	MR damper velocity
v_y	Pre-yield velocity
x	Displacement of the seal
ΔP	Pressure drop across the MR and passive valves
ΔP_{MR}	Pressure drop due to MR fluid effects across the MR valve
ΔP_{mr}	Pressure drop through the MR valve

ΔP_{relief}	Pressure drop across the relief valve
ΔP_{η_1}	Pressure drop due to viscous effects across the MR valve
ΔP_{η_2}	Pressure drop due to viscous effects across the passive valve center orifice
$\widetilde{\Delta P}_{MRF}$	Emulated pressure drop associated with the MR fluid yield stress
$\dot{\widetilde{\Delta P}}_{MRF}$	Low-pass filter
δ	Convergence rate of the estimation to the flow rate
ε	Average wall roughness
ϵ	Control gain of the bang-bang control
η	MR fluid viscosity
γ	Predefined error
$\dot{\gamma}$	Shear rate
μ_0	Vacuum magnetic permeability
μ_r	Relative permeability
ρ	MR fluid density
τ	Shear stress
τ_y	MR fluid yield stress

Disclaimer

This research was partially funded by the Government under Agreement No. W911W6-10-2-0003. The U.S. Government is authorized to reproduce and distribute reprints for Government purposes notwithstanding any copyright notation thereon. The views and conclusions contained in this document are those of the author and should not be interpreted as representing the official policies, either expressed or implied, of the Aviation Applied Technology Directorate or the U.S. Government.

CHAPTER 1: Introduction

The purpose of this chapter is to state the motivation for this study and to introduce the research objectives. Once the research objectives are identified, the means by which they are met will be discussed. Finally, an outline of this dissertation will conclude this chapter.

1.1 Research Motivation and Objectives

During hard landing or crash events of a helicopter and due to existing coupling between the fuselage and landing gear systems, there are impact loads that can be injurious to crew and other occupants and be detrimental to the helicopter structure. Landing gear systems are the first in line of an Active Crash Protection System (ACPS) to protect crew and passengers from detrimental crash loads. One of the main objectives of this dissertation is to improve landing gear systems of a lightweight helicopter.

The landing performance of a lightweight helicopter has evolved in recent years, and several more challenges have risen. Nevertheless, landing gear systems have to absorb the kinetic energy associated with the helicopter vertical velocity. An important challenge encountered is to tune the landing gear damper to operate at different operating conditions. Figure 1.1 shows a particular case that motivated this study. In the figure, the landing gear damper has to be tuned to operate at two conditions: a low sink rate, V_{low}, and a high sink rate, V_{high}, while maximizing the operating sink rate range hence maintaining a constant peak stroking load, F_s, over a desired sink rate range (from V_{low} to V_{high}); in addition to the energy dissipated by the landing gear damper, W.

$$W = \int_0^{La} F_s(S)dS \qquad [1.1]$$

Considering a passive solution could be costly in weight and can only satisfy one operating condition. For instance, the actual MD 500 helicopter passive hydraulic dampers can only be tuned to operate at a single condition (one payload and one excitation level) shown in Figure 1.2 (a) and (b); hence the MD 500 helicopter passive damper performance is limited. Several landing gear systems have been considered over the years that incorporate features such as sensing and control through position and velocity measurement systems or through real-time adaptive landing gear controllers. Other features adjusting landing gear characteristics in real time have been investigated such as piezo valves (Mikułowski *et al.*, 2013). However, controlling the behavior of the helicopter landing gear has great benefits. One prospective solution to reduce the touchdown impact and satisfy the landing performance challenge is to use adaptive landing gear dampers that can continuously adjust their stroking load in response to various operating conditions, such as adaptive magnetorheological (MR) landing gear dampers.

Landing gear systems, which play an important role in preventing the airframe from vibration and excessive impact forces and improving passenger comfort and aircraft flight safety, are one of the most essential components of the helicopter. In this study, adaptive landing gear dampers that can continuously adjust their stroking load in response to various operating conditions are investigated for improving the landing performance of a lightweight helicopter. MR dampers are considered as a potential solution to satisfy this challenge; however, in order to support and encourage this rotorcraft application, there is a need to substantiate that magnetorheological fluids (MRFs) are suitable for landing gear applications. First, in this study, certified landing gear hydraulic oils are used as carrier fluids to make MRFs. These carrier fluids are selected to preserve important parameters in the hydraulic oils and due to their low viscosity that is necessary to keep the weight of the MR device low. Also, the landing gear MRF stability

is investigated through particle re-dispersion. Then, this study attempts to demonstrate large yield force by comparing the newly manufactured MRFs to commercial MRFs performance. After investigating the suitability of MRFs for landing gear use, the second part of this study is an effort to achieve the landing performance challenge to maximize operating sink rate range of a lightweight helicopter. This is achieved by using adaptive MR landing gear dampers with a spring-assisted passive valve to decrease viscous forces at higher sink rates.

In prior work directly related to this study, adaptive MR landing gear dampers for a lightweight helicopter that maintained a constant peak stroking force of 4000 lb_f across sink rates ranging from 6-12 ft/s (1.8-3.7 m/s) were designed, manufactured and successfully tested. In this follow-on work, it is desired to expand the high end of the sink rate range, so that the peak stroking force could be held constant for sink rates ranging from 6-26 ft/s (1.8-7.9 m/s), thereby extending the high end of the speed range from 12 ft/s in the first study to 26 ft/s. To achieve this increase in the high end of the sink rate range, a spring-assisted passive valve MR landing gear damper is developed. The MR valve is designed to semi-actively control the peak stroking load over the 6-12 ft/s sink rate range, whereas the relief valve is designed to passively control the stroking load over the 12-26 ft/s sink rate range. Drop tests are first conducted using a single MR landing gear damper (with a total drop mass of 430 lbs and 1283 lbs, subsequently). In this study, in order to maintain the peak stroking load of the MR landing gear damper constant over the desired sink rate range of 6-26 ft/s, a bang-bang current control algorithm formulated using a force feedback signal is used. The controlled stroking loads achieved using the force feedback control algorithm is experimentally evaluated using a single damper drop test setup over the desired sink rate range. To emulate the landing gear system of a lightweight helicopter, an iron bird drop test apparatus (with a total drop mass of 2627 lbs) with four MR landing gear dampers

with spring-assisted passive valves is fabricated and successfully tested using the bang-bang control algorithm

1.2 Smart Materials Review: Magnetorheological Fluids

Discovered by Jacob Rabinow at the US National Bureau of Standards in 1948, magnetorheological fluids (MRFs) are a class of fluids that display variable yield stress. Simultaneously Willis Winslow was working on a competitive fluid technology called electrorheological fluid (ERF). Additional research was performed more on ERFs than MRFs. Although there are some similarities between the ERFs and MRFs technologies, such as the change in the fluids rheology under the application of a field (electric field for ERFs and magnetic field for MRFs), the dissimilarities are considerable. Table 1.1 presents an overview of the key features of ERFs and MRFs.

MRFs are suspensions of micron-sized magnetic particles, such as iron (Fe) or cobalt, in a silicone or hydraulic oil carrier fluid (Carlson and Jolly, 2000; Wereley *et al.*, 2006; Park *et al.*, 2009). MRF ferromagnetic particles are free to move in their fluid medium, but once a magnetic field is applied, MRFs have the ability to change rheological properties, such as yield stress and viscosity. In other words, MRFs have the ability to change from a fluid state in Figure 1.3 (a) to a semi-solid or plastic state instantly upon the application of a magnetic field. In fact, the magnetic particles acquire a polarization and attract one another, forming a chain-like structure in the direction of the applied magnetic field as illustrated in Figure 1.3 (b). In this semi-solid state, the fluid exhibits a behavior that is characterized by the field-dependent yield stress (viscoplastic behavior). Commercial MR fluids usually have a particle composition of 30 to 40 volume percent (vol%) in the carrier fluid. Increasing the size of MRF particles causes an increase in the shear strength of the fluid (Bell *et al.*, 2008); however, spherical particles larger than about

10 μm tend to settle too quickly even with the addition of special additives. Particles in the nanometer range settle more slowly (if the particles are not indefinitely suspended by Brownian motion), but contribute to the yield strength reduction of MRFs (Rosenfeld *et al*., 2002; Poddar *et al*., 2004; Chaudhuri *et al.*, 2005; Ngatu and Wereley, 2007). Sedimentation still occurs within particles with diameters within the "ideal" size range of 1-10 μm fluids due to the inherent density difference between the particles and the carrier fluid. Once settled, the spherical particles tend to form a hard cake caused by remnant magnetization and are not easily re-dispersed (Phulé and Ginder, 1998).

The field-dependent yield stress, MRFs fast response time (in milliseconds), the avertable moving parts, and the low voltage and power required make MRFs an attractive technology for many applications such as semi-active real-time control in civil, aerospace and automotive applications.

1.3 MR Fluid Devices and Applications: Literature Review

MRF devices have been very successful due to fluid technology advancements. The fact that MRFs can exceed yield stresses of 80 kPa is attractive and impressive for controllability and dynamic range. MRFs stability and durability have improved over the years through a number of interesting studies considering MRFs properties and behavior in order to better understand the behavior of the device in which the fluids operate for various applications. An MR device intended for one application often finds use in a different application in which the operating conditions of the fluid differ from the original application. For instance, the MR damper called MotionMaster™ damper by Lord Corporation was originally considered for use in trucks and buses suspensions, but it is also considered for use in prosthetic limbs. As different as these applications are, so are the MRF operating conditions.

An MR damper conventional valve configuration is shown in Figure 1.4. MR dampers can be used for vibration isolation. A particular helicopter seat and occupant system can be represented using a SDOF system in Figure 1.5 (a) and the system's response is shown on the transmissibility plot in Figure 1.6 (a). At resonance (where the frequency ratio equals to 1) the system vibrates considerably. Consequently, damping needs to be added to reduce the peak as shown in Figure 1.6 (b). In the isolation region (region of frequency ratio located after $\sqrt{2}$) the damping needs to be low, as illustrated in Figure 1.6 (c), to keep transmissibility low because it increases with damping. In the amplification zone (region of frequency ratio located before $\sqrt{2}$), damping needs to be increased to keep transmissibility close to 1.The desired performance is illustrated with the blue curve in Figure 1.6 (d). Using an MR damper instead of conventional damper can satisfy this performance, and the damper can be turned on or off using commonly used controllers, such as skyhook control (Hiemenz *et al*., 2008).

MR dampers can also be used for energy absorption. The energy absorber MR dampers provide vibration and shock mitigation potential to consider different operating conditions (payloads, vibration, shock pulses, and environmental factors). An important performance parameter is the dynamic range, which is the ratio of the maximum ON-state force (magnetic field activated) to the OFF-state force (magnetic field turned off). The passive force (OFF-state force) is assumed to increase proportionally to the velocity squared at higher damper piston velocities during impact events; hence, the damper exhibits nonlinear damping effects. The total MR damper force is expressed in Equation 1.2, and the sum of those two forces gives the constant stroking load (Figure 1.7). The energy is pulled during stroke.

$$F_{total} = F_{MR} + F_{passive} \quad [1.2]$$

$$F_{MR} = F_y sgn(V_p) \text{ with } F_y = \frac{2n\tau_y L_a}{d} A_p \quad [1.3]$$

Equation 1.3 of the force versus velocity relationship is illustrated in Figure 1.8 with the Bingham Plastic model typically used to analyze the nonlinear behavior of MR dampers.

1.4 Modes of Operation of MR Dampers

Depending on the fluid flow and on the rheological stress, there are three different modes of MRF operation: the flow mode (or valve or Poiseulle flow mode), the direct shear mode, and the squeeze mode.

In the flow mode (Figure 1.8), the MRF is made to flow through a passage, across which the field can be applied. In this case, the electrodes (plates) are stationary. This is also the configuration typically utilized to construct MR valves in dampers and in shock absorbers. The pressure drop created in this mode, for instance in a damper, is the sum of the viscous (pure rheological) component and the magnetic field dependent (MR) component.

In the shear mode (Figure 1.9), the MRF is enclosed between two electrodes (or magnetic poles). One of the electrodes or poles is kept fixed, while the other undergoes a displacement and is connected to the system that requires damping. The relative displacement between the two electrodes, or magnetic poles, results in shearing of the MRF while maintaining a constant gap between the electrodes. The strength of the applied field stays constant with the motion of the electrode. The total force in the shear mode can be separated into a viscous (pure rheological) component and a magnetic field dependent (MR) component. The shear mode is also used in MR dampers, and other applications of the shear mode appear in MR brakes and clutches.

The third mode of operation is called the squeeze mode (Figure 1.10), and it has not been studied as thoroughly as the flow mode and the shear mode. The squeeze mode working principle is that the MR fluid is enclosed between two electrodes or magnetic poles that undergo relative motion along the direction of the field. The field strength varies with the displacement

of the electrodes. Some small-amplitude vibration dampers use this mode. For small motions, this mode seems to offer the possibility of very large forces which can be controlled by the MRF effect (Carlson, J.D., 1999).

1.5 Literature Review of MR Damper Quasi-Static and Dynamic Models

A great deal of efforts has been dedicated towards MR dampers theoretical models. Quasi-static models are Bingham Plastic or Hershel-Bulkley based models that do not incorporate hysteresis phenomenon in the MR damper force velocity behavior. Phillips, R.W. (1969) developed a nondimensional analysis based on the Bingham Plastic model to determine ERF/MRF pressure drop through a rectangular duct. Gavin *et al*. (1996) used an axisymmetric model to improve the description of ER/MR dampers quasi-static behavior as well as the previous analysis conducted by Phillips. Wereley *et al*. developed quasi-static nondimensional models using different variables, such as the damping coefficient and the Bingham number (Kamath and Wereley, 1997; Wereley and Pang, 1998; Hu and Wereley, 2003).

Hershel-Bulkley based models (Lee and Wereley, 1999; Wereley, 2008; Wang and Gordaninejad, 2001) to incorporate shear thinning/thickening effects and to predict MR fluid behavior through a rectangular duct and circular pipes were developed. The models described are applicable to the design and analysis of the majority of controllable fluid devices. Particularly, the Bingham plastic based quasi-static model is practical due to its simplicity.

In order to practically describe damper hysteresis effects due to the force-velocity relationship, dynamic models have been investigated. For instance, a phenomenological model, which is numerically tractable and is capable of exhibiting a wide variety of hysteretic behaviors, was developed for MR dampers by Spencer *et al.* (1997) and Yang (2001). The phenomenological model was based on the Bouc-Wen hysteresis model. In addition, an Eyring-

plastic model was developed by Bitman *et al*. (2005). The Eyring-plastic model was constructed by combining simple nonlinear functions, and the model had a simple design and formulation, even though it was in the form of a nonlinear function. The model can capture practical electrorheological (ER) damper responses, particularly in both the pre-yield and the post-yield states.

The analysis of the MR landing gear damper with a spring-assisted passive valve developed in this current dissertation was based on a nonlinear quasi-static Bingham Plastic-based model, and it was sufficient even in the case of higher speed impacts.

1.6 Literature Review of Adaptive Landing Gear Dampers

A primary goal of an adaptive landing gear system is to adapt the load stroke profile in response to payload and sink rate variations of a helicopter, while considering several challenges that have been encountered in prior work, such as controlling of the load stroke profile for short duration event (50-200 ms), keeping adaptive landing system compact and lightweight, and adjusting the load with control algorithms based on real-time measurements of sink rate and crash harshness (Choi *et al.*, 2012). In order to meet these challenges as well as satisfy this study's goal, a spring-based passive (or relief) valve MR landing gear system that has a constant cracking pressure, was proposed in this study. The motivation behind this current work stems from different aspects of adaptive MR landing gear systems. MR application to adaptive landing gear systems has been investigated by several research groups. For instance, the ability and effectiveness of an ERF/MRF-based landing gear system for dynamic load and vibration attenuation under different sink rates and payloads were analytically demonstrated by Choi and Wereley (2003). A telescopic type ER/MR damper shock strut was built, and its vibration control performance was investigated by using a two degree-of-freedom (2 DOF) landing gear system

model. The MR landing gear system achieved better performance results than passive landing gear systems. Batterbee *et al.* (2007) designed and constructed an oleo-pneumatic MR landing gear system by retrofitting a lightweight trainer aircraft commercial passive landing gear damper. It is important to note that all these studies mentioned about adaptive MR landing gear systems were designed and tested with scaled-down stroking loads intended for laboratory testing. Also, studies to suppress the fuselage vibration for improving the ride quality and safety of aircraft have been explored. Lin *et al.* developed a control algorithm using fuzzy proportional-integral-derivative (PID) hybrid control for adaptive capability to nonlinear system variations (Lin *et al.*, 2009). The fuzzy PID hybrid control algorithm could effectively reduce the fuselage acceleration when compared to passive control and PID control. Mikulowski and LeLetty (2008) proposed a closed loop feedback control algorithm to recognize the impact energy based on the initial velocity and mass of the falling structure (velocity sensor), determine the optimal acceleration value for the adaptive impact absorber, and execute the control signal in the closed loop during the process (acceleration sensor feedback). Their closed loop feedback control algorithm was successfully implemented to maintain the optimal acceleration level with reference to the identified impact energy and the stroke of the adaptive absorber. Choi *et al.* (2012) proposed a flow-mode type MR landing gear damper for a lightweight helicopter skid landing gear system, which was designed, at full-scale and maintained a desired stroking load of 4000 lb_f over a desired sink rate range of 6-12 ft/s. The performance of the MR landing gear damper was experimentally validated over the desired sink rate range under the iron-bird drop testing stand which is equipped with four MR landing gear dampers and uses a skid landing gear.

1.7 Outline and Description of Thesis

In the subsequent chapter, which is Chapter 2, the focus is on the feasibility of synthesizing MRFs utilizing three different hydraulic oils employed as carrier fluids, which are licensed for use in landing gear systems. The key objective in this chapter is to assess the effectiveness and feasibility of using these newly synthesized MRFs in landing gear stroking elements such as shock struts or oleos. In order to determine the suitability of these newly synthesized MRFs for this application, a series of measurements is conducted and the performance of MRFs is characterized. First, rheological properties (yield stress and viscosity) are measured using a parallel disk rheometer as a function of magnetic field. Then, sedimentation rate is measured using an inductance-based sensor to measure particle settling rates and investigate the fluid stability after being quiescent for a long period of time. Finally, the dynamic behavior is measured using a small-scale MR damper, and dynamic impact loads are measured as a function of varying magnetic field strengths utilizing a drop tower facility. Chapter 2 reviews common viscoplastic models, often used to describe the field dependent yield stress of MRFs. The performance of MRFs synthesized in Chapter 2 is compared to commercially available MRFs with similar solid loadings or volume percent (vol %) of iron (Fe) powder.

Chapter 3 consists of investigating MRFs that employ passive particles. Carbonyl iron (CI) powder has been the primary ferromagnetic dispersant used to prepare MRFs because those powders enable high yield stress. However, particles in such MRFs do settle, and in the absence of remixing, the particles descend to the bottom of the container forming a hard cake that is hard to remix. An MRF is desired that essentially does not settle, but instead provides the full MR effect the first time it is used even in the absence of remixing. Methods have been proposed to reduce settling particularly for shear mode magneto-rheometers (Klingenberg and Ulicny, 2011;

Ulicny *et al.*, 2010). However, such a study is lacking in the context of MR dampers or flow mode devices. Therefore, chapter 3 considers two MRF samples having 40 volume percent (vol%) of particles that are synthesized in a carrier fluid: MRF-40 and MRF-37. MRF-40 has 40 vol% of CI particles, and MRF-37 contains 35.7 vol% of CI particles and 4.3 vol% of passive particles (glass beads). A comparative study of MRF characteristics is conducted to determine the impact of the nonmagnetic glass beads on yield stress, as well as viscosity, and settling rate. Both MRFs are characterized through magnetorheology as a function of magnetic field, sedimentation rate in a fluid column measured using an inductance-based sensor, and cycling of a small-scale damper undergoing sinusoidal excitations for characterization and endurance tests. Optical micrographs of the passive particles (glass beads) are taken before and after damper cycling to assess durability. The main goal of chapter 3 is to determine the impact of replacing a small volume percent (vol%) of CI magnetic particles with the same vol% of passive particles on MRF (yield stress and sedimentation rate) and MR damper (yield force and post-yield damping) performance.

Chapter 4 focuses on an MR device modeling, design, and construction. In this chapter, a particular MR device is proposed to undertake the main goal of an adaptive landing gear system, which is to adapt the load stroke profile in response to payload and sink rate variations of the lightweight helicopter. The effort in this chapter is to satisfy a lightweight helicopter specific landing challenge by maintaining a constant stroking load of 4000 lb_f over an extended equivalent sink rate range (6-26 ft/s) while considering other important challenges encountered in previous studies on adaptive landing gear dampers. The MR landing gear damper proposed in this chapter for this study is an MR landing gear damper with a spring-based passive (relief) valve. This chapter briefly discusses the nonlinear model used to design the landing gear device

considering the field dependent Bingham-plastic behavior of MRFs and nonlinear viscous loss factors that are dependent on velocity squared. In addition to the modeling of the MR valve with a spring-assisted passive valve, Chapter 4 also focuses on the design and construction of the MR and passive valves. The MR landing gear ON-state force performance is further examined via simulations using the commercial software ANSYS. For the ON-state case, an electromagnetic analysis is conducted to predict the magnetic field strength in the MR gap and estimate the MR yield force. Two different springs are designed and used (a conventional coil spring and a spiral wave spring) for the analysis. Two spring-assisted passive relief valves are constructed, and an experimental study using a material testing systems (MTS) machine is conducted to evaluate the damper force behavior of the spiral wave and coil spring-based MR landing gear dampers to verify that the passive valve operates properly to crack the pressure and maintain a stroking force of 4000 lb_f over the desired sink rate range.

In chapter 5, the intent is to expand the high end of the sink rate range, so that the peak stroking load can be held constant for sink rates ranging from 6-26 ft/s hence extending the high end of the speed range from 12 ft/s (from prior work) to 26 ft/s. This can be achieved through the use of an adaptive landing gear system. The main purpose of an adaptive landing gear system is to adapt the load stroke profile in response to payload and sink rate variations of a helicopter. To experimentally investigate the behavior of the MR landing gear damper fabricated, single damper drop tests conducted at the University of Maryland, College Park to measure the stroking load of the MR landing gear damper coupled with the passive valve over equivalent sink rates up to about 18 ft/s are considered. The total drop mass is 430 lbs. Chapter 5 focuses on a control algorithm used in order to maintain the peak stroking load of the MR landing gear damper constant over the desired sink rate range of 6-26 ft/s. The bang-bang current control algorithm is

formulated in this chapter using a force feedback signal. This control algorithm is experimentally evaluated using the single damper drop test setup. To experimentally measure the stroking load of the MR landing gear damper with the spring-assisted passive valve over higher desired equivalent sink rates up to 26 ft/s, single damper drop tests (with a total drop mass of 1283 lbs) conducted at Boeing Structures Test Laboratory in Mesa, Arizona are considered. Finally, a ballasted frame called an iron-bird, which emulates the lightweight helicopter with a complete skid landing gear system and incorporates four MR landing gear dampers that are each coupled with a spring-based passive valve, is drop tested at Boeing as well (with a total drop mass of 2627 lbs). The bang-bang current control algorithm is also used for the iron-bird drop test data to regulate the damper force of the MR landing gear dampers over the desired sink rate range of 6-26 ft/s.

Chapter 6 investigates the validation of the MR landing gear damper with a spring-assisted relief valve models. In order to experimentally validate the adaptive MR landing gear damper models, drop tests data are utilized. In fact, MR landing gear damper performance is characterized using drop tests, and the data is used to validate model predictions data from these drop tests at low and high speed impacts. This chapter focuses on better understanding the behavior of the MR landing gear damper coupled with a spiral wave spring-assisted passive valve and operating over sink rates ranging from 6 -26 ft/s. Two models are examined in this chapter. Model #1 is a nonlinear BP-type damper model including the Darcy friction and pressure drop due to viscous effects and MR valve minor losses, which are proportional to the velocity squared, and the pressure drop due to the spring-assisted relief valve seal's opening. The second model (model #2) is a modified version of the first as it considers, in addition to the pressure drop due to the relief valve seal's opening, the pressure drop across the center orifice of

the relief valve to better account for the damper force behavior at higher speeds. This model includes minor loss factors, Darcy friction and viscous forces across the MR valve and the center orifice of the relief valve. In addition, a gas pressure inside the MR damper piston is considered; hence, the total force of the MR landing gear damper with a spiral wave spring-assisted relief valve includes the gas force. The main objective of chapter 6 is to experimentally validate the models using single damper drop test data obtained from the drop tower facility at Boeing Structures Test Laboratory in Mesa, Arizona for nominal drop speeds of up to 26 ft/s (7.9 m/s).

Finally, chapter 7 provides a summary of the work and highlights the significant results. Research contributions as well as recommendations for future work are also presented in this chapter.

References

Batterbee, D.C., Sims, N.D., Stanway, R., and Wolejsza, Z., (2007a) Magnetorheological landing gear: 1. A design methodology. *Smart Materials and Structures*, 16: 2429-2440. DOI: 10.1088/0964-1726/16/6/046.

Batterbee, D.C., Sims, N.D., Stanway, R., and Rennison, M., (2007b) Magnetorheological landing gear: 2. Validation using experimental data. *Smart Materials and Structures*, 16: 2441-2452. DOI: 10.1088/0964-1726/16/6/047.

Bell, R.C., Karli, J.O., Vavreck, A.N., Zimmerman, D.T., Ngatu, G., and Wereley, N.M., (2008) Magnetorheology of submicron diameter iron microwires dispersed in silicone oil. *Smart Materials and Structures*, 17(015028): 1-6. DOI: 10.1088/0964-1726/17/01/015028.

Bitman L., Choi, Y.-T., Choi, S.B., and Wereley, N.M., (2005) Electrorheological damper analysis using an Eyring-plastic model. *Smart Materials and Structures*, 14(1): 237-246. DOI: 10.1088/0964-1726/17/14/1/024.

Carlson, J.D, Sprecher, A.F., and Conrad, H., (1990) Electrorheological fluids. Proceedings of the Second International Conference on ER Fluids, Technomic, Lancaster, Pa.

Carlson, J.D., Catanzarite, D.M., and St. Clair, K.A., (1995) Commercial magneto-rheological fluid device. Lord Corporation, Cary, NC 27511 USA. Proceedings of the 5th International Conference on ER Fluids, MR Fluids and Associated Technology, U. Sheffield, UK, 20-28.

Carlson, J.D., (1999) Magnetorheological Fluid Actuators. Adaptronics and Smart Structures, Editor H. Janocha Springer Berlin, 180-195, ISBN 3-540-61484-2.

Carlson, J.D., and Jolly, M.R., (2000) MR fluid, foam and elastomer devices. *Mechatronics*, 10 (4-5): 555-569. DOI: 10.1016/S0957-4158(99)00064-1.

Carlson, J.D., (2001) What makes a good MR fluid. Proceedings of the 8th International Conference on Electrorheological (ER) and Magnetorheological (MR) Suspensions.

Chaudhuri, A., Wereley, N.M., Kotha, S., Radhakrishnan, R., and Sudarshan, T., (2005) Viscometric characterization of cobalt nanoparticle-based magnetorheological fluids using genetic algorithms. *Journal of Magnetism and Magnetic Materials*, 293: 206–214. DOI: 10.1016/j.jmmm.2005.01.061.

Choi, Y.-T., and Wereley, N.M., (2003) Vibration control of a landing gear system featuring ER/MR fluids. *AIAA Journal*, 40(3): 432–439. DOI: 10.2514/2.3138.

Choi, Y.-T., Robinson, R., Hu, W., Wereley, N.M., Birchette, T.S., and Bolukbasi, A.O., (2012) Analysis and control of a magnetorheological landing gear system for a helicopter. Proceedings of the American Helicopter Society 68th Annual Forum & Technology Display, Fort Worth, TX, USA.

Gavin, H.P., Hanson, R.D., and Filisko, F.E., (1996) Electrorheological dampers, part I: analysis and design. *Journal of Applied Mechanics*, 63: 678-82. DOI: 10.1115/1.2823348.

Gonzales, F.D., (2005) Characterizing the behavior of magnetorheological fluids at high velocities and high shear rates. Ph.D Thesis, Mechanical Engineering, Virginia Polytechnic Institute and State University, Virginia.

Hiemenz, G., Hu, W., and Wereley, N.M., (2008) Semi-active magnetorheological helicopter crew seat suspension for vibration isolation. *Journal of Aircraft*, 45(3): 945-953. DOI: 10.2514/1.32736.

Hu, W., and Wereley, N.M., (2003) Nondimensional damping analysis of flow-mode magnetorheological and electrorheological damper. Proceedings of IMECE'03 ASME, International Mechanical Engineering Congress & Exposition, Washington, D.C., USA.

Jolly, M.R., Bender, J.W., and Carlson, J.D., (1998) Properties and applications of commercial magnetorheological fluids. Proceedings of the 5th SPIE Annual International Symposium on Smart Structures and Materials, San Diego, CA.

Kamath, G.M., and Wereley, N.M., (1997) A nonlinear viscoelastic-plastic model for electrorheological fluids, *Smart Materials and Structures*, 6: 351-359. DOI: 10.1088/0964-1726/6/3/012.

Klingenberg, D.J., and Ulicny, J.C., (2011) Enhancing magnetorheology. *International Journal of Modern Physics B*, 25(7): 911-917. DOI: 10.1142/S021797921105847X.

Lee, D.Y., and Wereley, N.M., (1999) Quasi-steady Herschel-Bulkley analysis of electro- and magnetorheological flow mode dampers. *Journal of Intelligent Material Systems and Structures*, 10(10): 761-769. DOI: 10.1106/E3LT-LYN6-KMT2-VJJD.

Lin, L.H., Yong, C., Qi, H., and Jian, L., (2009) Fuzzy PID control for landing gear based on magnetorheological (MR) damper. International Conference on Apperceiving Computing and Intelligence Analysis (ICACIA), 22-25. DOI: 10.1109/ICACIA.2009.5361162.

Lord Corporation, www.lord.com.

Lord Corporation (2014) Dr. Dave's Do-It-Yourself MR Fluid, Designing with MR Fluid, Magnetic Circuit Design, FAQs, www.lord.com.

Mikulowski, G.M., and LeLetty, R., (2008) Advanced landing gears for improved impact absorption. Proceedings of the 11th International Conference on New Actuators, 363-366, Bremen, Germany.

Mikułowski, G.M., Wiszowaty, R., and Holnicki-Szulc, J., (2013) Characterization of a piezoelectric valve for an adaptive pneumatic shock absorber. *Smart Materials and Structures*, 22(125011): 1-12. DOI: 10.1088/0964-1726/22/12/125011.

Ngatu, G.T., and Wereley, N.M., (2007) Viscometric and sedimentation characterization of bidisperse magnetorheological fluids. *IEEE Transactions on Magnetics*, 43(6): 2474–2476. DOI: 10.1109/TMAG.2007.893867.

Park, B.J., Song, K.H., and Choi, H.J., (2009) Magnetic carbonyl iron nanoparticle based magnetorheological suspension and its characteristics. *Materials Letters*, 63(15): 1350-1352. DOI: 10.1016/j.matlet.2009.03.013.

Phillips, R.W., (1969) Engineering Applications of Fluids with a Variable Yields Stress, Ph.D Thesis, Mechanical Engineering, University of California, Berkeley.

Phulé, P., and Ginder, J., (1998) The materials science of field-responsive fluids. *MRS Bulletin*, 23(8): 19–21. DOI: 10.1557/S0883769400030761.

Poddar, P., Wilson, J.L., Srikanth, H., Yoo, J.H., Wereley, N.M., Kotha, S., Barghouty, L. and Radhakrishnan, R., (2004) Nanocomposite magnetorheological fluids with uniformly dispersed Fe nanoparticles. *Journal of Nanoscience and Nanotechnology*, 4(1-2): 192–196. DOI: 10.1166/ jnn.2004.020.

Rosenfeld, N., Wereley, N.M., Radakrishnan, R., and Sudarshan, T., (2002) Behavior of magnetorheological fluids utilizing nanopowder iron. *International Journal of Modern Physics B*, 16(17-18): 2392–2398. DOI: 10.1142/S0217979202012414.

Spencer Jr., B.F., Dyke, S.J., Sain, M.K., and Carlson, J.D. (1997) Phenomenological model for a magnetorheological damper. *Journal of Engineering Mechanics*, ASCE, 123: 230-52.

Ulicny, J.C., Snavely, K.S., Golden, M.A., Klingenberg, D.J., (2010) Enhancing magnetorheology with nonmagnetizable particles. *Applied Physics Letters*, 96: 231903-1-3. DOI: 10.1063/1.3431608.

Wang, X., and Gordaninejad, F., (2001) Dynamic modeling of semi-active ER/MR fluid dampers, damping and isolation. Proceedings of SPIE Conference on Smart Materials and Structures, 4331; 82-91.

Wereley, N.M., and Pang, L., (1998) Nondimensional analysis of semi-active electro- and magneto-rheological dampers using parallel plate models. *Smart Materials and Structures*, 7: 732-743. DOI: 10.1088/0964-1726/7/5/015.

Wereley, N.M., Chaudhuri, A., Yoo, J.H., John, S., Kotha, S., Suggs, A., Radhakrishnan, R., Love, B.J., and Sudarshan, T.S., (2006) Bidisperse magnetorheological fluids using Fe particles at nanometer and micron scale. *Journal of Intelligent Material Systems and Structures*, 17(5): 393-401. DOI: 10.1177/1045389X06056953.

Wereley, N.M., (2008) Nondimensional Herschel-Bulkley analysis of magnetorheological and electrorheological dampers. *Journal of Intelligent Material Systems and Structures*, 19(3): 257-268.

Yang, G.Q., (2001) Large-scale magnetorheological fluid damper for vibration mitigation: modeling, testing and control. Ph.D dissertation, University of Notre Dame.

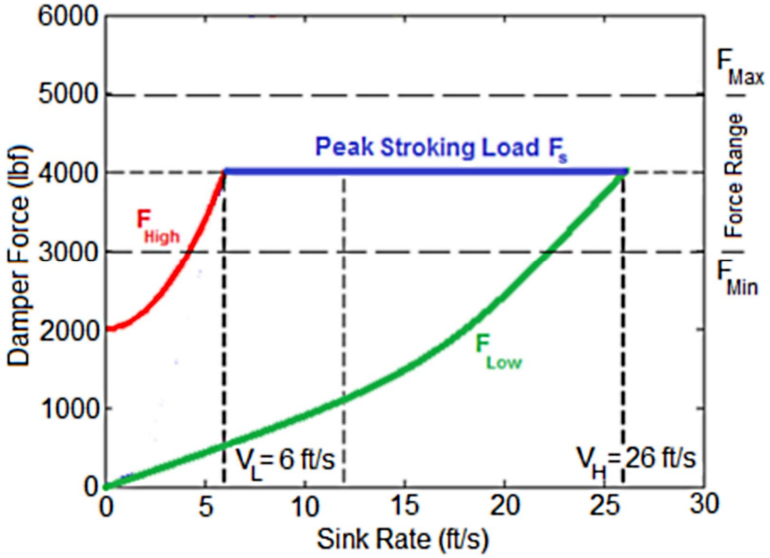

Figure 1.1. Design targets assigned by Boeing to maintain a constant stroking load of 4000 lb_f over an equivalent sink rate range of 6-26 ft/s

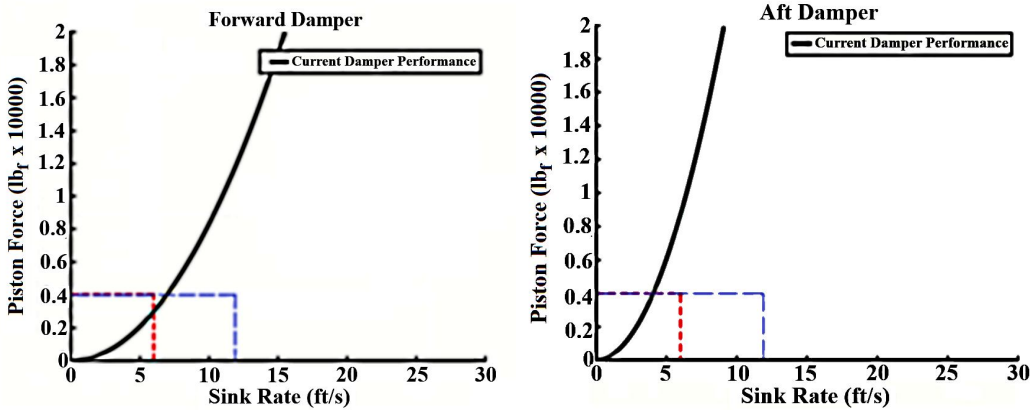

Figure 1.2. Passive hydraulic damper performances for the MD-500 helicopter fixed landing gear dampers. Each damper is tuned for only one condition.

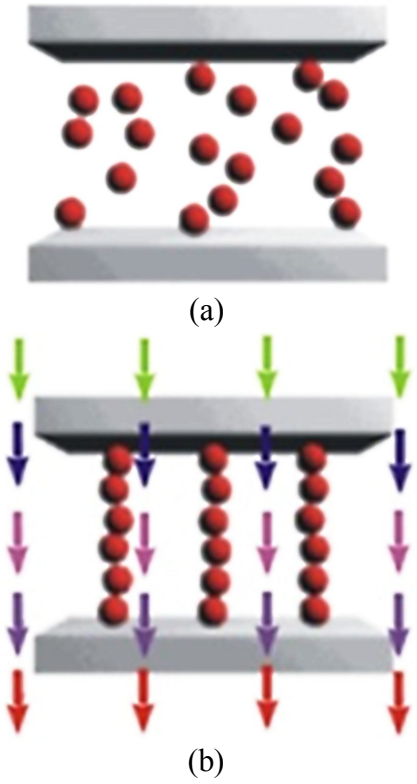

Figure 1.3. Activation of MRF: (a) no magnetic field applied; (b) magnetic field applied and ferromagnetic particle chains have formed (© 2005 Lord Corporation. All rights reserved)

MRF: Magnetorheological fluid

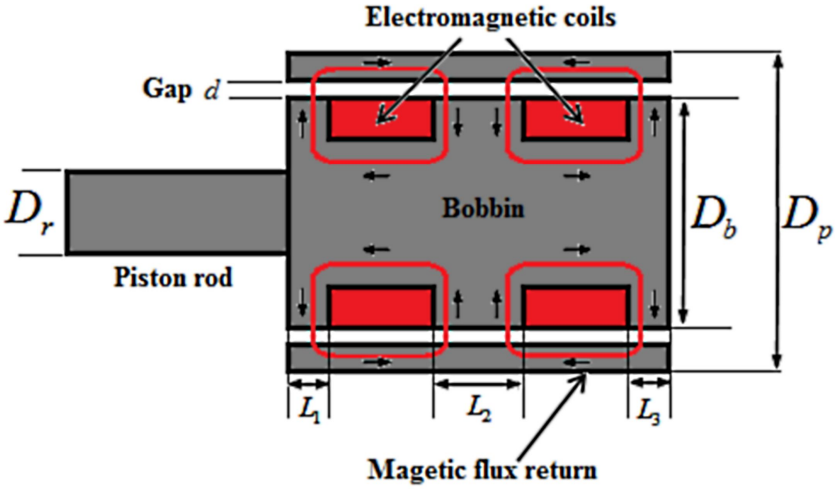

Figure 1.4. Typical conventional MR damper valve configuration

MR: Magnetorheological

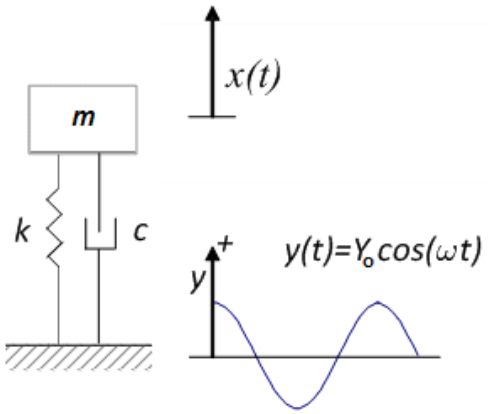

Figure 1.5. A particular helicopter seat and occupant system represented using a single-degree-of-freedom system (SDOF system)

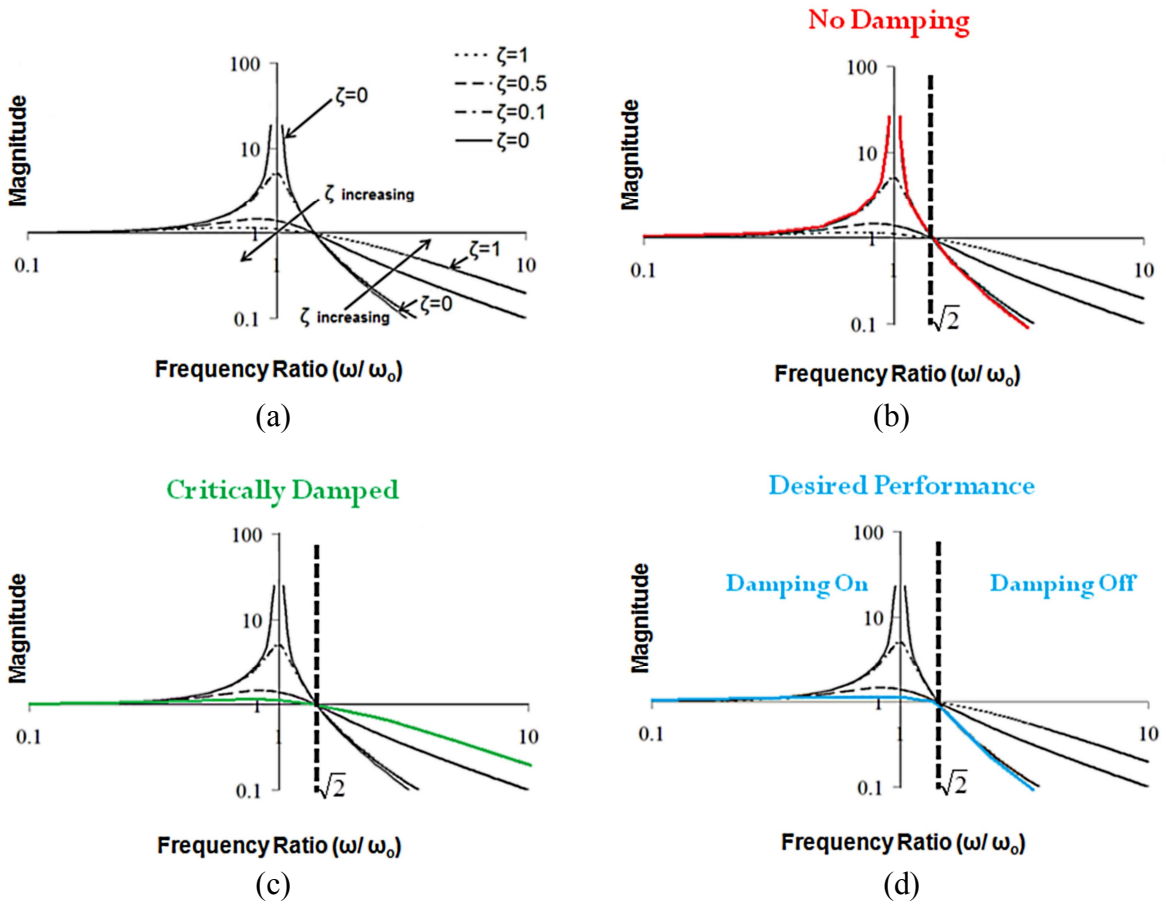

Figure 1.6. A particular helicopter seat and occupant system's response shown on a transmissibility plot

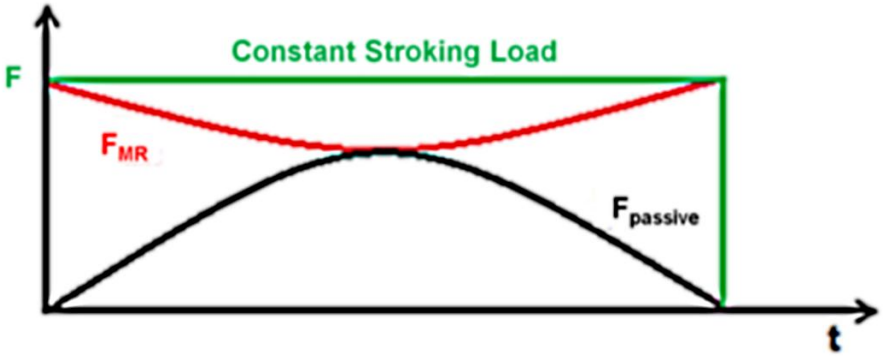

Figure 1.7. MR devices used for energy absorption. The constant stroking load is the sum of F_{MR} and $F_{passive}$.

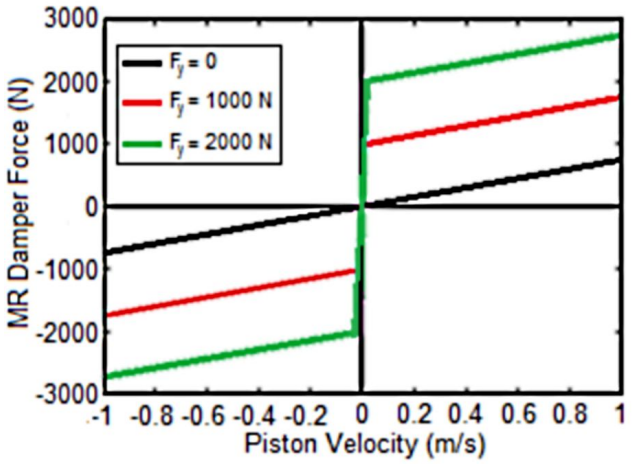

Figure 1.8. Force versus velocity relationship represented by the Bingham Plastic model

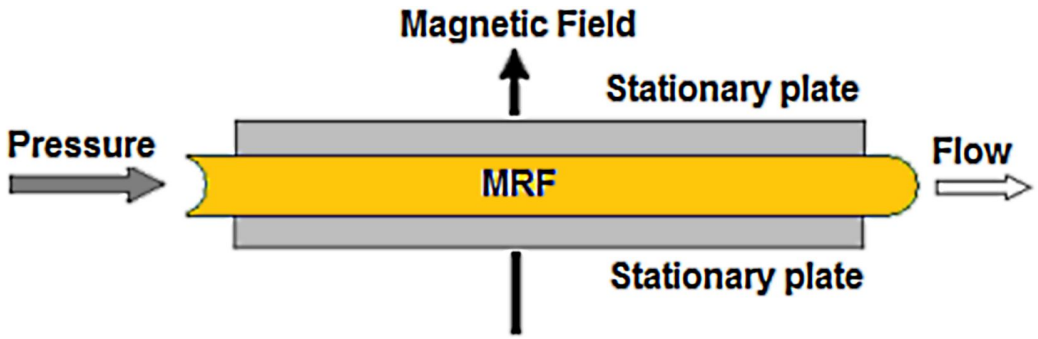

Figure 1.9. MR damper mode of operation: flow mode

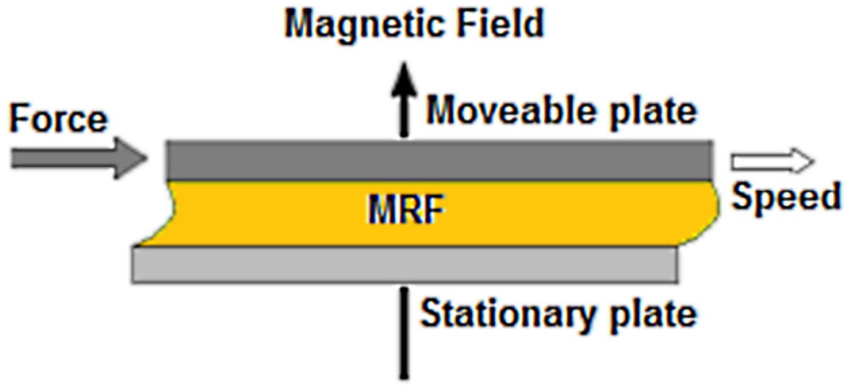

Figure 1.10. MR damper mode of operation: shear mode

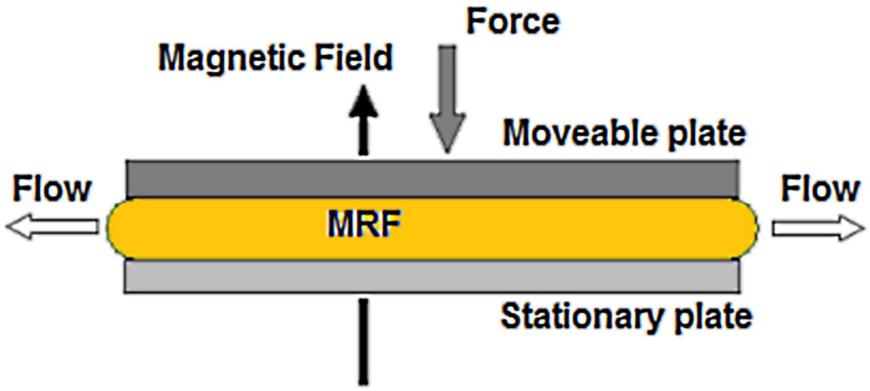

Figure 1.11. MR damper mode of operation: squeeze mode

Table 1.1. MRF and ERF key features comparison

Key Features	**MRF**	**ERF**
Maximum yield stress	50-100 kPa	2-5 kPa
Power supply	2-24 Volts @ 1-2 A	2-5 kilovolts @ 1-10 mA
Response time	Few milliseconds	Few milliseconds
Operational Field	~250 kA/m	~4kV/mm
Energy density	0.1 J/cm^3	0.001 J/cm^3
Stability	Good for most impurities	Poor for most impurities
Operational temperature	-40°C up to +150°C	-25°C up to +125°C

CHAPTER 2: Magnetorheological Fluids Synthesized for Helicopter Landing Gear Applications

2.1 Introduction and Overview

Magnetorheological fluids (MRFs) are used in an increasing range of applications, such as primary vehicle suspensions and semi-active vibration absorbing systems (Choi *et al.*, 2005a; Snyder *et al.*, 2001). However, the use of MRFs targeting such applications as landing gear systems has not been widely investigated (Batterbee *et al.*, 2007a; Choi *et al.*, 2003 and 2012).

During landing, an aircraft is subjected to a short-duration impulsive impact, which is a contributing factor to structural fatigue damage, crew and passenger discomfort, and dynamic stress. One possibility to reduce these impact loads is to incorporate MRFs into the shock struts of landing gear systems. By doing so, a landing gear can exploit the field adjustable yield stress to control the stroking load of a landing gear oleo to minimize impact loads transmitted to the aircraft fuselage.

Magnetorheology depends on several factors including particle shape (Bell *et al.*, 2007), and coatings (Fang *et al.*, 2008) or passive particles (Powell *et al.*, 2012). However, in this chapter, the focus is on the feasibility of synthesizing MRFs employing three different carrier fluids, which are hydraulic oils licensed for use in landing gear (MIL-H-5606, MIL-PRF-83282, and MIL-PRF-87257). The performance of MRFs was characterized through a series of measurements in order to assess the suitability of these synthesized MRFs: (1) rheological properties (yield stress and viscosity) were measured using a parallel disk rheometer as a function of magnetic field, (2) sedimentation rate was measured using an inductance-based sensor to measure particle settling rates, (3) dynamic behavior was measured using a small-scale

MR damper, and (4) dynamic impact loads were measured as a function of varying magnetic field strengths utilizing a drop tower facility. The MRFs synthesized here are also compared to commercially available MRFs with similar solids loading or weight percent (wt%) of iron (Fe) powder.

The key goal in this chapter is to assess the effectiveness and feasibility of using these newly synthesized MRFs in landing gear stroking elements such as shock struts or oleos.

2.2 Synthesis of MRF Composites

Three certified landing gear hydraulic oils were utilized as carrier fluids to prepare MRFs: a mineral oil (MIL-H-5606) and two synthetic hydrocarbon oils (MIL-PRF-83282 and MIL-PRF-87257). These particular oils were selected to preserve important characteristics needed for landing gear systems, such as wide operational temperature ranges (e.g. 265 ^{o}F to 275 ^{o}F), excellent anti-wear agents, and fire resistance properties (Aviation Maintenance and Training Manual, 2003).

Each hydraulic fluid was then used to prepare two categories of MRF composites, depending on the average diameter of spherical Fe particles present. The first sample set contained Fe particles of larger diameter (6–10 μm denoted by I), and the second set contained Fe particles of smaller diameter (1–3 μm denoted by II). Also, lecithin powder (2 wt%) was added as a surfactant to reduce agglomeration and to minimize particle settling rate. In order to prepare stable MRFs, a specific amount of hydraulic oil was mixed with lecithin powder using a high speed shear mixer (IKA-Ultra-Turrax® T 25 basic) operating at 11,000 rpm. After consistently mixing for 30 min, Fe particles were added in specific quantity to each fluid sample and remixed for an additional hour. Accordingly, samples varying from 60 to 80 wt% (15 to 32 vol%) in Fe particle concentrations were synthesized, and each sample notation includes three

important parts: first is the hydraulic oil number used (e.g. 83282, 87257, or 5606), second are Fe particle sizes (e.g. I for 6–10 μm or II for 1–3 μm), and third is the Fe particle concentration (e.g. ‘‘d’’ for 75 wt% Fe and ‘‘e’’ for 80 wt% Fe). The synthesis chart is presented in Figure 2.1.

2.3 Characterization of MRF Composites

2.3.1 Magnetorheology

2.3.1.1 Setup and Instrumentation

MRF characterization was performed on all the MRF samples using a Paar Physica MCR 300 parallel disk rheometer (Figure 2.2). This instrument was used to measure the flow curves (i.e. shear stress vs. shear rate) as a function of applied field. The prepared samples (0.3 ml) were loaded onto the rheometer, which had a standard 1 mm gap separating the rotating disk from the platen. The current was increased from 0.2 to 5 A to measure flow curves as a function of the applied field and to determine magnetic saturation of each sample.

2.3.1.2 Results and Discussion

Rheological tests were performed on all of the prepared MRFs at room temperature. The fluid was sheared by the rotating top disk of the rheometer as the bottom disk stayed stationary. Figure 2.3 shows selected flow curves with the Bingham Plastic (BP) model of mr83282-Ie with synthetic oil (MIL-PRF-83282). A synthetic oil-based MRF containing larger (6–10 μm) Fe particles with 75 wt% (or 26 vol%) Fe concentration (referred as mr83282-Id) rheology was compared to a commercial MRF from Lord Corporation (MRF126CD) of the same Fe concentration. The MRF sample (mr83282-Id) had an off-state (dynamic) viscosity lower than that of the commercial MRF, as illustrated in Figure 2.4. It is important to keep the off-state viscosity as low as possible in order to maintain high-frequency transmissibility in a base-excited

isolation mount as low as possible (Choi *et al.*, 2005a). Also, both fluids had field-dependent yield stress curves that followed similar trends, as shown in Figure 2.5.

2.3.1.3 Bingham Plastic Modeling of MRF Composites Flow Curves

The flow curves were characterized using the Bingham plastic (BP) model (Wereley *et al.*, 2006). In this model, when a shear stress is applied to the fluid, it behaves as a solid until a specific yield stress, τ_y is reached. At stress levels higher than the yield stress, the fluid performs like a Newtonian liquid with a constant viscosity. Above the yield point, the stress in the fluid can be expressed as the following constitutive law:

$$\tau = \tau_y + \mu\dot{\gamma} \text{ for } \dot{\gamma} > 0 \qquad [2.1]$$

where μ is the post-yield viscosity and $\dot{\gamma}$ the shear rate. The post-yield viscosity is the slope of the high shear rate asymptote of the BP model, and the yield stress is the intercept of the high shear rate asymptote to the shear stress axis.

2.3.2 Sedimentation Testing

2.3.2.1 Setup and Instrumentation

The effectiveness of the MRF composite to maintain the suspension was analyzed by quantifying the settling rates of Fe particles using a 1/4-in inductance-based sensing coil. In fact, after settling, the Fe particles may form a hard cake due to remnant particle magnetization, which is difficult to redisperse, rendering the MRF ineffective. Therefore, in order to prepare stable MRFs, adding a surfactant, such as lecithin, improves mixability by reducing this tendency to form a hard cake. The sedimentation setup is described in (Ngatu and Wereley, 2007; Powell *et al.*, 2012).

As settling progresses, the sensing coil tracks a distinct boundary, or "mudline," between the clarified carrier fluid above and the MRF below, and it measures the inductance, L, which depends on the permeability of MRFs (also dependent on the volume fraction of dispersed particles) enclosed by the sensing coil, as illustrated in Equation 2.2:

$$L = \frac{N^2 A \mu_0}{l} \mu_r \qquad [2.2]$$

n is the number of turns, A is the cross-sectional area of the sensing coil wire, μ_0 is the vacuum magnetic permeability, μ_r is the relative permeability of the enclosed MRF, and $l\ is\ the\ sensing\ coil\ length.$ As the mudline travels downwards through the sensing coil, the permeability of the fluid volume contained therein decreases. The slope of this curve yields the sedimentation rate (Ngatu and Wereley, 2007; Powell *et al.*, 2012). The samples were tested twice: a sedimentation test was performed immediately after synthesizing the fluid and a second test after being stored quiescent for one month in order to assess remixability.

2.3.2.2 Results and Discussion

Particle sedimentation rates of the tested MRFs were measured several times to verify redispersion consistency. For example, the MRF containing synthetic oil and larger particles at 80 wt% (i.e.: mr83282-Ie) inductance was measured while the fluid mudline descended through the sensor. After performing the first set of tests, the fluid was not remixed for one month until the second set of tests was conducted. Testing was repeated several times on the same sample, and Figure 2.6 shows that the results are similar. This demonstrates that the particles were easily remixed in the MRF after being left alone for at least one month.

2.3.3 Low Speed Dynamic Testing of MR Damper

2.3.3.1 Setup and Instrumentation

Performance of the MRFs was determined by the response of a modified Rheonetics SD-1000-2 MR damper from Lord Corporation to sinusoidal loads. Only MRFs containing Fe particle concentration of 80 wt% or 32 vol% were tested for this experiment. The damper was subjected to sinusoidal loading on an 810 MTS servo-hydraulic testing machine. Figure 2.7 shows the setup for the MR damper characterization and further discussion of this MR damper can be found in (Snyder *et al.*, 2001; Powell *et al.*, 2012).

The MR damper was connected to a load cell through an extension bolt that was screwed into an upper bracket, which in turn was holding the MR damper in place. The lower mounting bracket was attached to the MR damper through a mounting rod that is slotted at the mounting hole of the shaft displacement, located at the center of the MR damper assembly. The other end of the lower mounting bracket was attached to the MTS actuator through another extension bolt. The displacement and MR damper force were measured by the linear variable differential transformer (LVDT) sensor and load cell of the MTS machine.

2.3.3.2 Test Inputs

The frequencies of excitations were chosen to be 2.5 Hz and 5.0 Hz. The damper excitation amplitudes ranged from 1.27 mm to 7.62 mm with a 2.54 mm increment. In order to apply a magnetic field inside the damper, electric current from a DC power supply (from 0 to 4 A with 1 A increment) was used to power the magnetic circuit.

2.3.3.3 Results and Discussion

The hysteretic behavior of the linear stroke MR damper containing MRF was studied using high Fe particle concentration fluids of 80 wt% or 32 vol% (specifically, MRFs denoted

mr83282-Ie and mr5606-Ie). The Nonlinear BiViscous (NBV) model was used to characterize the yield force of the MR damper. The performances of both MRF samples, i.e., mr83282-Ie and mr5606-Ie, were compared to a commercial MRF from Lord Corporation (MRF132) of the same particle concentration. The yield force of all three fluids followed the same trend as a function of applied field, particularly at 5 Hz. Figure 2.8 illustrates these results, and all three fluid yield forces plotted versus current show that the maximum yield forces are within 5%.

2.3.3.4 Nonlinear BiViscous Model of MR Damper

Force versus displacement data were analyzed using the NBV model (Wereley *et al.*, 2004). The NBV model was employed to represent force versus velocity damper response, and provided a means to estimate yield force (F_y) and post-yield damping (C_{po}). The model is piecewise continuous in velocity and assumes that the MRF is plastic in both the pre-yield, C_{pr}, and the post-yield, C_{po}, conditions with the pre-yield damping being much greater than the post-yield damping as illustrated in Figure 2.9 (Wereley *et al.*, 2004). The piecewise continuous equations describing the model are shown in Equations 2.3 and 2.4:

$$f(t) = \begin{cases} C_{po}v + F_y & v \geq v_y \\ C_{pr}v & -v_y \geq v \leq v_y \\ C_{po}v - F_y & v \leq -v_y \end{cases} \quad [2.3]$$

The pre-yield velocity is:

$$v_y = \frac{F_y}{C_{pr} - C_{po}} \quad [2.4]$$

2.3.4 High Speed Impact Testing of MR Damper

2.3.4.1 Setup and Instrumentation

A free-flight drop test facility with a 59 kg drop carriage, as shown in Figure 2.10, was used to conduct impact tests on a MR energy absorber (MREA) filled with synthetic oil-based MRF containing 6-10 μm Fe particles at a concentration of 80 wt% (denoted mr83282-Ie).

Recently, MREAs have been highlighted as a promising candidate for crashworthiness systems, and several impact tests have been conducted (Facey *et al.*, 2005; Mao *et al.*, 2007). Therefore, the performance of mr83282-Ie in a MREA subjected to drop testing is important to verify the adjustability of MREA response at impact velocities representative of sink rates that occur during a helicopter landing.

The experiment instrumentation included a load cell located on a base plate as shown in Figure 2.11, which was safely bolted to the ground, an LVDT fastened to the damper to monitor the displacement of the damper piston as a function of time, and a power supply to provide electric current necessary to generate a magnetic field in the damper magnetic circuit. In addition, the raw signal from the sensor was filtered through a 2311 VISHAY signal conditioning amplifier, and the data was transferred to a computer using a SCC-68 National Instruments data acquisition interface (which changed analog data to digital). Finally, the data was exported to MATLAB compatible formats for analysis.

Testing of the MRF composite enclosed in the damper was achieved by positioning the damper vertically on the base plate. Then, a block of aluminum honeycomb measuring 90x60x60 mm was taped on a small plate, which was mounted on the top end of the damper. The purpose of using the aluminum honeycomb block was to prevent the ringing in the load cell due to metal-to-metal contact and reduce the inertial spike associated with the impact acceleration of the

piston rod (Browne *et al.*, 2004). Additional larger honeycomb blocks were placed on top of cement bricks and wood blocks (on each side of the damper) to stop the drop carriage platform after about 3.8 cm of stroke, which needed to be less than the LVDT stroke of 4.6 cm to prevent damaging it.

2.3.4.2 Results and Discussion

An MREA was filled with a synthetic hydraulic oil-based MRF with 6–10 μm and 80 wt% Fe particles concentration (denoted mr83282-Ie) and subjected to drop tests. This particular fluid was selected due to its favorable performance based on the rheological and damper test results. Peak stroking loads measured for a range of impact velocities and applied magnetic field strengths are in Table 1. The peak force increased as magnetic field and impact velocities increased. In Table 1, for a given field strength, the peak stroking load increased as velocity increased as a result of the velocity squared viscous force component. As the current (or magnetic field) increased, the peak stroking load also increased, which resulted in the increase in yield stress or MREA force. Tunability of the stroking load was greater at lower impact velocity and reduced slightly as the velocity increased. The MRF (mr83282-Ie) enabled tunable behavior as the magnetic field varied. The peak stroking load, as well as the energy absorbed by the MREA, could be adjusted by increasing magnetic field for an impact velocity of 2.8 m/s as shown in Figure 2.12.

2.4 Conclusions

Magnetorheological fluids (MRFs) were synthesized using three different carrier hydraulic oils certified for landing gear use, and the feasibility of these MRFs for potential use in landing gear systems was assessed. A series of sample MRFs were synthesized for different solid loadings (vol% of iron, Fe, particles) using landing gear fluids as the carrier fluids: MIL-H-5606,

MIL-PRF-83282, and MIL-PRF-87257. A lecithin surfactant was used (2 wt%) to maintain the suspension and to prevent particle agglomeration. These fluids were also compared to commercially available fluids from Lord Corporation with comparable solid loadings.

First, magnetorheological (MR) properties were tested as a function of applied field, and the experimental data were characterized using the Bingham Plastic (BP) model. Using flow curve data, the yield stress and viscosity of the MRF composites were identified. The MR landing gear fluid composite compared favorably with a commercial MRF (both containing 26 vol% magnetic particles).

Second, a particle sedimentation study was performed on the fluids using an inductance coil-based sedimentation rate monitoring system. Consequently, particle dispersion stability was effective, and redispersion showed similar results, even though fluids were left quiescent for over a month.

Third, the performance of a linear stroke MR damper, filled with MRFs, was characterized using a Nonlinear BiViscous (NBV) model. The NBV model was used to successfully identify the yield force. MR damper behavior was compared to the damper behavior using a commercial MRF (of 32 vol% particle concentration). The yield forces of the MRFs containing the larger (6-10 μm) Fe particles (32 vol%) compared favorably with that of the commercial MRFs, and measured yield forces of the MR damper with either MRF were within 5% of each other.

Finally, synthetic oil-based MRF (of 32 vol% Fe particles) was utilized in an MR damper and subjected to high shear rate drop testing to experimentally verify the tuning nature of the MR device at different impact velocities and magnetic field strengths. Consequently, the peak

stroking force and the energy dissipated by the MR damper strongly depended on the changes in the magnetic field strengths.

Based on this range of tests used to characterize MRFs synthesized, using certified landing gear fluids, it has been shown that it is feasible to utilize such hydraulic oils as the carrier fluids in suitable MRFs. Additional testing is warranted to ensure that the addition of particle solids and surfactants does not affect key properties of the hydraulic carrier fluids such that operating temperature range and resistance to flammability are preserved in landing gear applications.

References

Aviation Maintenance and Training Manual (2003). Integrated Publishing, Inc. Port Richey, FL. Available at: www.tpub.com

Batterbee, D.C., Sims, N.D., Stanway, R., and Wolejsza, Z., (2007a) Magnetorheological landing gear: 1. A design methodology. *Smart Materials and Structures*, 16: 2429-2440. DOI: 10.1088/0964-1726/16/6/046.

Bell, R.C., Miller, E.D., Karli, J.O., Vavreck, A.N., and Zimmerman, D.T., (2007) Influence of particle shape on the properties of magnetorheological fluids. *International Journal of Modern Physics B*, 21(28–29): 5018-5025. DOI: 10.1142/S0217979207045979.

Browne, A.L., McCleary, J.D., Namuduri, C.S., and Webb, S.R., (2004) Impact performance of magnetorheological fluids. ASME International Mechanical Engineering Congress and Exposition, Paper No. IMECE 2004-60542.

Choi, Y.-T., and Wereley, N.M., (2003) Vibration control of a landing gear system featuring ER/MR fluids. *AIAA Journal*, 40(3): 432–439. DOI: 10.2514/2.3138.

Choi, Y.-T., Wereley, N.M., and Jeon, Y.S., (2005a) Semi-active vibration isolation using magnetorheological isolators. *Journal of Aircraft*, 42(5): 1244-1251. DOI: 10.2514/1.7919.

Choi, Y.-T., Robinson, R., Hu, W., Wereley, N.M., Birchette, T.S., and Bolukbasi, A.O., (2012) Analysis and control of a magnetorheological landing gear system for a helicopter. Proceedings of the American Helicopter Society 68th Annual Forum & Technology Display, Fort Worth, TX, USA.

Facey, W.B., Rosenfeld, N., Choi, Y.-T., Wereley, N.M., Choi, S.B., and Chen, P., (2005) Design and testing of a compact magnetorheological damper for high impulsive loads. *International Journal of Modern Physics B*, 19(7-9): 1549-1555. DOI: 10.1142/S0217979205030578.

Fang, F.F., and Choi, H.J., (2008) Noncovalent self-assembly of carbon nanotube wrapped carbonyl iron particles and their magnetorheology. *Journal of Applied Physics*, 103(7): 07A301-1-3. DOI: 10.1063/1.2829019.

Mao, M., Hu, W., Choi, Y.-T., Wereley, N.M., (2007) A magnetorheological damper with bifold valves for shock and vibration mitigation. *Journal of Intelligent Material Systems and Structures*, 18(12): 1227-1232. DOI: 10.1177/1045389X07083131.

Ngatu, G.T., and Wereley, N.M., (2007) Viscometric and sedimentation characterization of bidisperse magnetorheological fluids. *IEEE Transactions on Magnetics*, 43(6): 2474–2476. DOI: 10.1109/TMAG.2007.893867.

Powell, L.A., Wereley, N.M., and Ulicny, J.C., (2012) Magnetorheological fluids employing substitution of nonmagnetic for magnetic particles to increase yield stress. *IEEE Transactions on Magnetics*, 48(11): 3764-3767. DOI: 10.1109/TMAG.2012.2202885.

Snyder, R.A., Kamath, G.M., and Wereley, N.M., (2001) Characterization and analysis of magnetorheological damper behavior under sinusoidal loading. *AIAA Journal*, 39(7): 1241-1253. DOI: 10.1117/12.384563.

Wereley, N.M., Lindler, J, Rosenfeld, N., Choi, Y.-T., (2004) Biviscous damping behavior in electrorheological shock absorbers. *Smart Materials and Structures*, 13(4): 743-752. DOI: DOI: 10.1088/0964-1726/13/4/012.

Wereley, N.M., Chaudhuri, A., Yoo, J.H., John, S., Kotha, S., Suggs, A., Radhakrishnan, R., Love, B.J., and Sudarshan, T.S., (2006) Bidisperse magnetorheological fluids using Fe particles at nanometer and micron scale. *Journal of Intelligent Material Systems and Structures*, 17(5): 393-401. DOI: 10.1177/1045389X06056953.

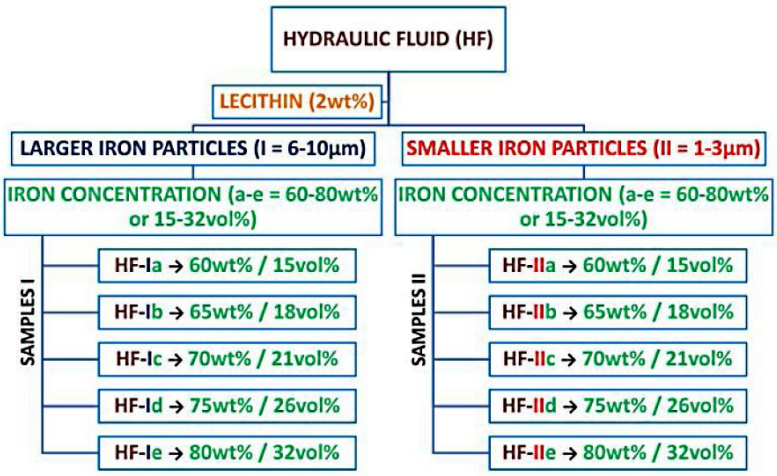

Figure 2.1. Fluid sample preparation and notation

Figure 2.2. Paar Physica MCR 300 parallel disk rheometer

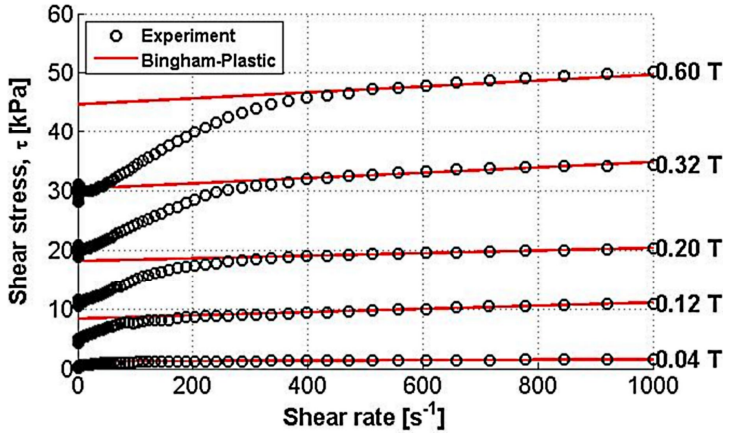

Figure 2.3. Sample flow curves or shear stress versus shear rate for oil-based mr83282-Ie (80 wt% Fe)

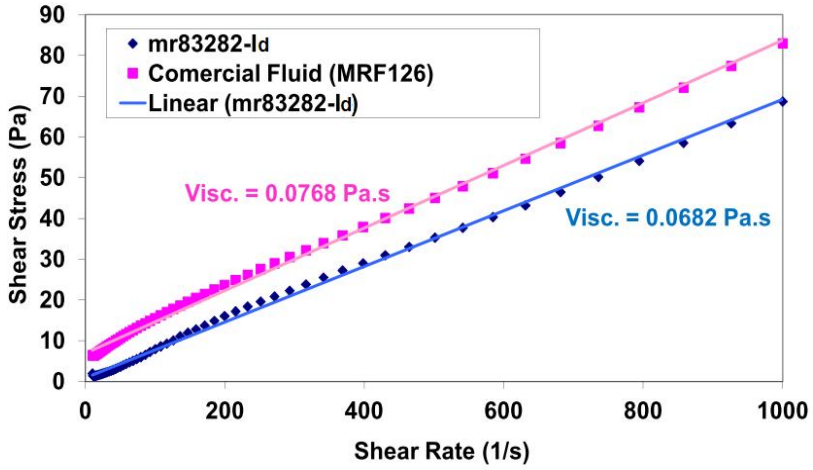

Figure 2.4. Off-state viscosity (Pa s) of mr83282-Id and MRF126CD (both 75 wt% and 26 vol% particle concentration)

MRF: magnetorheological fluid

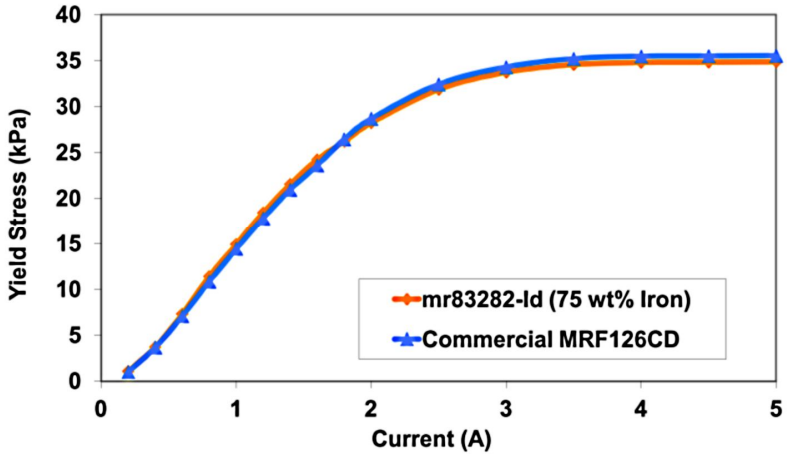

Figure 2.5. Yield stress (kPa) as a function of applied current (A)

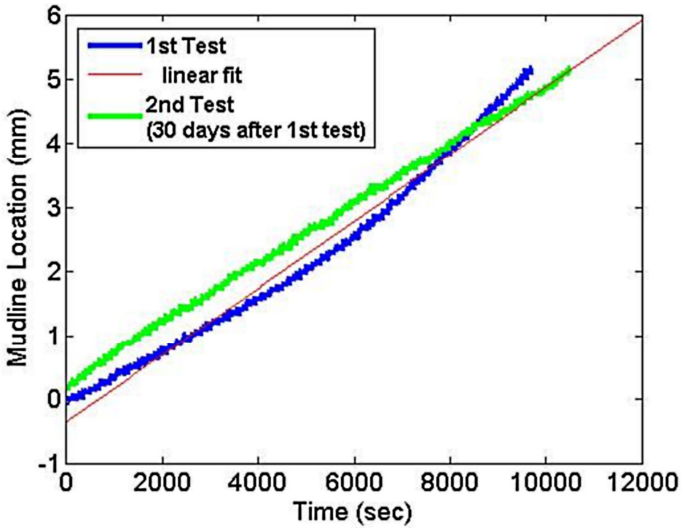

Figure 2.6. Settling rates of mr83282-Ie (containing 6-10 m particles at 80 wt% concentration). Testing was performed one month apart.

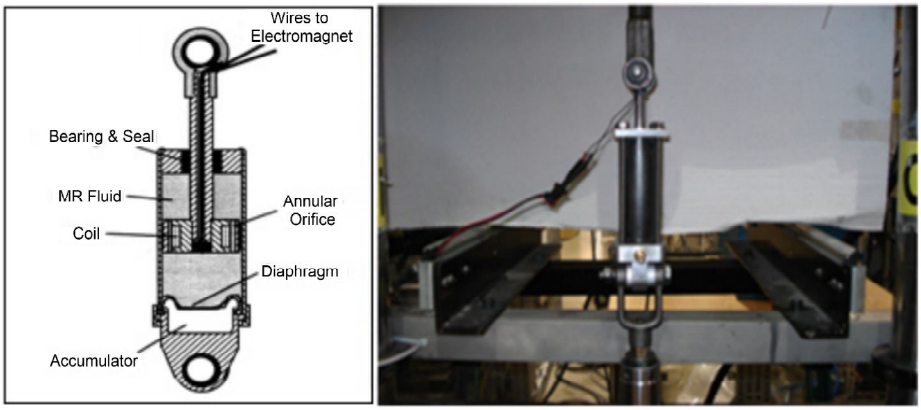

Figure 2.7. Cross section and setup of MR damper on 810 MTS servo-hydraulic testing machine

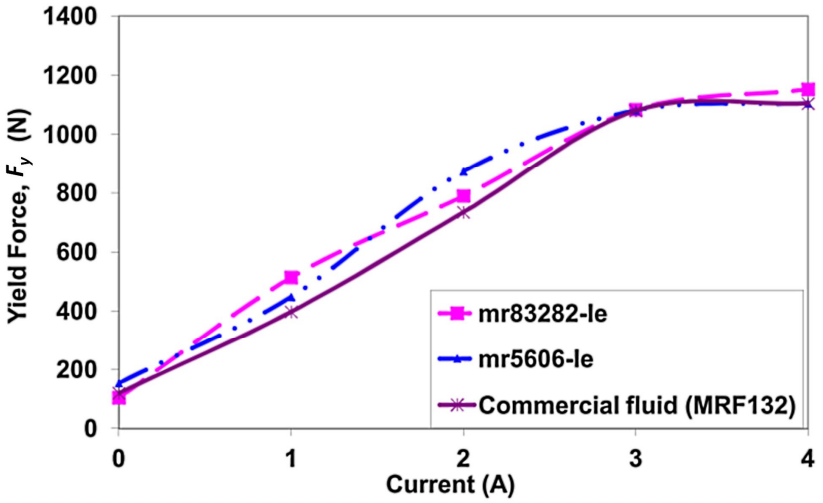

Figure 2.8. Yield force (N) versus current (A) for synthetic oil-based (mr83282-Ie) and mineral oil-based (mr5606-Ie) MRFs and commercial MRF (Lord MRF132) at 5 Hz

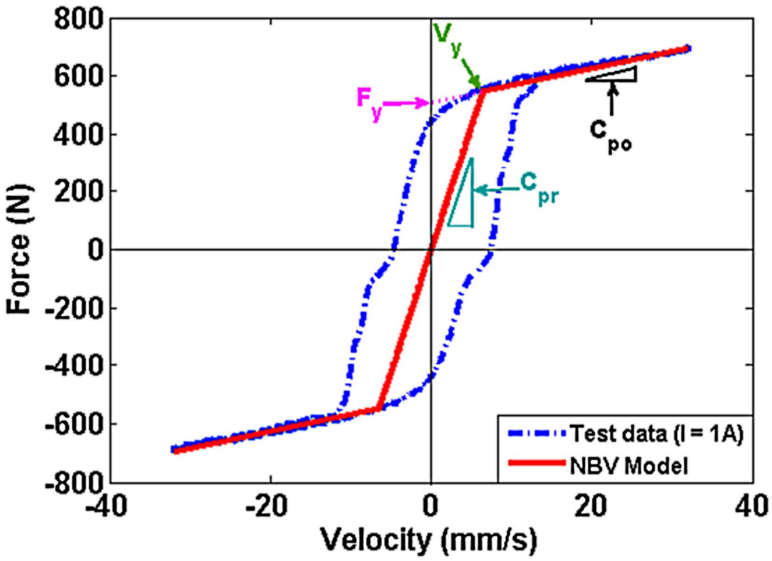

Figure 2.9. Force versus velocity with Nonlinear BiViscous (NBV) model of mr83282-Ie (containing 6-10 m particles at 80 wt% concentration)

Figure 2.10. Drop test carriage at the University of Maryland College Park

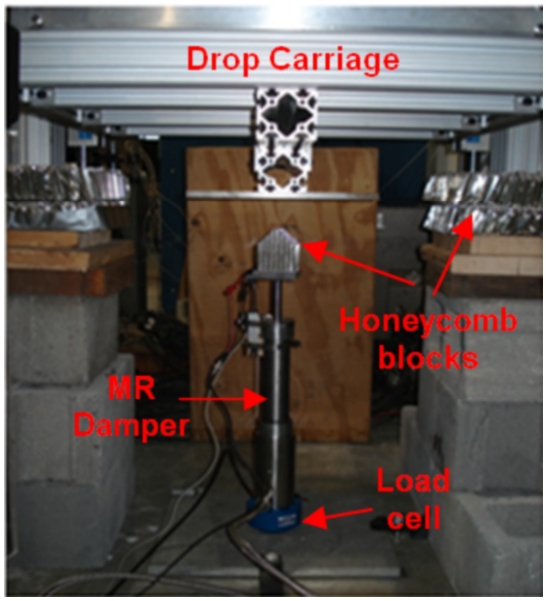

Figure 2.11. MREA drop testing setup at the University of Maryland

MREA: magnetorheological energy absorber

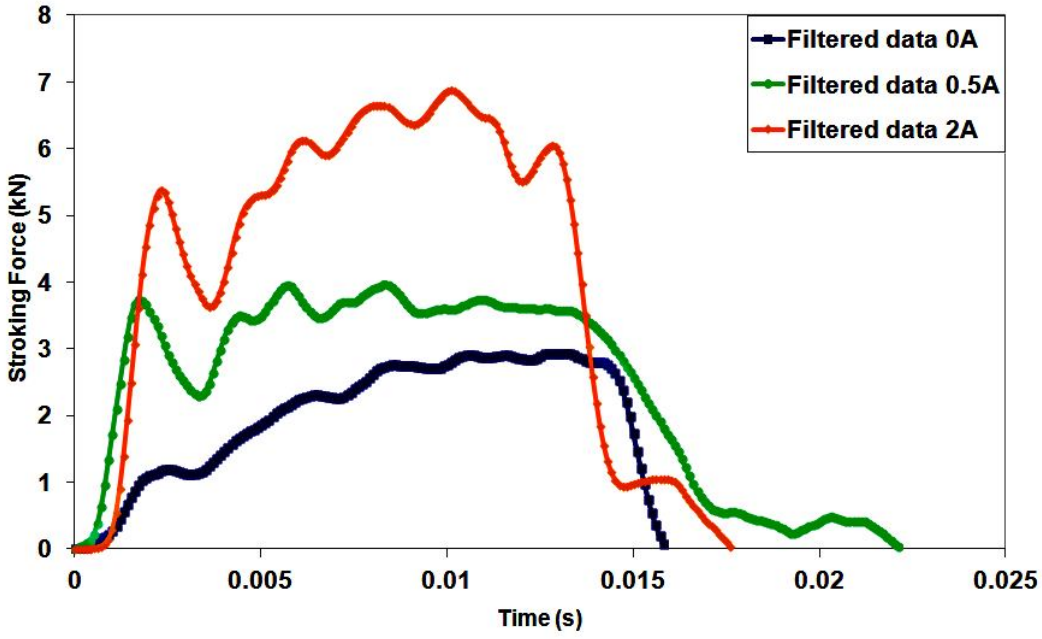

Figure 2.12. Stroking load time history for three different applied field strengths for an impact velocity of 2.8 m/s

Table 2.1. Peak stroking load (N) for applied current and impact velocity

Velocity (m/s)	**Current (Amperes)**		
	0	0.5	2
1.1	950	1360	3770
2.8	2940	3960	6880
4.1	7530	9080	10100

CHAPTER 3: Magnetorheological Fluids Employing Passive Particles

3.1 Introduction and Overview

Magnetorheological fluids (MRF) (Rabinow, 1951; Carlson and Jolly 2000), magnetorheological (MR) foams (Carlson and Jolly, 2000), and MR elastomers (Carlson and Jolly, 2000; Padalka *et al.*, 2010; Eem *et al.*, 2011; Shunta *et al.*, 2012) are used in an increasing range of applications such as semi-active vibration and shock isolation systems. Carbonyl iron (CI) powder has been the primary ferromagnetic dispersant used to prepare MRFs because such powders enable high yield stress. Unfortunately, particles in such MRFs do settle, and in the absence of remixing, the particles descend to the bottom of the container. A MRF is desired that essentially does not settle, but instead provides the full MR effect the first time it is used even in the absence of remixing. Methods have been proposed to reduce settling, such as chemical modification of CI particles (Park *et al.*, 2009; Jiang *et al.*, 2009), or substitution of micro-scale magnetic particles for nano-scale particles (Wereley *et al.*, 2006; Ngatu and Wereley, 2007; Patel, 2011). Although substitution of nonmagnetic particles for magnetic CI particles in MRFs has been investigated for shear mode magneto-rheometers (Klingenberg and Ulicny, 2011; Ulicny *et al.*, 2010), such a study is lacking in the context of MR dampers or flow mode devices.

Two MRF samples having 40 volume percent (vol%) of particles were synthesized: MRF-40 and MRF-37. MRF-40 had 40 vol% of CI particles, and MRF-37 contained 35.7 vol% of CI particles and 4.3 vol% of glass beads. A comparative study of MRF characteristics was conducted to determine the impact of the nonmagnetic glass beads on yield stress, as well as viscosity, and settling rate. Both MRFs were characterized as follows: 1) magnetorheology as a

function of magnetic field, 2) sedimentation rate in a fluid column measured using an inductance-based sensor, and 3) cycling of a small-scale damper undergoing sinusoidal excitations at frequencies of 1 Hz for characterization and 4 Hz for endurance tests. Optical micrographs of the glass beads were taken before and after damper cycling to assess durability.

Our goal is to determine the impact of replacing a small volume percent (vol%) of CI magnetic particles with the same vol% of nonmagnetic glass beads on MRF (yield stress and sedimentation rate) and MR damper (yield force and post-yield damping) performance.

3.2 Characterization of MRF

3.2.1 Magnetorheology

3.2.1.1 Setup and Instrumentation

Magnetizable particles used in this study were carbonyl iron (CI) particles, nominally 2 and 8 micron average diameter, in a 50-50 bidisperse mixture (BASF Corp.). Non-magnetizable particles were 11 micron average diameter hollow non-porous fused borosilicate microspheres (Potters Sphericel 110P8, hollow spheres). Carrier fluid was a hydrogenated poly-alpha-olefin (PAO) carrier fluid, SHF 21 (Exxon-Mobil). The first fluid, MRF-40, had a density of 3.53 g/cm, a CI concentration of 40 vol%, and no glass beads. The second fluid, MRF-37, had a density of 3.26 g/cm, a CI concentration of 35.7 vol%, and a glass bead concentration of 4.3 vol%. A standard additive package of lithium-12-hydroxystearate and ZBPD was also used in both fluids.

The off-state viscosity and yield stress of both MRF samples were determined using the same Paar Physica MCR 300 parallel disk rheometer mentioned in chapter 2, section 2.2.1. In the absence of magnetic field, a test was run to measure off-state viscosity. A volume of 0.15 ml MRF sample was placed in the rheometer test section, which had a 0.5 mm gap separating the rotating disk from the platen. When current was applied, the magnetic field lines were oriented

normal to the parallel disks. The flow curves (shear stress vs. shear rate) were then measured. To measure flow curves in the presence of magnetic field, a volume of 0.3 ml MRF sample was placed between the platen and rotating disk separated by a 1 mm gap. The current was increased from 0.2 A to 4 A during sequential tests.

Flow curves were characterized using the Bingham Plastic (BP) model (Ngatu and Wereley, 2007) described in chapter 2, section 2.3.1.3.

3.2.1.2 Results and Discussion

The flow curves are shown in Figure 3.1. The BP model was used to characterize the flow curves for the viscosity and yield stress of both fluids. It allowed for a better visualization of the MR effect on the MRF shear stress as the current (i.e., magnetic field) increased.

From Figure 3.2, the MRF-37 (with glass beads) had a 22% higher off-state viscosity, and from Figure 3.3, both fluids exhibited a variation in maximum yield stress of only 10%.

Using a similar parallel disk rheometer (Anton-Paar MCR 501), measurement uncertainty was estimated to be ±1-5 kPa (5-13%) in the measured on-state yield stress over the range of approximately 0-1.1 Tesla. This is based on repeat measurements of MRFs with iron (Fe) solids loading of 20, 30 and 45 vol%.

3.2.2 Sedimentation Testing

3.2.2.1 Setup and Instrumentation

Sedimentation tests were performed in order to measure settling rates. Sedimentation tests were conducted with an inductance-based sensing coil fabricated in-house (Ngatu and Wereley, 2007), a GW INSTEK LCR-816 inductance meter, and a height gauge to mount and gradually move the sensor (Figure 3.4).

A uniformly dispersed (well-mixed) MRF was placed in a vertical column (1/4-inch test tube). As settling progressed, there was a distinct boundary, or mudline, between the clarified carrier fluid above and the MRF below. The permeability of a volume of fluid in the test tube was measured using the sensing coil, and data were logged via computer. As the mudline traveled downwards through the sensing coil, the permeability of the fluid volume contained therein decreased. A mudline position curve (Figure 3.5) was first constructed for both MRFs (MRF-37 and MRF-40). Inductance was measured by manually shifting the sensing coil upward at fixed increments. The MRF was initially fully enclosed in the sensor. Then the sensor was moved to a final position, which was above the mudline location, hence enclosing no fluid. The mudline position curve exhibited a linear region between inductance and mudline location. The sedimentation velocity or settling rate was determined by continuously calculating the inductance as the MR fluid settled. As the mudline traveled down through the sensor in the tubular column, reducing the volume fraction of the CI particles in the fluid, the experimental data was generated. The slope of the mudline descent versus time yielded the sedimentation rate (Ngatu and Wereley, 2007).

3.2.2.2 Results and Discussion

The settling rates of both MRFs were measured with the inductance-based sensor. Impedance data were measured as the mudline descended a distance of 6.35 mm in a column filled with a well-mixed MRF sample. The impedance meter measured the inductance of the MRF inside the fluid column and enclosed within a coil sensor. The mudline descents of the MRF-40 and MRF-37 samples are compared in Figure 3.6. This testing method was previously used for other studies in chapter 2 section 2.3.2 and in reference (Ngatu and Wereley, 2007) as well, in which procedures and error measurements were discussed in detail. The error in the

mudline descent measurement was estimated to be 6.35 mm ±0.05 mm based on noise statistics. The sedimentation rate was taken as the rate of change of the mudline descent. The sedimentation rate of the MRF-37 sample (with glass beads) had a slightly lower sedimentation rate (0.041μm/s) than the MRF-40 sample (0.043 μm/s) with no glass beads, as expected, due to its lower specific gravity. However, this effect was not substantial.

3.2.3 Low Speed Dynamic Testing of an MR Damper

3.2.3.1 Setup and Instrumentation

The yield force and post-yield damping of MR dampers, filled with either MRF-40 or MRF-37, were determined by analyzing the behavior of a modified Rheonetic SD-1000-2 MR damper from Lord Corporation, which was tested for characterization under sinusoidal loading at a frequency of 1 Hz. The MR damper and test setup on a servo-hydraulic testing machine (MTS-810) are depicted in Figure 2.7 of chapter 2. Forces versus displacement data were analyzed using the Nonlinear BiViscous (NBV) model (Stanway *et al.*, 1996).

3.2.3.2 Test Inputs

The frequency of excitations was chosen to be 1.0 Hz for characterization. The damper excitation amplitude was 5.08 mm. In order to apply a magnetic field inside the damper, electric current from a DC power supply (from 0 to 3 A with 1 A increment) was used to power the magnetic circuit.

3.2.3.3 Results and Discussion

The MRF-40 and MRF-37 (with glass beads) samples were studied using a linear stroke MR damper (Snyder *et al.*, 2001). Data shown in Figures 3.7 and 3.8 are the force versus displacement and the force versus velocity curves varying from 0 to 3 A, reconstructed using the

NBV model, respectively. The NBV model was employed to represent force versus velocity damper response, and provided a means to estimate yield force (F_y) and post-yield damping (C_{po}).

3.2.4 Fatigue Testing

3.2.4.1 Instrumentation and Test Inputs

The yield force of the MR damper, filled with MRF-37, was determined by analyzing the behavior of the same modified Rheonetic SD-1000-2 MR damper from Lord Corporation, which was tested under sinusoidal loading at a frequency of 4 Hz for an endurance test conducted, and the damper excitation amplitude was also 5.08 mm.

Testing was done with no electric current hence no magnetic field in the electromagnet. Forces versus displacement data were analyzed using the Nonlinear BiViscous (NBV) model.

3.2.4.2 Results and Discussion

An endurance test was carried out where the MR damper was cycled at 4 Hz for a total of 518,400 cycles. The yield force was characterized by fitting the NBV model to the force versus velocity data taken at 1 Hz during a number of breaks in the endurance tests indicated by the symbols in Figure 3.9. For 518,400 cycles, the peak value of the yield force followed similar trends for each current value, that is, the force decreased markedly until nominally 250,000 cycles at 4 Hz had been completed, and leveled off to remain relatively constant (Figure 3.9). The constant yield force levels (dashed lines) correspond to the single point baseline yield force measured for MRF-40 and extended across the plot for comparison only. Based on the experimental results, the glass beads do not seem to contribute toward shear thickening. In

Figure 3.10, the post-yield damping decreased then remained constant as the number of cycles increased.

The ratio of maximum to minimum yield force at a particular current value is plotted as a function of number of cycles (Figure 3.11). It was observed that adding glass beads to the MRF increased the yield force by multiplicative factors ranging from 2 to 3.2 for current values between 1 to 3 A. These results show experimentally that the glass beads increased the yield force of the MR damper, thereby enhancing magnetorheology (Klingenberg and Ulicny, 2011; Ulicny *et al.*, 2010).

3.2.4.3 Nonmagnetic Particles Mechanical Separation

The glass beads were mechanically separated from the MRF using a solvent. In this study, acetone was added to a small volume of MRF (10 ml) in a beaker and stirred for about 10 minutes. The CI particles settled at the bottom of the container, and the clear solution of acetone and carrier oil was transferred to a different beaker, which was heated to the acetone boiling point of 56 degrees Celsius. The carrier oil, which floated atop the surface of the solution was then separated using a spoon, and the resultant solution of acetone was left to boil until complete evaporation and a white residue became clearly visible. This residue was placed on a thin slide and examined under an optical microscope with a magnification of x25.

3.2.4.4 Nonmagnetic Particles Investigation: Pre-Cycle and Post-Cycle

The durability of the glass beads during the endurance test was examined before and after 518,400 sinusoidal loading cycles at 4 Hz using an optical microscope with a magnification of x25. Photomicrographs of the glass beads, both before and after the endurance test are shown in Figure 3.12 (a) and (b), respectively. The glass beads were mechanically separated from the MRF using a solvent, pre-and-post cycling of the MR damper. Before cycling, the micrometer-

scale glass beads were spherical and undamaged. After the endurance test, the glass spheres were completely crushed and no longer visible in the MRF, in Figure 3.12 (b). Therefore, damper cycling caused the glass beads to break into ultra-fine pieces, which did not contribute to an increase in MRF off-state viscosity.

3.3 Conclusions

The behavior of two MRF compositions was investigated. The first fluid, MRF-37, had 35.7 vol% of iron powder, 4.3 vol% glass beads, and 60 vol% carrier fluid. The second fluid, MRF-40, had 40 vol% of iron powder, and 60 vol% carrier fluid. Based on this study, the following conclusions are made:

1. MRF-37 (with glass beads) presented a substantial enhancement (increase) in yield force in the as-mixed fluid damper cycling tests. The yield force more than doubled in the damper tests at high field strengths (here 2 to 3 A in the electro-magnet) suggesting that nonmagnetic fillers can substantially increase damper yield force.

2. MRF-37 (with glass beads) had an off-state viscosity 22% greater than the MRF-40 (no glass beads).

3. After subjecting MRF-37 to endurance testing (i.e., 518,400 cycles of sinusoidal loading at 4 Hz), the yield force enhancement effect was eliminated because the glass beads were eroded or crushed to very small sizes. This further supports the conclusion that the glass beads are the strong contributing factor to the damper yield force enhancement.

MRF-37 would provide a lower specific gravity fluid with a much higher damper yield force at full field, thereby providing performance improvements for applications where the MR device is intended for single or infrequent use. For cases where extensive cycling would be required, a more durable filler that is not subject to erosion, as glass beads are, would be more

appropriate. Further study (Klingenberg and Ulicny, 2011) is needed to better describe the underlying physics contributing to the yield force enhancement in the MR damper when using MRF with glass beads.

References

Carlson, J.D., and Jolly, M.R., (2000) MR fluid, foam and elastomer devices. *Mechatronics*, 10 (4-5): 555-569. DOI: 10.1016/S0957-4158(99)00064-1.

Eem, S.H., Jung, H.J., and Koo, J.H., (2011) Application of MR elastomers for improving seismic protection of base-isolated structures. *IEEE Transactions on Magnetics*, 46(6): 2901–2904. DOI: 10.1109/TMAG.2011.2156771.

Jiang, W., Cao, Z., Gu, R., Ye, X., Jiang, C., and Gong, X., (2009) A simple route to synthesize $ZnFe_2O_4$ hollow spheres and their magnetorheological characteristics. *Smart Materials and Structures*, 18(12): 125013-1-4. DOI: 10.1088/0964-1726/18/12/125013.

Klingenberg, D.J., and Ulicny, J.C., (2011) Enhancing magnetorheology. *International Journal of Modern Physics B*, 25(7): 911-917. DOI: 10.1142/S021797921105847X.

Ngatu, G.T., and Wereley, N.M., (2007) Viscometric and sedimentation characterization of bidisperse magnetorheological fluids. *IEEE Transactions on Magnetics*, 43(6): 2474–2476. DOI: 10.1109/TMAG.2007.893867.

Padalka, O., Song, H.J., Wereley, N.M., Filer II, J.A., and Bell, R.C., (2010) Stiffness and damping in Fe, Co, and Ni nanowire-based magnetorheological elastomeric composites. *IEEE Transactions on Magnetics*, 46(6): 2275-2277. DOI: 10.1109/TMAG.2010.2044759.

Park, B.J., Song, K.H., and Choi, H.J., (2009) Magnetic carbonyl iron nanoparticle based magnetorheological suspension and its characteristics. *Materials Letters*, 63(15): 1350-1352. DOI: 10.1016/j.matlet.2009.03.013.

Patel, R., (2011) Mechanism of chain formation in nanofluid based MR fluids. *Journal of Magnetism and Magnetic Materials*, 323(10): 1360–1363. DOI: 10.1016/j.jmmm.2010.11.046.

Rabinow, J., (1951) Magnetic fluid torque and force transmitting device. U.S. Patent 2575360.

Shunta, K., Fumikazu, M., and Katsuhiro, H., (2012) Novel soft actuator using magnetorheological elastomer. *IEEE Transactions on Magnetics*, 48(4): 1649-1652. DOI: 10.1109/TMAG.2011. 2173669.

Snyder, R.A., Kamath, G.M., and Wereley, N.M., (2001) Characterization and analysis of magnetorheological damper behavior under sinusoidal loading. *AIAA Journal*, 39(7): 1241-1253. DOI: 10.1117/12.384563.

Stanway, R., Sproston, J.L., and El-Wahed, A.K., (1996) Application of electrorheological fluids in vibration control: a survey. *Smart Materials and Structures*, 5(4): 464–482. DOI: 10.1088/094-1726/5/4/011.

Ulicny, J.C., Snavely, K.S., Golden, M.A., Klingenberg, D.J., (2010) Enhancing magnetorheology with nonmagnetizable particles. *Applied Physics Letters*, 96: 231903-1-3. DOI: 10.1063/1.3431608.

Wereley, N.M., Chaudhuri, A., Yoo, J.H., John, S., Kotha, S., Suggs, A., Radhakrishnan, R., Love, B.J., and Sudarshan, T.S., (2006) Bidisperse magnetorheological fluids using Fe particles at nanometer and micron scale. *Journal of Intelligent Material Systems and Structures*, 17(5): 393-401. DOI: 10.1177/1045389X06056953.

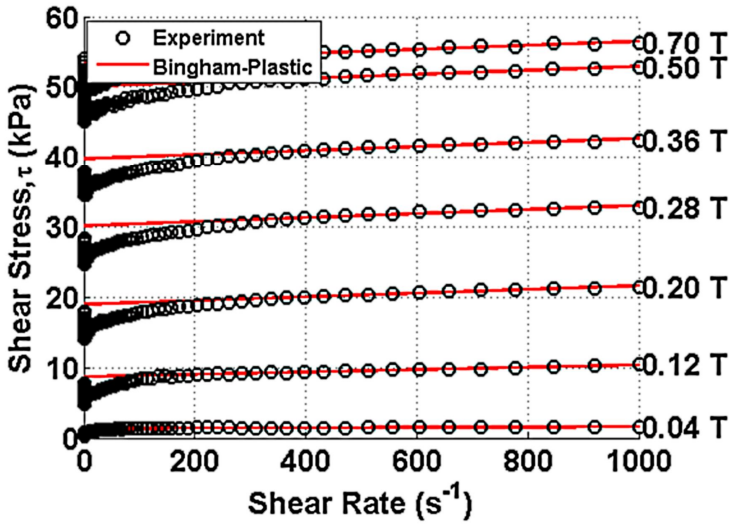

Figure 3.1. Flow curves, or shear stress vs. shear rate, measured using a parallel disk magneto-rheometer

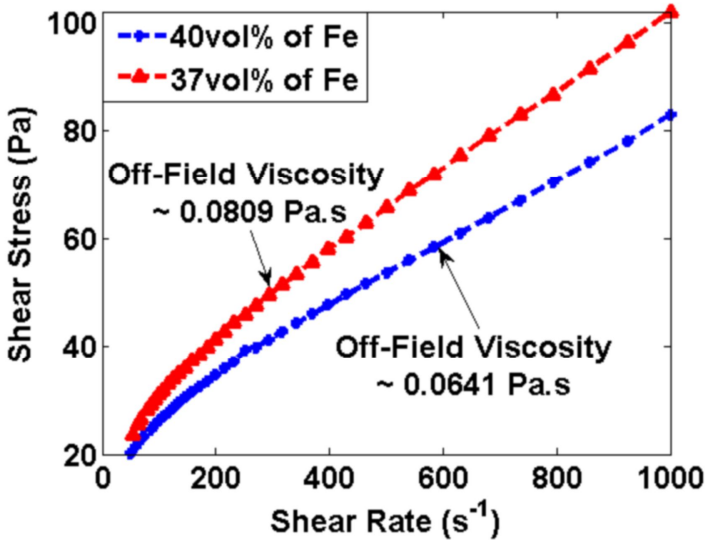

Figure 3.2. Magnetorheology: off-state viscosity

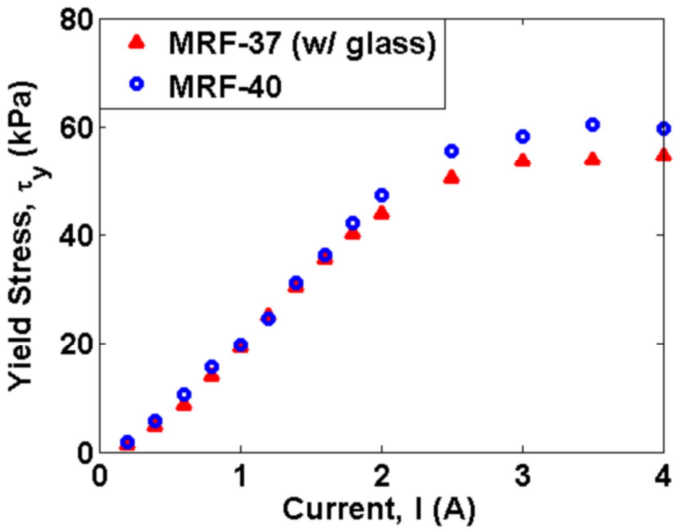

Figure 3.3. Magnetorheology: yield stress as a function of current

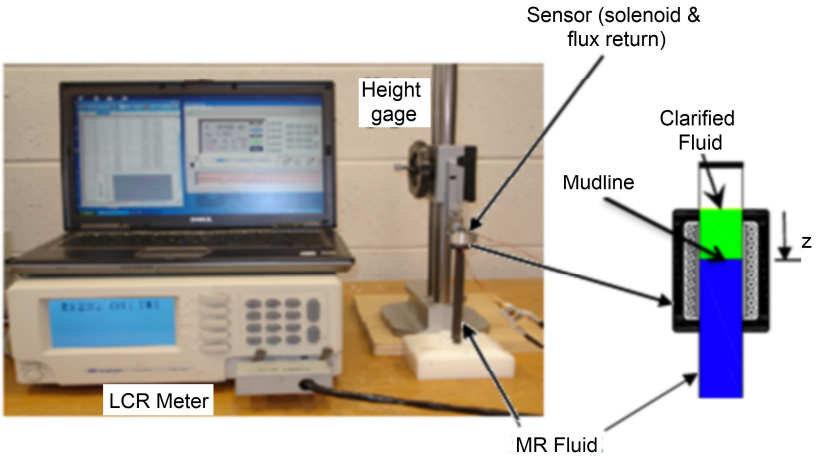

Figure 3.4. Sedimentation rate measured using a column of MRF and an inductance sensor interrogated using an inductance meter

MRF: Magnetorheological fluid

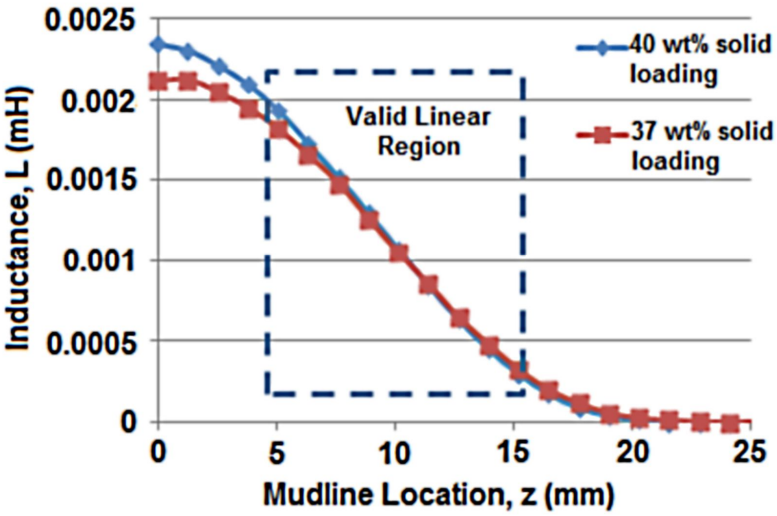

Figure 3.5. Inductance as a function of mudline location within the sensor

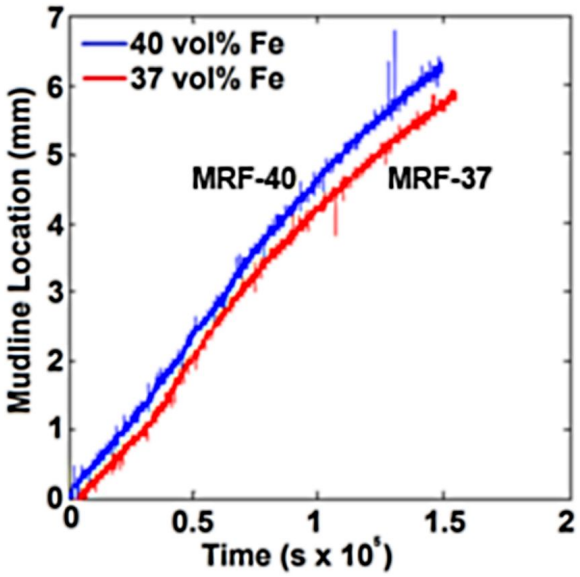

Figure 3.6. Mudline descent versus time for MRF-40 and MRF-37 (with glass beads)

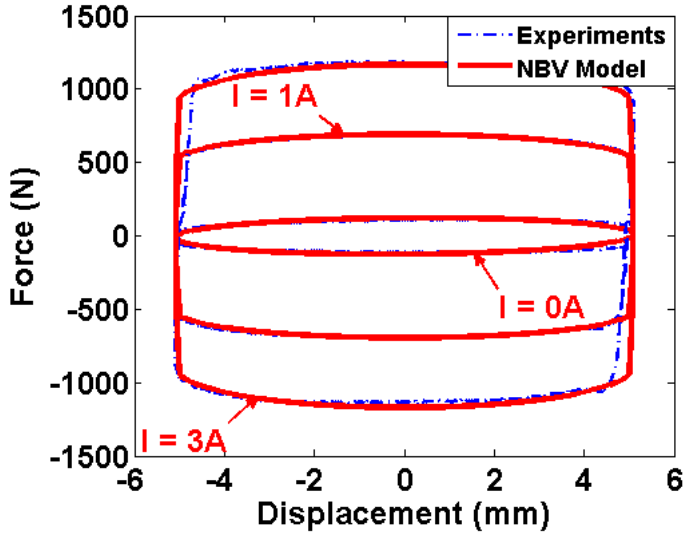

Figure 3.7. Cyclic damper data compared with NBV model for MRF-37: force vs. displacement

NBV: Nonlinear BiViscous

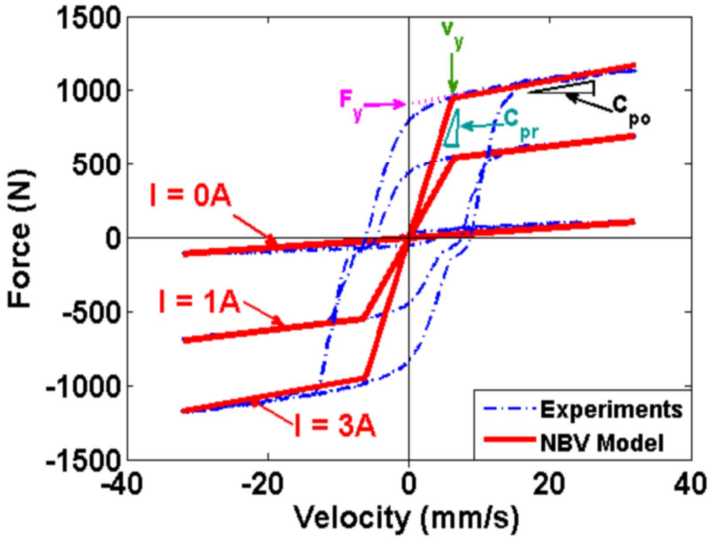

Figure 3.8. Cyclic damper data compared with NBV model for MRF-37: force vs. velocity

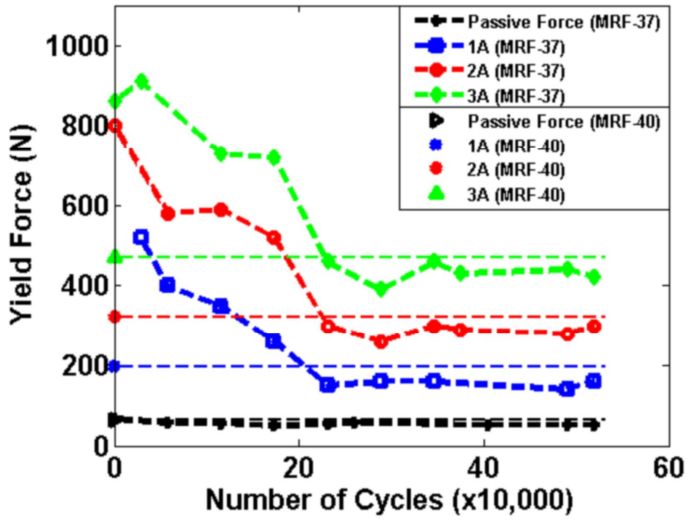

Figure 3.9. MR damper yield force as a function of number of cycles

MR: Magnetorheological

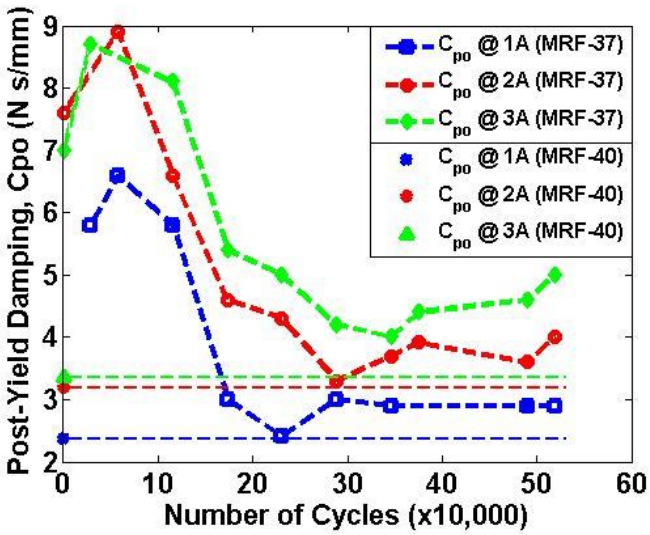

Figure 3.10. MR damper post-yield damping as a function of number of cycles

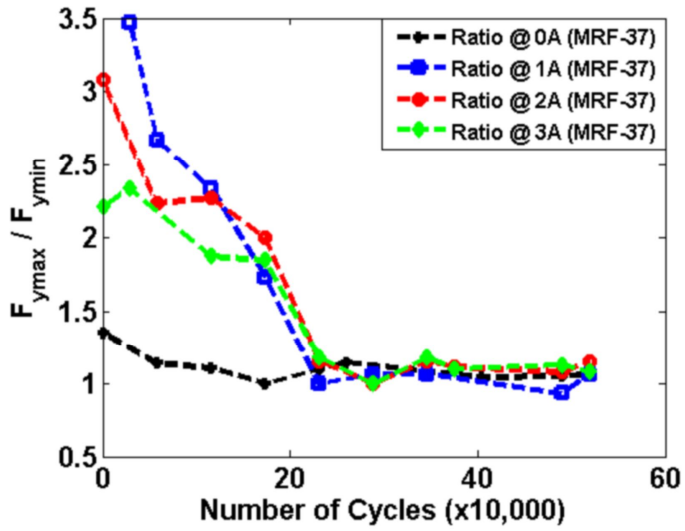

Figure 3.11. Ratio of maximum to minimum yield force vs. number of cycles

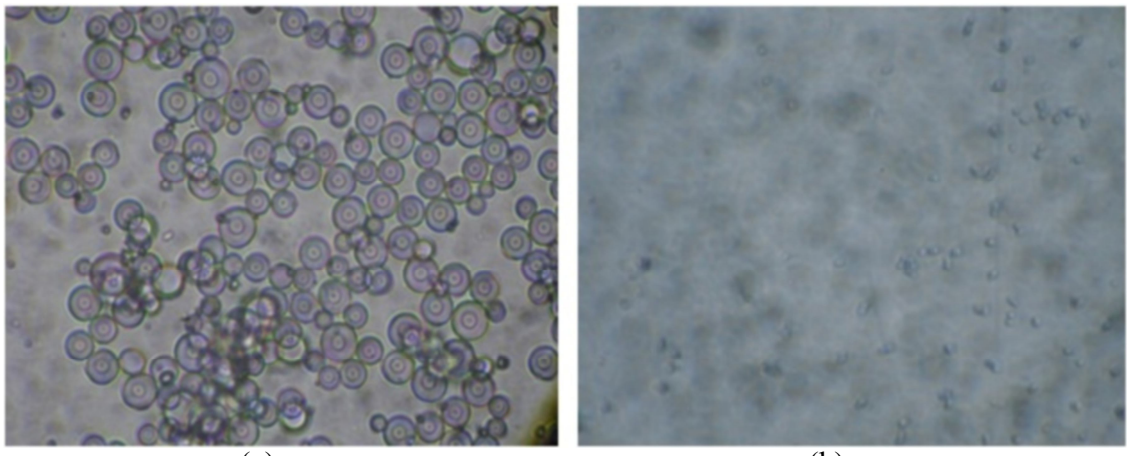

(a) (b)

Figure 3.12. Optical micrographs of glass beads: (a) Glass beads prior to cycling magnified 25x (b) Glass beads post-cycling magnified 25x

CHAPTER 4: Adaptive Magnetorheological Landing Gear Damper Using Passive Valves to Maximize Sink Rate Range

4.1 Introduction and Overview

Adaptive landing gear dampers that can continuously adjust their stroking load in response to various operating conditions are investigated to improve the landing performance of a lightweight helicopter. In our prior work, adaptive magnetorheological (MR) landing gear dampers for a lightweight helicopter that maintained a constant peak stroking force of 4000 lb_f across sink rates ranging from 6-12 ft/s were designed, fabricated and successfully tested. This represented a 300% increase in the energy attenuation requirement over the entire sink rate range when compared to the performance of the current passive hydraulic landing gear dampers utilized in the MD-500 helicopter (Choi *et al.*, 2012). In this follow-on effort, it was desired to expand the high end of the sink rate range further, so that the peak stroking load could be held constant for sink rates ranging from 6-26 ft/s, thereby extending the high end of the speed range from 12 ft/s in the first study to 26 ft/s, while preserving low speed force levels. To achieve this increase in the high end of the sink rate range, the U.S. Army Aviation Development Directorate - Aviation Applied Technology Directorate (AATD), Boeing, and the University of Maryland jointly developed an adaptive MR landing gear damper that can continuously adjust its stroking load during hard landing and crash impact events to protect the occupants and minimize aircraft damage. This adaptive landing gear damper is part of a comprehensive Active Crash Protection System (ACPS) being developed by Boeing and AATD. The ACPS under development can predict an impending hard landing or a crash event as well as activate and control a crashworthy subsystems such as adaptive landing gears, active seats and restraint systems, and external

airbags to maximize the crash survivability of the aircraft and occupants. The adaptive landing gear damper developed in this study operates with a spring-based passive (or relief) valve. The MR valve was designed to semi-actively control the peak stroking load over the 6-12 ft/s sink rate range, whereas the relief valve was designed to passively control the stroking load over the 12-26 ft/s sink rate range.

A main goal of an adaptive landing gear system is to adapt the load stroke profile in response to payload and sink rate variations of a helicopter. Consequently, the objective of this current effort in this chapter is to maintain a constant stroking load of 4000 lb_f over an extended equivalent sink rate range (6-26 ft/s) while considering the same challenges encountered in prior work, such as controlling of the load stroke profile for short duration event (50-200 ms), keeping adaptive landing system compact and lightweight, and adjusting the load with control algorithms based on real time measurements of sink rate and crash harshness (Choi *et al.*, 2012). The motivation behind this current work stems from different aspects of adaptive MR landing gear systems and applications that have been investigated by several research groups (Choi *et al.*, 2012; Choi and Wereley, 2003; Mikulowski and Holnicki-Szulc, 2007; Batterbee *et al.*, 2007a; Batterbee *et al.*, 2007b; Lin *et al.*, 2009; Mikulowski and LeLetty, 2008) and discussed in chapter 1.

The MR valve of the proposed landing gear system was designed using a nonlinear analytical damper model considering the field dependent Bingham-plastic behavior of MR fluids and nonlinear viscous loss factors that are dependent on velocity squared. The passive valve was designed based on a computer simulation related to spring dynamic equations of motion, which estimated the force behavior of the passive valve of the MR landing gear damper to meet the

desired stroking load of 4000 lb_f over the desired sink rates of 12-26 ft/s. Using the MR damper analysis, a spring-based passive valve MR landing gear damper was designed and constructed.

A nonlinear analysis based on the pressure drop across the MR valve and the passive relief valve center orifice was performed to estimate the center orifice diameter. Two different springs were designed and used (a conventional coil spring and a spiral wave spring) for the analysis. In addition, an electromagnetic analysis of the MR valve in the landing gear damper was conducted to predict the magnetic field strength in the MR gap. Two spring-assisted passive relief valves were constructed, and an experimental study using an MTS machine was conducted to evaluate the damper force behavior of the spiral wave and coil spring-based MR landing gear dampers to verify that the relief valve operated properly.

4.2 Summary of the Design Targets

Passive hydraulic landing gear dampers, currently used on the MD-500 helicopter fixed landing gear systems, are single-staged and cannot reach the low and high-speed design targets while maintaining a constant stroking force of 4000 lb_f over a wide equivalent sink rate range. The equivalent sink rate is determined by a multiplicative factor of 2.7, which is used to emulate the kinematic relationship between the skid of the helicopter and the location of the installed MR landing gear damper. In prior work related to this study, the equivalent sink rate range was 6-12 ft/s, and the existing MD-500 helicopter passive hydraulic forward and aft dampers were not capable of maintaining a constant stroking load over these particular speeds targeted, as shown in Figure 4.1 (a) and (b). Consequently, a flow-mode type MR landing gear damper (MRLGD) was initially proposed, in prior study, as a retrofit to the existing passive landing gear damper. The MR landing damper was successfully designed, tested, and analyzed, and it was capable of holding constant, a desired stroking load of 4000 lb_f over the desired equivalent sink rate range

of 6-12 ft/s. The initial MRLGD was designed using a Bingham-plastic model (BPM) incorporating minor viscous loss factors (proportional to velocity squared). Figure 4.2 depicts the stroking load or damper force of the MRLGD versus the equivalent sink rate. As seen in this figure, the MRLGD was designed to theoretically meet the desired stroking load of 4000 lb_f at the lowest design equivalent sink rate of 6 ft/s by activating the magnetic circuit of the MR valve and maintaining the stroking load at 4000 lb_f. However, at the high-end equivalent sink rate range of 12 ft/s, the MRLGD met the desired stroking load of 4000 lb_f when the MR valve was turned off (Choi *et al.*, 2012).

The new unconventional MR landing gear damper with a spring-assisted passive valve, discussed in this chapter, intends to maintain a constant stroking load of 4000 lb_f over an extended equivalent sink range of 6-26 ft/s. The desire is to increase the high-end of the sink rate range from 12 ft/s (from prior work) to 26 ft/s, which is a larger increase of the operating sink rate range compared to the passive hydraulic damper and the prior designed conventional MRLGD, as shown in Figure 4.3.

4.3 Modeling of the MR Landing Gear Damper with a Spring-Assisted Passive Valve

4.3.1 Valves Operation: Semi-Active MR Valve and Spring-Assisted Passive Relief Valve

The schematic diagram of the passive (or relief) valve inside the MR landing gear damper used in this study is presented in Figure 4.4. In this figure, the MR valve has one annular single flow path, one center orifice contributing to the spring-assisted relief valve, three layers of magnetic coil windings, a spring, and a seal. The spring in the relief valve is pre-compressed; hence, the seal does not open until the MR valve force develops to a desired stroking load of 4000 lb_f.

The working principle of the MR valve is that, by activating a magnetic field input inside the MR valve, the desired stroking load is produced at an equivalent sink rate of 6 ft/s (Choi *et al.*, 2012). At higher equivalent sink rates of about 12 ft/s, the MR valve is turned off and works as a passive valve to maintain the desired stroking load. At this point, the spring compresses, and the seal is open for the center orifice to work as an additional fluid path such as a bypass valve. As a result, the damper force decreases because the MR fluid pressure in the center orifice drops.

4.3.2 Passive Relief Valve Orifice Diameter Range Optimized

The diameter of the center orifice of the passive relief valve inside the MR landing gear damper is a very important parameter in the design of the system. The diameter size depends on the pressure drop across the annular gap and the center orifice flow passage, with magnetic field strength turned off in the MR valve. Equations 4.1 and 4.2 are representative of the pressure drops across the MR valve and the passive valve center orifice, respectively.

$$\Delta P_{\eta_1} = f_1 \frac{\rho L_1 V_{d_1}^2}{4 d_1} + \frac{\rho \sum K_1 V_{d_1}^2}{2} \qquad [4.1]$$

$$\Delta P_{\eta_2} = f_{or} \frac{\rho L_o V_{d_o}^2}{4 d_o} + \frac{\rho \sum K_{tot.or} V_{d_o}^2}{2} \qquad [4.2]$$

Here, ρ is the MR fluid density, L_1 and L_o are the MR annular gap and center orifice passage lengths, respectively. V_{d_1} and V_{d_o} are the fluid velocities in the annular gap and center orifice passages, and K_1 and $K_{tot.or}$ are the minor loss coefficients. Also, f_1 and f_{or} are the Darcy friction factors, which are piecewise continuous and Reynolds number dependent (White, 1986; Franzini and Finnemore, 1997). In this case, the Darcy friction factors f_1 and f_{or} were assumed to be the same based on the assumption that the Reynolds number at high speed was fixed at ~ 5000; hence, the flow was turbulent (Reynolds number, Re ~ 5000, which has to be greater than 4000 for turbulent flow). The Darcy friction factor is defined in Equation 4.3 as:

$$\frac{1}{f^{1/2}} = -1.8\log_{10}\left[\left\{\frac{\varepsilon/(2d_1)}{3.7}\right\}^{1.11} + \frac{6.9}{Re}\right] \quad [4.3]$$

where d_1 is the diameter of the MR valve gap.

When the spring-assisted relief valve is open, the seal through the center orifice is displaced, and the MR fluid passes through the MR valve as well as the center orifice relief valve; hence, Equation 4.4 applies. The flow velocity, V_{d_1} in the MR valve annular gap can be defined in terms of the flow velocity V_{d_o} in the center orifice, as shown in Equation 4.5:

$$\Delta P_{\eta_1} = \Delta P_{\eta_2} \quad [4.4]$$

$$V_{d_1} = V_{d_o}\sqrt{\frac{f\rho\frac{L_o}{4d_o} + \frac{\rho\sum K_{tot.or}}{2}}{f\rho\frac{L_1}{4d_1} + \frac{\rho\sum K_1}{2}}} \quad [4.5]$$

Equation 4.5 can be re-written as:

$$V_{d_1} = V_{d_o}\bar{R} \quad [4.6]$$

The total flow rate in term of the flow rates in each flow passage was then calculated and is illustrated in Figure 4.5:

$$Q_{total} = Q_1 + Q_2 \quad [4.7]$$

$$Q_{total} = A_1 V_{d_1} + A_{relief} V_{d_o} \quad [4.8]$$

The total flow rate can also be expressed in terms of effective piston area, A_p, and piston velocity, V_p, as shown in Equation 4.9:

$$Q_{total} = A_p V_p \quad [4.9]$$

Substituting Equation 4.6 into Equation 4.8 and solving for V_{d_o}, in terms of A_p and V_p from Equations 4.9 lead to Equation 4.10:

$$V_{d_o} = \frac{A_p V_p}{A_1 \bar{R} + A_{relief}} \quad [4.10]$$

which can be written as Equation 4.11,

$$V_{d_o} = \frac{A_p V_p}{A_1 \bar{R} + \frac{\pi}{4} d_o^2} \quad [4.11]$$

where $\bar{R}$ is defined as:

$$\bar{R} = \sqrt{\frac{f\rho \frac{L_o}{4d_o} + \frac{\rho \sum K_{tot.or}}{2}}{f\rho \frac{L_1}{4d_1} + \frac{\rho \sum K_1}{2}}} \quad [4.12]$$

Then, substituting Equation 4.11 into Equation 4.6 leads to the following:

$$V_{d_1} = \bar{R} \left(\frac{A_p V_p}{A_1 \bar{R} + \frac{\pi}{4} d_o^2} \right) \quad [4.13]$$

The MR damper force equation is given by:

$$F = \Delta P_{\eta_1} A_p \quad [4.14]$$

Equation 4.1 is then substituted to the MR damper force equation defined in Equation 4.14, and the flow velocity expression for V_{d_1} from Equation 4.13 is substituted as well; all of which lead to the equation below:

$$F = \bar{R} \left(\frac{A_p V_p}{A_1 \bar{R} + \frac{\pi}{4} d_o^2} \right)^2 \left(f_1 \frac{\rho L_1}{4d_1} + \frac{\rho \sum K_1}{2} \right) A_p \quad [4.15]$$

Equation 4.15 is expressed in terms of the passive relief valve center orifice diameter, d_o, and the MR damper force versus the sink rate is illustrated in Figure 4.6 for different passive relief valve center orifice diameters. The maximum achievable center orifice diameter of the passive relief valve is $d_o = 9.398$ mm (or 0.37 inches) and is illustrated in Figure 4.7.

4.3.3 *Electromagnetic Analysis of the MR Valve using ANSYS*

A commercial simulation software (ANSYS) was used to perform an electromagnetic analysis of the MR valve in the landing gear damper. This analysis was carried out to predict the magnetic field strength in the MR gap, while taking into consideration the diameter of the center orifice of the passive relief valve. This analysis was also performed to calculate the MR yield force using Equation 4.16 for the pressure drop across the MR gap due to the MR fluid yield stress effect. In this equation, L_a is the total active length of the MR valve, τ_y is the MRF yield stress, and D_h is the hydraulic diameter ($D_h = 2d_1$, where d_1 is the MR valve gap diameter).

$$\Delta P_{MR} = \frac{4L_a\tau_y}{D_h} \qquad [4.16]$$

The design parameters of the MR valve with the center orifice of the passive relief valve are presented in Table 4.1, and the low speed design target of maintaining a constant damper stroking load of 4000 lb_f at 6 ft/s is satisfied, as presented in Figure 4.8. These results were generated based on the Bingham Plastic modeling (BPM) used in prior work related to this study in reference (Choi *et al.*, 2012).

The MR fluid used for this study was Lord Corporation MRF-132DG with a density of 2.95-3.15 g/cm^3. This particular fluid magnetic saturation is around 49 kPa. The center orifice diameter of the passive relief valve was adjusted to meet the high-end of the sink rate range of the design target, which is to maintain the damper stroking load constant at 4000 lb_f at a sink rate of 26 ft/s. Meanwhile, it is important to note that the center orifice diameter adjustment was done while keeping the maximum attainable yield stress at or higher than 45 kPa, which is as high as the previous study (Choi *et al.*, 2012) and necessary to maintain the low speed design target satisfied. In order to satisfy both (low and high speed) design targets, the center orifice diameter

was selected within the range of 4.8 mm (0.189 inches) to 9.398 mm (0.37 inches), specifically 7.62 mm (0.30 inches) as shown in Figure 4.9.

The electromagnetic analysis of the MR valve in the landing gear damper was conducted to estimate the magnetic field strength inside the MR valve gap and relate it to the yield stress of the MRF used in the damper (Lord Corporation MRF-132CG) to determine whether the MRF yield stress could produce sufficient force to satisfy the low speed design target. Figure 4.10 (a) shows the yield stress of the MRF-132CG versus the magnetic field strength, H, and Figure 4.10 (b) is the estimated magnetic field strength inside the MR valve gap. The estimated maximum attainable magnetic field strength, $H_{max_{att.}}$, within the MR valve gap is 249 kAmp/m. Relating the estimated field strength to the plot (courtesy of Lord Corp.) in Figure 4.10 (a) shows that the maximum attainable yield stress is about 47 kPa, which is sufficient to satisfy the low speed design target. Figure 4.11 (a) and (b) illustrate the estimated magnetic flux lines generated by the magnetic coil windings and the magnetic field strength, H, inside the MR valve gap, respectively. Figure 4.12 (a) and (b) show the magnetic field density, B, inside the MR valve gap.

4.3.4 Analysis of MR Landing Gear Damper with Spring-Assisted Passive Valve

A hydraulic model of the MR and passive valves of the landing gear damper is presented in Figure 4.13. The total damping force, F_t, of the MR damper can be expressed as follows:

$$F_t = A_p \Delta P \qquad [4.17]$$

Here, A_p is the effective piston area of the MR landing gear damper and ΔP is the pressure drop across the valves.

4.3.4.1 Passive Valve Closed

When the seal closes the spring-assisted relief valve of the center orifice, the MR fluid's only path is through the MR valve as shown in Figure 4.13 (a); hence, the following equations apply:

$$\Delta P = \Delta P_{mr} \quad [4.18]$$

$$\Delta P_{relief} = \infty \quad [4.19]$$

$$Q_p = A_p V_p = Q_{mr} \quad [4.20]$$

$$Q_{relief} = 0 \quad [4.21]$$

ΔP_{mr} is the pressure drop through the MR valve, and ΔP_{relief} is the pressure drop through the relief valve. Q_p is the total flow rate passing through the piston, and V_p is the piston velocity. Q_{mr} is the flow rate passing through the MR valve, and Q_{relief} is the flow rate passing through the relief valve. The pressure drop through the MR valve, ΔP_{mr}, is derived from a Bingham-plastic type damper model incorporating minor loss factors, which are proportional to velocity squared, and is given as follows:

$$\Delta P_{mr} = \left[nf \frac{\rho\left(L_{a_1} + L_c\right)}{4d_1} \left(\frac{Q_{mr}}{A_{mr}}\right)^2 + \frac{\rho\left(K_{entry} + K_{exit}\right)}{2} \left(\frac{Q_{mr}}{A_{mr}}\right)^2 \right] + \frac{2nL_{a_1}\tau_y}{d_1} \quad [4.22]$$

Here, ρ is the density of the MR fluid, L_{a_1} is the active MR valve length associated with one magnetic coil winding, and L_c is the length of one magnetic coil winding. A_{mr} is the flow area of the MR valve; n is the number of magnetic coil windings, and d_1 is the gap diameter of the MR valve. K_{entry} and K_{exit} in Equation 4.22, are the minor loss factors in the MR valve associated with sudden entrance and exit effects, respectively. In this study, it was assumed that $K_{entry} = 0.7$ and $K_{exit} = 0.5$ (White, 1986; Idel'chik, 1994; Franzini and Finnemore, 1997; Spurk and Aksel, 2008). The Darcy friction factor, f, is a piecewise continuous function of the Reynolds

number, and detailed equations are given in (Choi *et al.*, 2012). In addition, in Equation 4.22, τ_y is the MR fluid yield stress (Mao *et al.*, 2005; Wereley and Pang, 1998).

4.3.4.2 Passive Valve Open

When the spring-assisted relief valve is open, the seal through the center orifice is displaced, and the MR fluid passes through the MR valve and the center orifice relief valve as shown in Figure 4.13 (b); hence, the following equations apply:

$$\Delta P = \Delta P_{mr} = \Delta P_{relief} \quad [4.23]$$

$$Q_p = Q_{mr} + Q_{relief} \quad [4.24]$$

Here, the pressure drop of the relief valve, ΔP_{relief}, is determined by the pressure drop due to the seal's opening as follows (Choi *et al.*, 2005; Merritt, 1967):

$$\Delta P_{relief} = \frac{\rho Q_{relief}^2}{2\left(A_{open} C_d\right)^2} \quad [4.25]$$

Note that Equation 4.25 is held under the assumption that the diameter of the center orifice is big enough, so that its pressure drop is negligibly smaller than the pressure drop due to the seal's opening. Here, the discharge coefficient, C_d, is given by:

$$C_d = \frac{C_v C_c}{\sqrt{1 - C_c^2 \left(\frac{A_{open}}{A_p}\right)^2}} \quad [4.26]$$

where, C_v is the velocity coefficient (C_v = 1), and C_c is the contraction coefficient (C_c = 0.611) (Merritt, 1967). In addition, A_{open} is the flow area of the opened relief valve orifice, and is calculated using:

$$A_{open} = \pi d_o x \quad [4.27]$$

where d_o is the center orifice diameter and x is the displacement of the seal.

i. Single-Degree-of-Freedom Mass Spring Damper Lumped Model

Using a single DOF mass-spring-damper lumped model shown in Figure 4.13, the displacement of the seal was calculated by numerically solving the following equation

$$M\ddot{x} + c\dot{x} + kx = F_t\left(\frac{A_{relief}}{A_p}\right) - F_{s0} \quad [4.28]$$

where

$$F_{s0} = \left(\frac{A_{relief}}{A_p}\right) 4000\ lb_f \quad [4.29]$$

Here, M is the mass of the seal, and c is the damping of the spring, k is the stiffness of the spring, and A_{relief} is the cross-sectional area of the center orifice.

ii. Calculation of Flow Rates

The flows at each path depend on the pressure drop, and the fluid resistances are nonlinear functions of flow rates. As a result, the flow rates Q_{mr} and Q_{relief} are not straightforwardly determined from the total flow rate, Q_p. Hence, a numerical iteration method (Choi, 2005b) was used to calculate each flow rate. The first step in the process of the iteration method starts by guessing the initial flow rates as follows:

$$Q_{mr}^{-} = \frac{Q_p}{2} \text{ and } Q_{relief}^{-} = \frac{Q_p}{2} \quad [4.30]$$

Using Eq. 4.22 with initial flow rates Q_{mr}^{-} and Q_{relief}^{-}, the new flow rate, Q_{relief}^{+} is computed as follows:

$$Q_{relief}^{+} = \left| A_{open} C_d \sqrt{\frac{2\Delta P_{mr}|_{Q_{mr}=Q_{mr}^{-}}}{\rho}} \right| \quad [4.31]$$

Where $\Delta P_{mr}|_{Q_{mr}=Q_{mr}^{-}}$ is obtained from replacing Q_{mr} with Q_{mr}^{-} in Eq. 4.22. Then, it is necessary to calculate the error of the estimated total flow rate as follows:

$$\left|\left(Q_{relief}^{+} + Q_{mr}^{-}\right) - Q_p\right| \leq \gamma \quad [4.32]$$

Here, γ is the predefined error. If the error of the estimated total flow rate is not smaller than the predefined error, then the new initial flow rate, Q_{mr}^{+}, of the MR valve needs to be increased or decrease by:

$$Q_{mr}^{+} = (1 \pm \delta) Q_{mr}^{-} \quad [4.33]$$

Here, δ is the convergence rate of the estimation to the flow rate.

4.4 Design of MR Landing Gear Dampers with a Spring-Assisted Passive Relief Valve

4.4.1 Design of the Spring-Assisted Passive Relief Valve

Using equations 4.17- 4.33, the damper force of the MR landing gear damper with the spring-based passive valve was estimated to meet the desired stroking load of 4000 lb_f over the desired sink rate range of 6-26 ft/s. Figure 4.14 represents the estimated force of the MR landing gear damper with the spring-assisted passive valve versus sink rate. In this case, a spring stiffness of $k = 50$ lb_f/in was chosen as soft stiffness is necessary for a better relief performance of the passive relief valve. As illustrated in Figure 4.14, the damper force generated by the activation of the MR valve (F_{on}) can theoretically meet the desired stroking load of 4000 lb_f at the low sink rate of 6 ft/s. Then, at higher sink rate, the MR landing gear damper theoretically meets the desired stroking load by turning off (F_{off}) the MR valve and releasing additional MR fluid by cracking the pressure when the center orifice relief valve opens up.

4.4.1.1 Spring Design and Construction of the MR Landing Gear Damper Coupled with the Passive Valve

i. Spring Design

Two different types of springs were custom designed and compared in order to implement the spring stiffness of 50 lb_f/in while taking into account the dimensions and configuration of the MR landing gear damper. One was a crest-to-crest spiral wave spring (Smalley Steel Ring Company, 2011), and the other spring was a conventional coil spring (Mid-West Spring and Stamping, 2011). Table 4.2 highlights each spring properties, and Figure 4.15 illustrates their dissimilarities. The fundamental formula to custom design the spiral wave spring stiffness was as follows:

$$k_{Wavo} = \frac{Ebt_s^3 N^4}{KD_m^3 Z} * \frac{O.D.}{I.D.} \quad [4.34]$$

Here, E is the Modulus of elasticity, b is the radial width of material $\left(\frac{Outside\ Diameter\ (O.D.) - Inside\ Diameter\ (I.D.)}{2}\right)$, and t_s is the spring material thickness. N is the number of waves per turn, and K is the multiple wave factor, which was selected to be 3.88 as it depended on the number of waves per turn, N (Smalley Steel Ring Company, 2011). D_m is the mean diameter $\left(\frac{Outside\ Diameter\ (O.D.) + Inside\ Diameter\ (I.D.)}{2}\right)$, and Z is the spring number of turns. Figure 4.16 illustrates the spiral wave spring stiffness and its nomenclature. Based on calculations from Equation 4.34, the spiral wave spring stiffness was selected to be 59.8 lb_f/in (or 10472.6 N/m) considering the bore diameter (1.30 in or 3.30 cm) within which the spring operates inside the landing gear damper and the pre-compressed spring force of 72 lb_f (or 320.27 N), as shown in table 4.2.

The fundamental formula to custom design the conventional coil spring stiffness was as follows (Wahl, 1963):

$$k_{coil} = \frac{Gd^4}{8nD^3} \qquad [4.35]$$

where, G is the modulus of elasticity of spring material in shear, d is the diameter of spring wire, n_s is the number of active coils, and D is the mean coil diameter, $\left(\frac{Outside\ Diameter\ (O.D.) + 2d}{2}\right)$. Based on calculations from Equation 4.35, the coil spring stiffness was selected to be 47.5 lb_f/in (or 8318.5 N/m), as shown in table 4.2.

ii. Valve Construction and Assembly

Two spring-based relief valves of the MR landing gear damper (one with the spiral wave spring and the other with the coil spring) were manufactured and assembled (see Figure 4.17 and 4.18), and their damper force performance was experimentally tested. As illustrated in Figures 4.17 and 4.18, either spring was positioned and pre-compressed between the spring assembly top and bottom parts and secured with nuts and bolts. The seal was fastened on the lower part of the spring assembly and positioned to regulate the release of MR fluid through the orifice located in the center of the magnetic bobbin. Finally, a cap was fitted at the lower end of the bobbin and was designed to keep the magnetic flux return safely in place.

4.4.1.2 Passive Relief Valve Implementation Verification using a "Dummy Bobbin"

i. Testing Strategy with a Material Testing System (MTS) Machine

After manufacturing two different spring-assisted relief valves (spiral wave and coil springs) for the MR landing gear damper, their damper force performance was experimentally tested using an 810 MTS servo-hydraulic testing machine (MTS machine) at lower sink rates in

order to verify that the relief valve was working appropriately (see figure 4.19 for the damper setup on the MTS machine). In order to experimentally evaluate the damper force behavior of the spiral wave or coil spring-based MR landing gear damper, a series of ramp damper tests was conducted. In this ramp damper test, a constant piston velocity was applied to the MR landing gear damper using the hydraulic exciter of the MTS machine (see Figure 4.19). Under the estimated damper force designed and shown in Figure 4.14, the relief valve for the magnetic field-off case starts to open between 11-12 ft/s. It is important to note that the MTS machine can only reach speeds up to about 2.3 ft/s (0.7 m/s), which corresponds to an equivalent sink rate of about 6.2 ft/s (1.89 m/s), as illustrated in Figure 4.20. Consequently, The desired equivalent sink rate range of 11 ft/s-26ft/s for the magnetic field-off case cannot be implemented by the MTS machine.

ii. Design of an MR bobbin with No Electromagnetic Coil (Dummy Bobbin)

The testing strategy to perform the ramp tests on the MTS machine was to modify a "dummy" bobbin design parameters to have the relief valve opening at 4.4 ft/s (1.34 m/s), as simulated in Figure 4.21 to prevent reaching the MTS equivalent sink rate limit of 6.2 ft/s (or 1.89 m/s), while maintaining the damper force at the desired stroking load of 4000 lb_f. In this case, instead of the electromagnetic coil winding that activates the MR fluid inside the MR landing gear damper, the dummy bobbin was used to check if the relief valve worked correctly. This dummy bobbin was designed to make the MR landing gear damper without current input produce similar damper force as the force level of the MR landing gear damper with a constant current of 4 A. The annular gap of the dummy bobbin was reduced from 0.79 mm (or 0.0311 inches) from the designed electromagnetic coil winding gap to 0.50 mm (or 0.0197 inches) in

order to increase the field-off damper force. The Figures 4.22 and 4.23 show the different components needed for the dummy bobbin valve assembly with the spiral wave and coil springs, respectively.

4.4.2 *Ramp Testing and Results of MR Landing Gear Damper with Spring-Assisted Passive Valve*

Figure 4.24 presents a comparative study of the damper force performance of the spiral wave or coil spring-based MR landing gear dampers with the "no orifice" MR landing gear damper, both equipped with a dummy bobbin. In this figure, "no orifice" implies that the center orifice of the dummy bobbin was closed with a setscrew; thus, the relief valve was blocked. In addition, the MRF amount filled in the MR landing gear damper was 767 grams for the spiral wave spring-based damper case and 775 grams for the coil spring-based damper case due to the different relief valve assembly volumes. The initial gas pressure of the MR landing gear damper was 100 psi (6.89 bar), and the magnetic field was turned off for each case. As shown in figures 4.24 (a) and (b), the MR landing gear dampers for the three different configurations show similar damper forces at low constant velocities of 0.1 m/s (0.33 ft/s) and 0.4 m/s (1.31 ft/s) because the damper force level was below the relief valve pre-set force level of 4000 lb_f; hence, the seal does not open. However, at higher constant velocities of 1.2 m/s (3.94 ft/s) and 1.6 m/s (5.25 ft/s), as shown in figures 4.24 (c) and (d), the no orifice case shows higher damper force than the spiral wave and coil spring-based MR landing gear damper cases. It means that the relief valve is open because the damper force level passes the pre-set force level of 4000 lb_f. On the other hand, compared to the coil spring-based MR landing gear damper case, the spiral wave spring-based MR landing gear damper case shows more stable transient behavior as shown in figure 4.24 (d).

This phenomenon may occur due to the fact that the spiral wave spring is axisymmetric to the center guide of the bottom part of the spring assembly and more balanced than the coil spring.

4.5 Conclusions

An adaptive magnetorheological (MR) landing gear damper with a spring-assisted passive relief valve for a lightweight helicopter was designed to maintain a constant peak stroking force of 4000 lb_f across sink rates ranging from 6-26 ft/s. It was desired to expand the high end of the sink rate range from 12 ft/s from a prior study to 26 ft/s, while preserving low speed force levels. To achieve this increase in the high end of the sink rate range, the adaptive landing gear damper developed in this study was equipped with an MR valve that was designed to semi-actively control the peak stroking load over the 6-12 ft/s sink rate range and a spring-assisted passive (or relief) valve that was designed to passively control the stroking load over the 12-26 ft/s sink rate range.

The MR valve was designed using a nonlinear analytical damper model or Bingham-plastic model that depended on the behavior of MR fluids and nonlinear viscous factors. The passive relief valve was designed based on a computer simulation related to spring dynamic equations of motion, which estimated the damper force behavior to meet the desired stroking load of 4000 lb_f over the desired sink rate range of 12-26 ft/s.

A nonlinear analysis based on the pressure drop across the MR valve and the passive relief valve center orifice was carried out to estimate the center orifice diameter range. The optimal diameter of the center orifice was estimated to be 0.3 inches (7.62 mm).

Two different springs were used (a conventional coil spring and a spiral wave spring) for the analysis and construction of the valves. Moreover, an electromagnetic analysis of the MR valve in the landing gear damper using the commercial software ANSYS was performed to

predict the magnetic field strength in the MR gap while taking into consideration the center orifice diameter selected.

Finally, an experimental study using an MTS machine was performed to evaluate the damper force behavior of the spiral wave and coil spring-based MR landing gear dampers to verify that the relief valve operated properly. A dummy bobbin was designed, fabricated, and tested using ramp damper tests. In these ramp tests, instead of the electromagnetic coil winding that activates the MR valve, the dummy bobbin was used to check if the relief valve worked correctly due to the speed limitation of the servo-hydraulic testing machine. Using the MTS machine, the stroking load (or damper force) of the MR landing gear damper coupled with a spring-assisted relief valve was measured for constant velocity inputs to verify that the spring-based relief valve was working appropriately. Three different damper configurations such as a dummy bobbin with no relief valve, a bobbin with a spiral wave spring-based relief valve, and a bobbin with a coil spring-based relief valve were tested. At a constant velocity of 5.25 ft/s, the no relief valve case showed higher damper force performance than the spiral wave and coil spring-based MR landing gear damper cases. This implies that the spiral wave and coil spring-based relief valves were opening, hence working properly. Also, the spiral wave spring-based MR landing gear damper case showed more stable transient behavior, which could be due to the fact that the spiral wave spring was axisymmetric hence well balanced around its center axis as compared to the coil spring.

References

Batterbee, D.C., Sims, N.D., Stanway, R., and Wolejsza, Z., (2007a) Magnetorheological landing gear: 1. A design methodology. *Smart Materials and Structures*, 16: 2429-2440. DOI: 10.1088/0964-1726/16/6/046.

Batterbee, D.C., Sims, N.D., Stanway, R., and Rennison, M., (2007b) Magnetorheological landing gear: 2. Validation using experimental data. *Smart Materials and Structures*, 16: 2441-2452. DOI: 10.1088/0964-1726/16/6/047.

Choi, Y.-T., and Wereley, N.M., (2003) Vibration control of a landing gear system featuring ER/MR fluids. *AIAA Journal*, 40(3): 432–439. DOI: 10.2514/2.3138.

Choi, Y.-T., Yoo, J.H., and Wereley, N.M., (2005b) Double adjustable magnetorheological dampers for a gun recoil system. International Mechanical Engineering Congress and Exposition (IMECE), Orlando, FL, USA.

Choi, Y.-T., Robinson, R., Hu, W., Wereley, N.M., Birchette, T.S., and Bolukbasi, A.O., (2012) Analysis and control of a magnetorheological landing gear system for a helicopter. Proceedings of the American Helicopter Society 68th Annual Forum & Technology Display, Fort Worth, TX, USA.

Franzini, J.B., and Finnemore, E.J., (1997) *Fluid Mechanics with Engineering Applications*, McGraw Hill.

Idel'chik, I.E., (1994) *Handbook of Hydraulic Resistance,* 3rd Edition, CRC Press, FL, USA.

Lin, L.H., Yong, C., Qi, H., and Jian, L., (2009) Fuzzy PID control for landing gear based on magnetorheological (MR) damper. International Conference on Apperceiving Computing and Intelligence Analysis (ICACIA), 22-25. DOI: 10.1109/ICACIA.2009.5361162.

Lord Corporation, www.lord.com.

Mao, M., Choi, Y.-T., and Wereley, N.M., (2005) Effective design strategy for a magnetorheological damper using a nonlinear flow model. Proceedings of SPIE, 5760: 446-455. DOI: 10.1117/12.601061.

Merritt, H.E., (1967) *Hydraulic Control Systems*. John Wiley & Sons, New York, USA.

Mid-West Spring and Stamping (2011) retrieved from <http://www.mwspring.com/>.

Mikulowski, G.M., and Holnicki-Szulc, J., (2007) Adaptive landing gear concept- feedback control validation. *Smart Materials and Structures*, 16: 2146-2158. DOI: 10.1088/0964-1726/16/6/017.

Mikulowski, G.M., and LeLetty, R., (2008) Advanced landing gears for improved impact absorption. Proceedings of the 11th International Conference on New Actuators, 363-366, Bremen, Germany.

Smalley Steel Ring Company (2011) retrieved from <http://www.smalley.com>.

Spurk, J.H., and Aksel, N., (2008) *Fluid Mechanics*, 2nd Edition. Springer-Verlag, Berlin Germany. DOI 10.1007/978-3-540-73537-3.

Wahl, A.M., (1963) *Mechanical Springs*, 2nd Edition, McGraw-Hill, New York, USA.

Wereley, N.M., and Pang, L., (1998) Nondimensional analysis of semi-active electro- and magneto-rheological dampers using parallel plate models. *Smart Materials and Structures*, 7: 732-743. DOI: 10.1088/0964-1726/7/5/015.

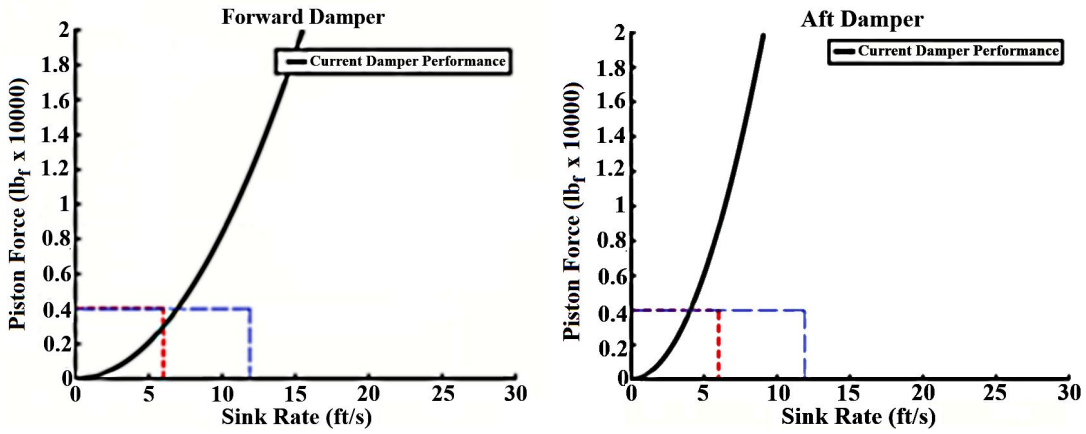

(a) (b)

Figure 4.1. Passive hydraulic damper performance for MD-500 helicopter: (a) forward damper and (b) aft damper

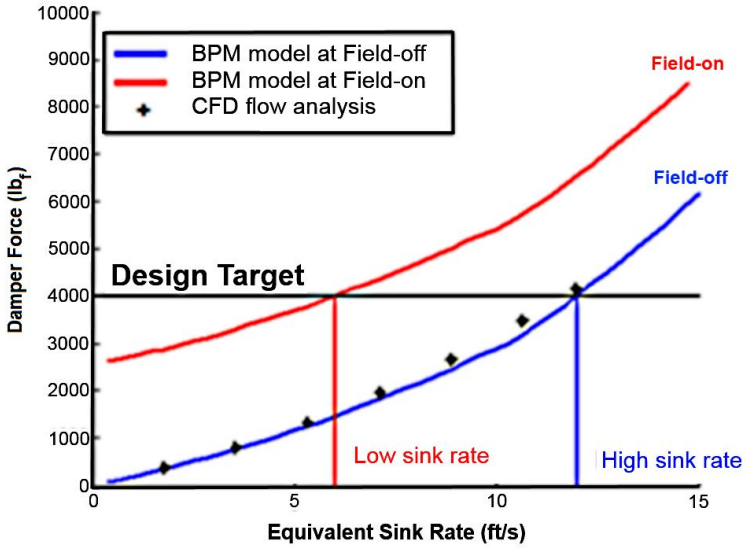

Figure 4.2. Initial MR landing gear damper stroking load or damper force versus equivalent sink rate (adapted from Choi *et al*., 2012)

MR: Magnetorheological

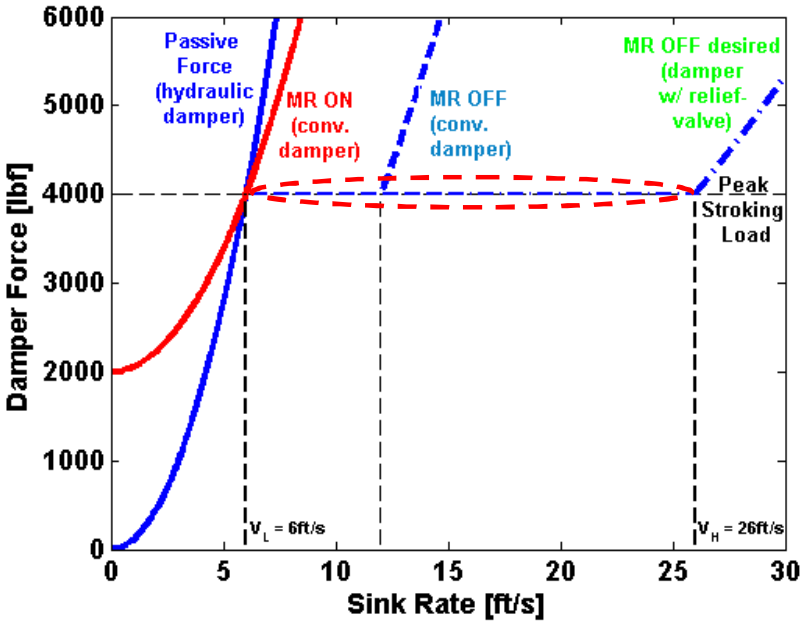

Figure 4.3. Design targets comparing the predicted performances of MR landing gear damper with spring-assisted relief valve to the original MD-500 passive hydraulic damper and the previously designed conventional MRLGD

MRLGD: Magnetorheological landing gear damper

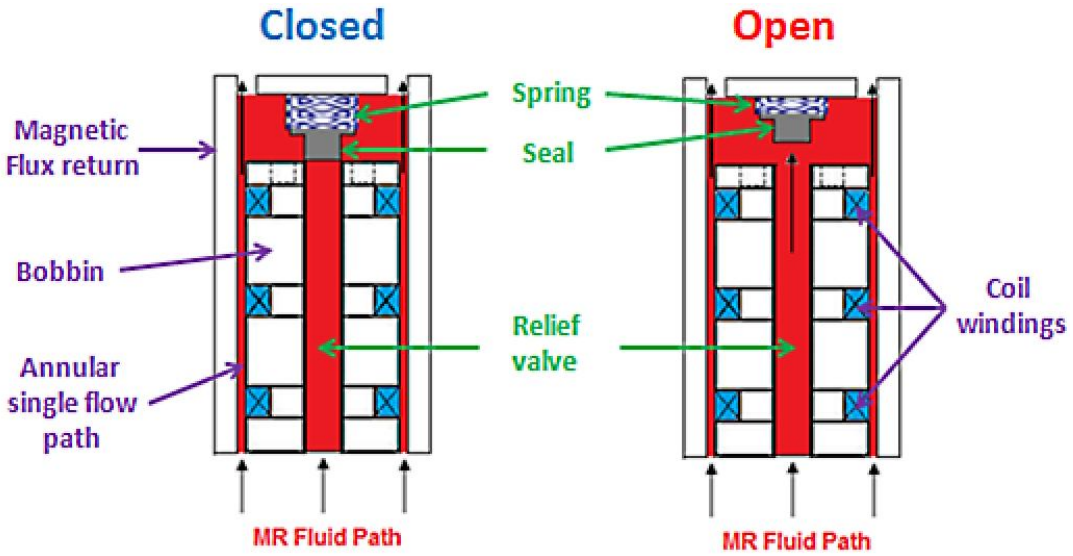

Figure 4.4. Schematic of the MR valve coupled with a spring-assisted passive (or relief) valve in the landing gear damper for a lightweight helicopter

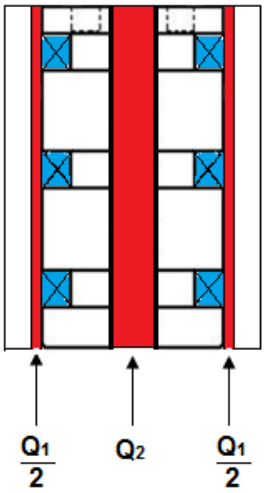

Figure 4.5. Flow rates in each flow passage of the MR valve and the center orifice of the passive valve

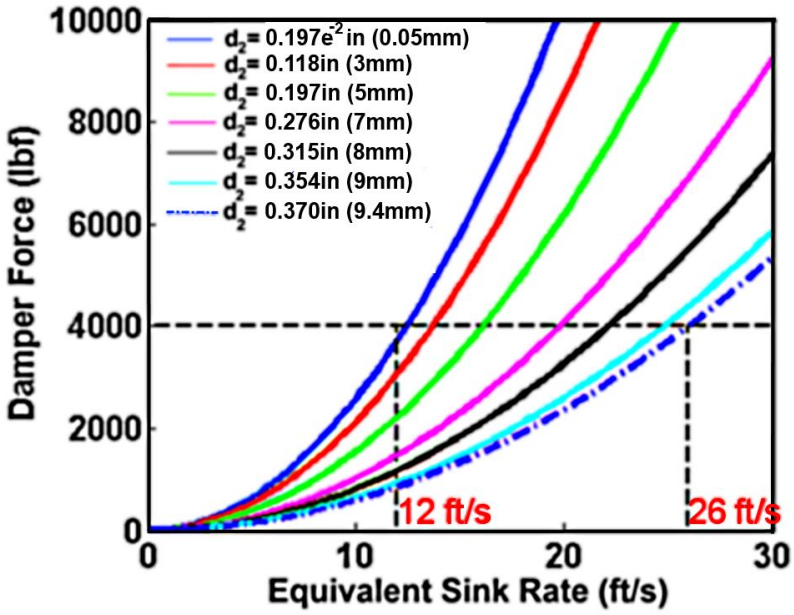

Figure 4.6. Damper force (in lb_f) versus sink rate (in ft/s) for different orifice diameters, d_2

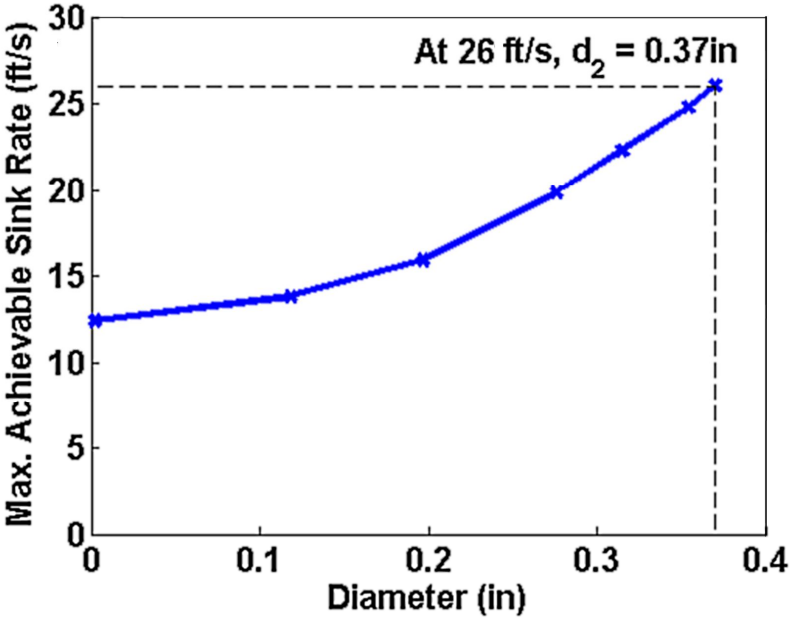

Figure 4.7. Maximum achievable orifice diameter needed to reach the high-end of the sink rate range target of 26 ft/s

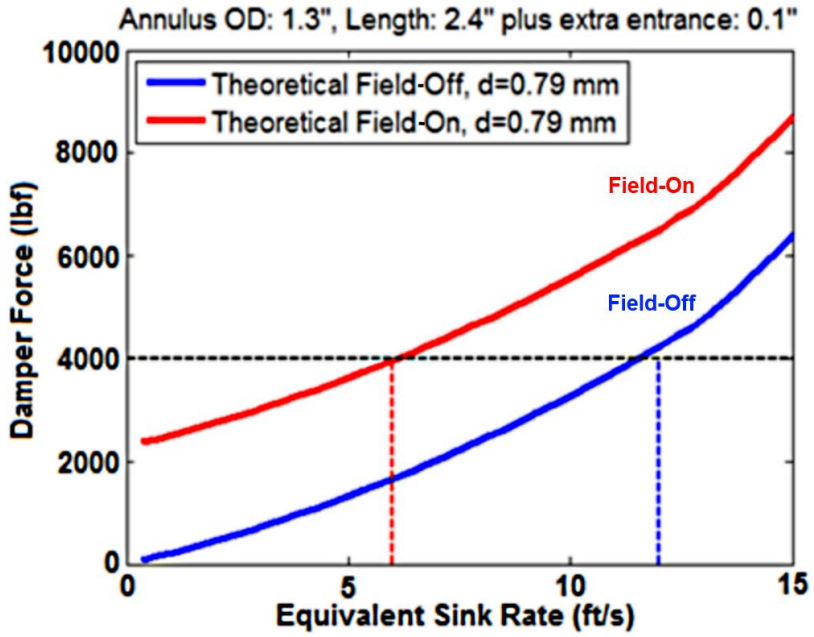

Figure 4.8. Theoretical damper force of the MR landing gear damper with spring-based passive valve versus equivalent sink rate with the low speed design target satisfied

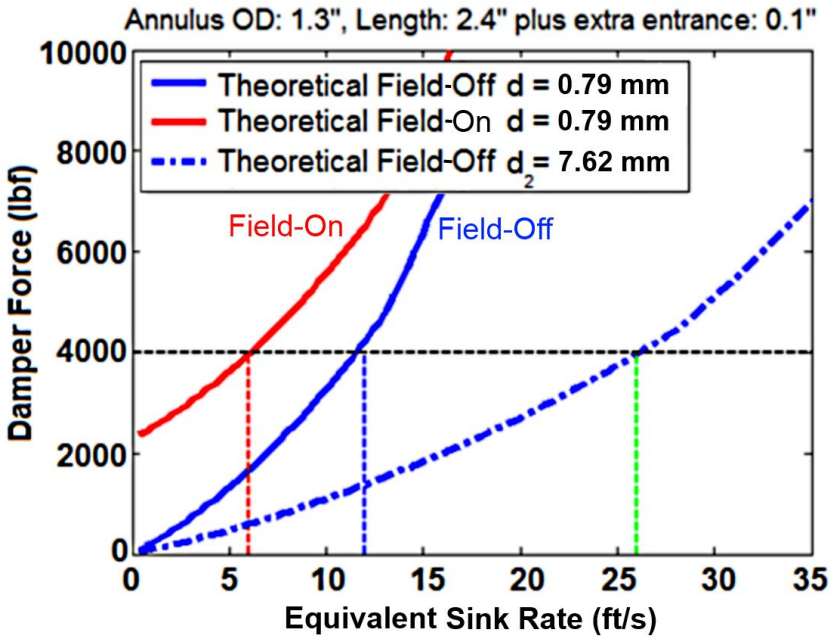

Figure 4.9. Theoretical damper force of the MR landing gear damper with spring-based passive valve versus equivalent sink rate with the low and high speed design targets satisfied. Center orifice diameter d_2 = 0.30 in (7.62 mm)

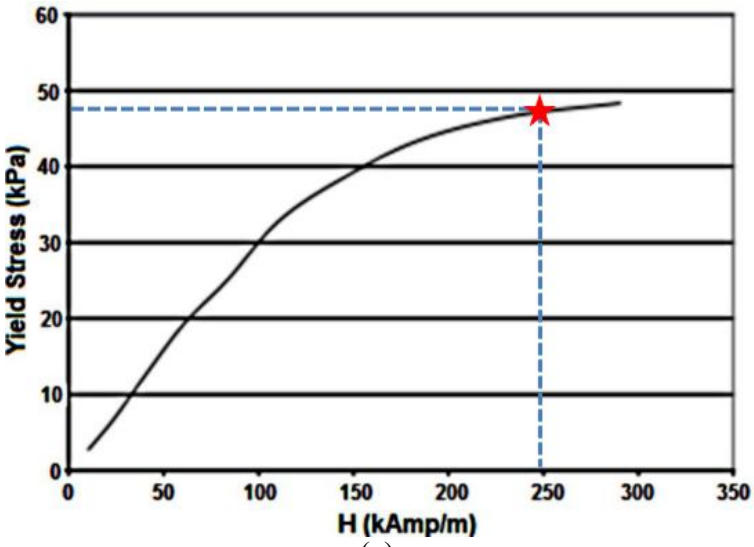

(a)

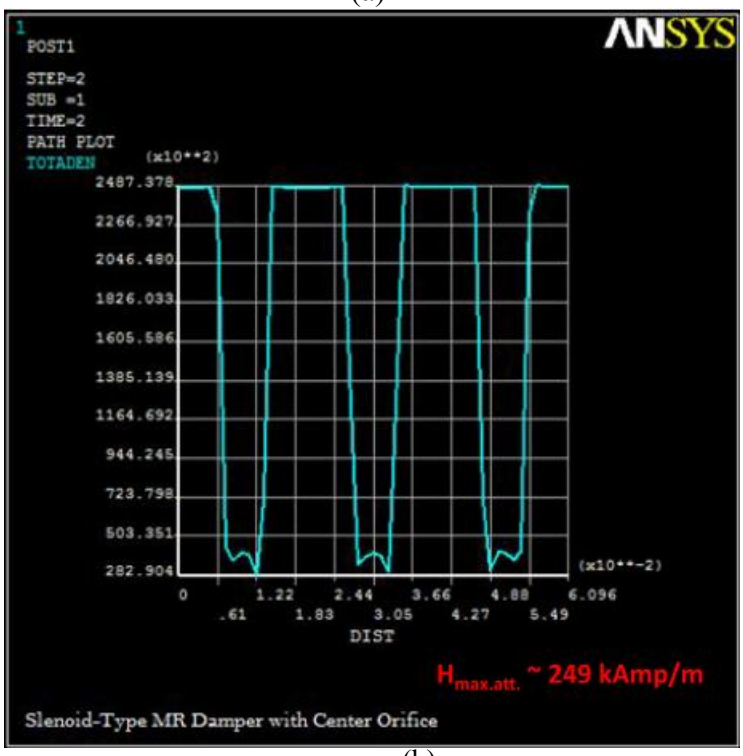

(b)

Figure 4.10. Electromagnetic analysis of the MR valve in the landing gear damper to relate the magnetic field strength inside the MR valve gap to the yield stress of the MRF used in the damper (a) yield stress versus magnetic field strength of the Lord Corporation MRF-132CG (b) magnetic field strength inside the MR valve gap

MRF: magnetorheological fluid

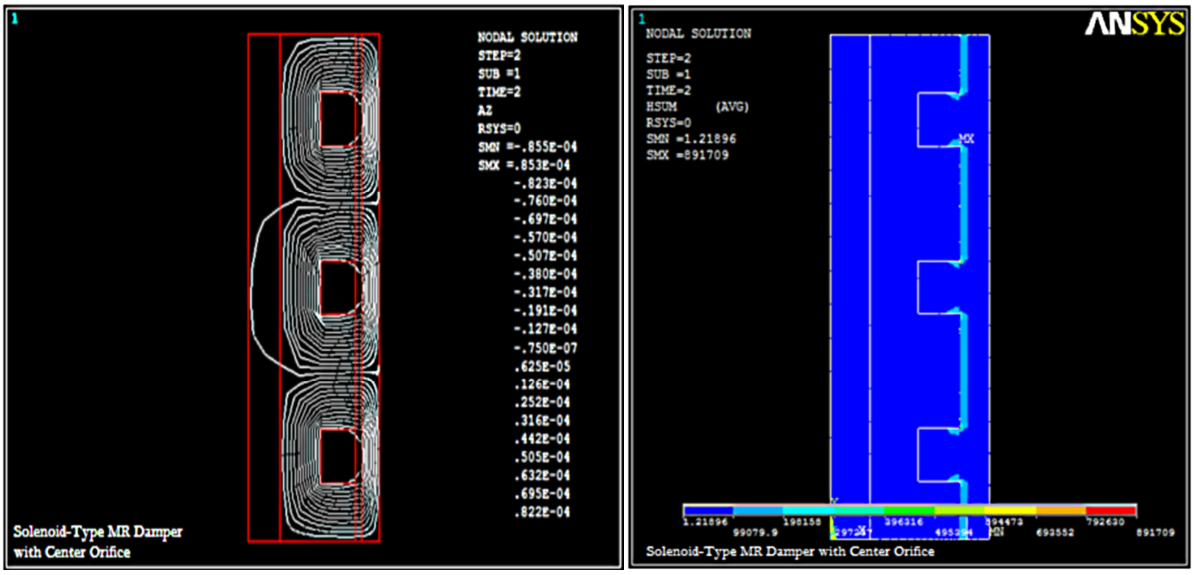

(a) (b)

Figure 4.11. Electromagnetic analysis of the MR valve in the landing gear damper: magnetic field strength, H, (a) magnetic flux lines to be generated by the magnetic coil windings (b) magnetic field strength inside the MR valve gap illustrated

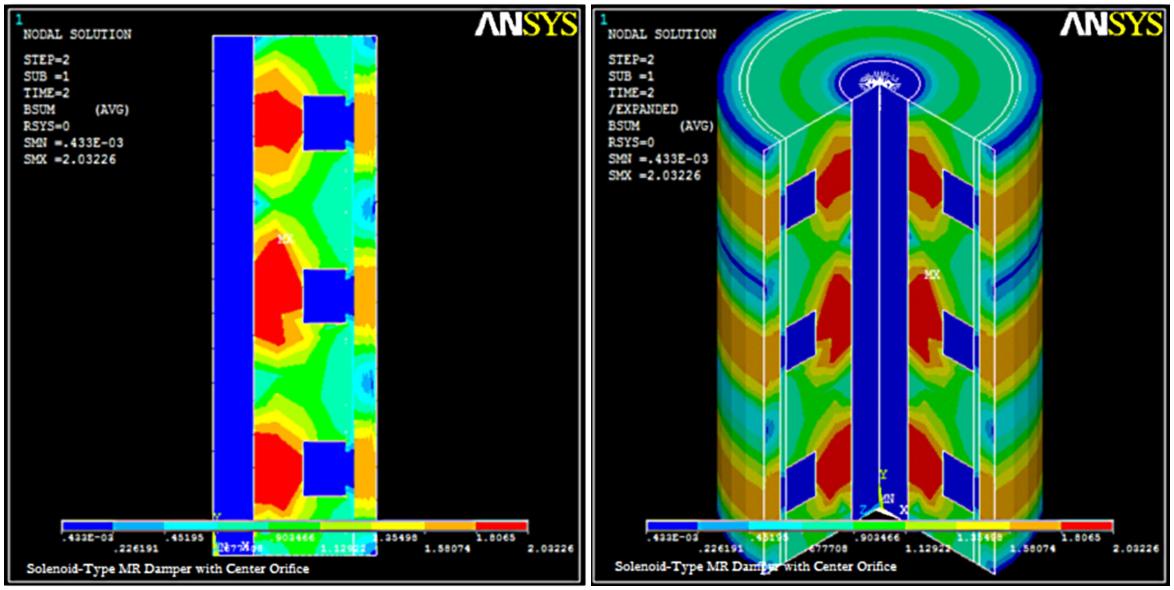

(a) (b)

Figure 4.12. Electromagnetic analysis of the MR valve in the landing gear damper: magnetic field density, B (a) front view (b) axisymmetrical view

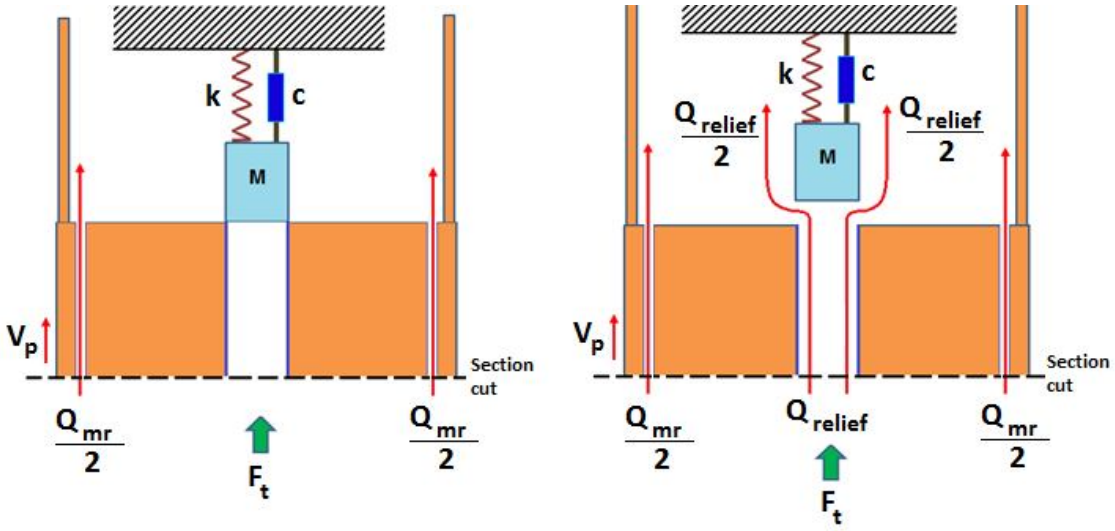

(a) (b)

Figure 4.13. Hydraulic model of the MR and passive valves of the MR landing gear damper: (a) relief valve is closed and MRF only flows through the MR valve; (b) relief valve is open and MRF flows through two paths (the MR valve and the center orifice relief valve)

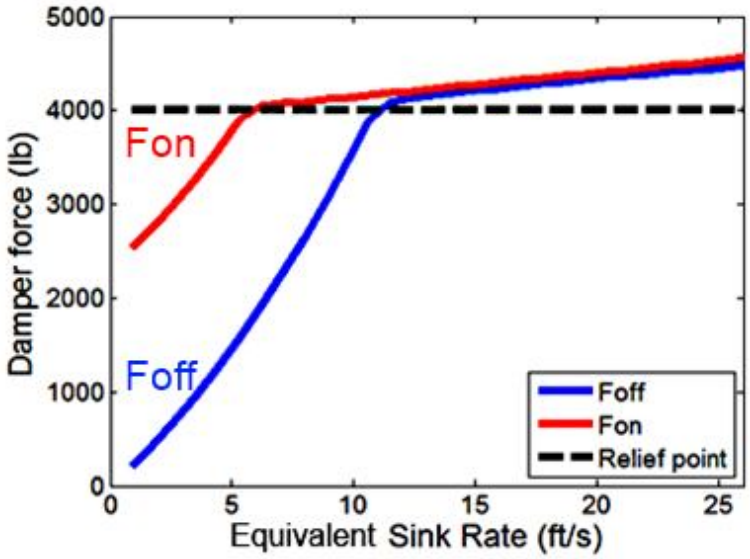

Figure 4.14. Estimated damper force of the relief valve of the MR landing gear damper versus sink rate (with a spring stiffness of 50 lb_f/in)

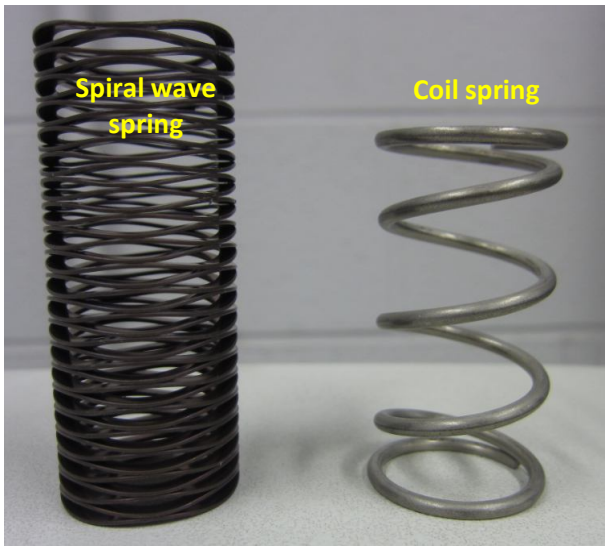

Figure 4.15. Custom designed crest-to-crest spiral wave and conventional coil springs

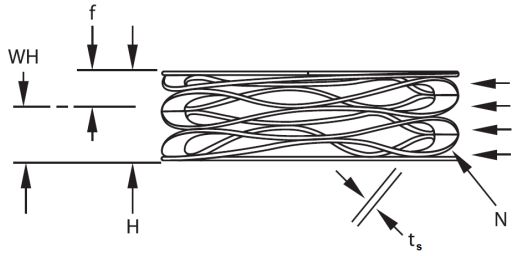

P	Load, lb
S	Operating Stress, psi
t_s	Thickness of Material, in
WH	Work Height, in (H-f)
Z	Number of Turns

b	Radial Width of Material, in [(O.D. - I.D.)÷2]
D_m	Mean Diameter, in [(O.D. + I.D.)÷2]
E	Modulus of Elasticity, psi
f	Deflection, in
H	Free height, in
I.D.	Inside Diameter, in
K	Multiple Wave Factor, see Table 1
L	Length, Overall Linear, in
N	Number of Waves (per turn)
O.D.	Outside Diameter, in

Figure 4.16. Custom designed spiral wave spring nomenclature (Courtesy of Smalley®. All rights reserved)

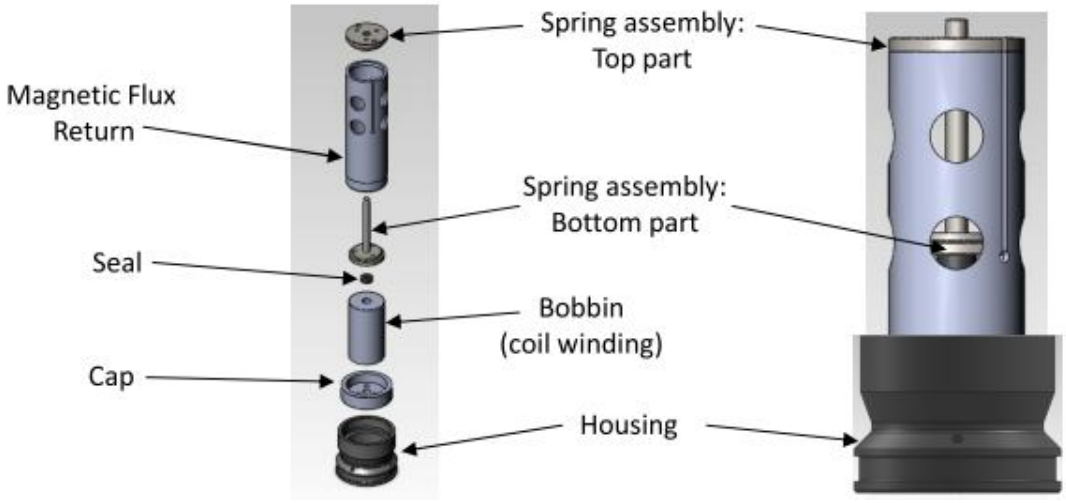

Figure 4.17. Components and assembly of the spring-based relief valve for the MR landing gear damper (either spring is installed between the top and bottom parts of the spring assembly)

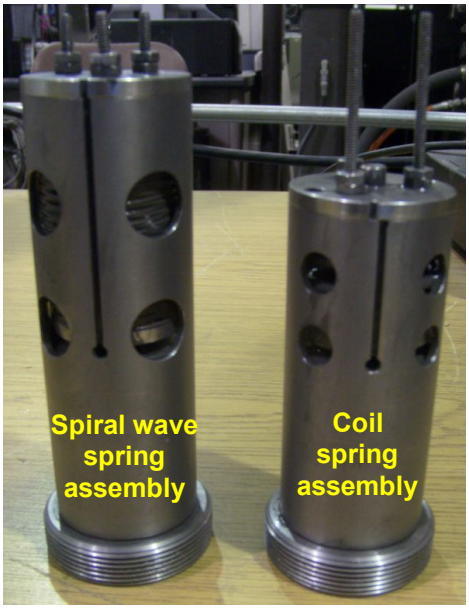

Figure 4.18. Fully assembled MR valves coupled with spiral wave and coil spring-based passive valves

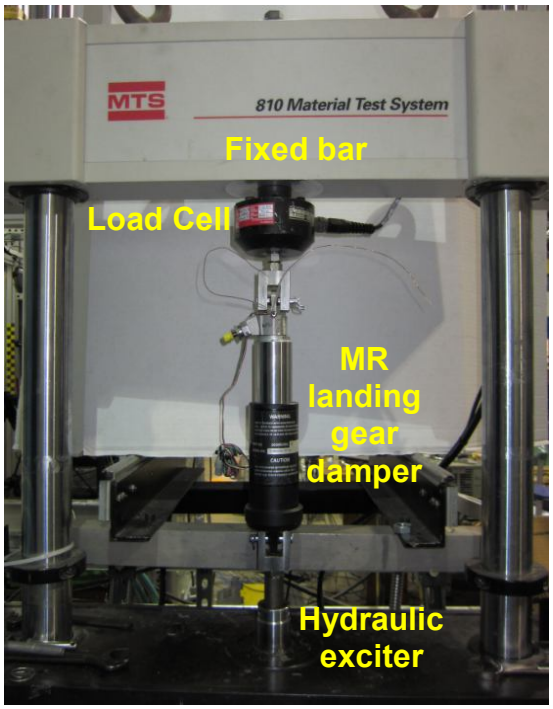

Figure 4.19. Damper ramp test setup of the MR landing gear damper on the MTS machine

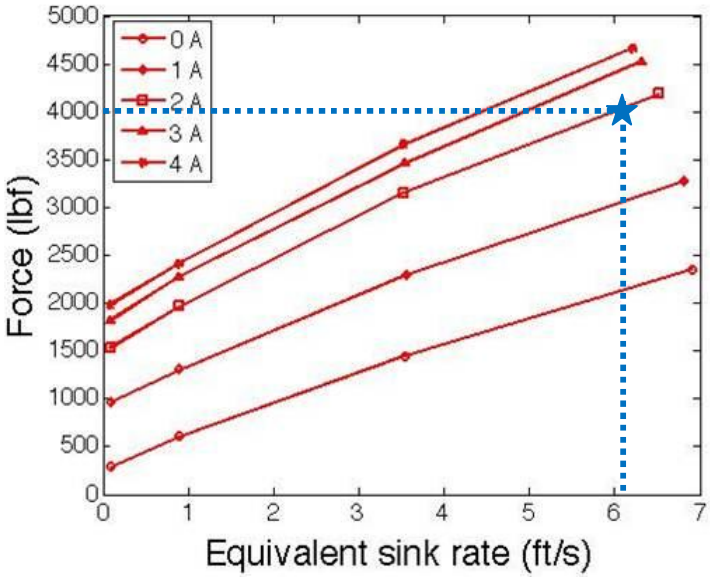

Figure 4.20. MTS machine capability of reaching equivalent sink rates of about 6.2 ft/s (or 1.89 m/s) while maintaining a stroking load of 4000 lb_f in the landing gear damper at the University of Maryland

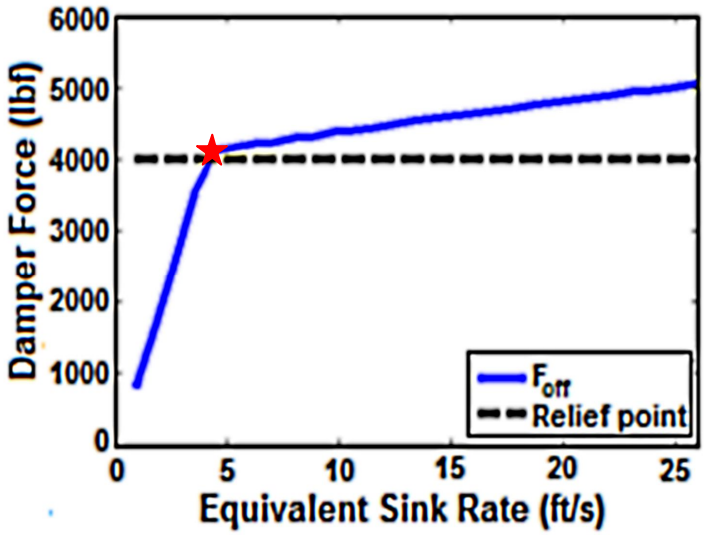

Figure 4.21. MR passive relief valve damper force is designed to open around an equivalent sink rate of 4.4 ft/s (1.34 m/s) for MTS ramp tests using the spiral wave spring with a stiffness of 59.8 lb_f/in and the coil spring using a stiffness of 47.5 lb_f/in

MTS: material test system

(a) (b)

Figure 4.22. Spiral wave spring-based passive relief valve with a dummy bobbin; (a) components of the spiral wave spring-based relief valve and (b) Valve assembly

(a) (b)

Figure 4.23. Coil spring-based passive relief valve with a dummy bobbin; (a) components of the coil spring-based relief valve and (b) Valve assembly

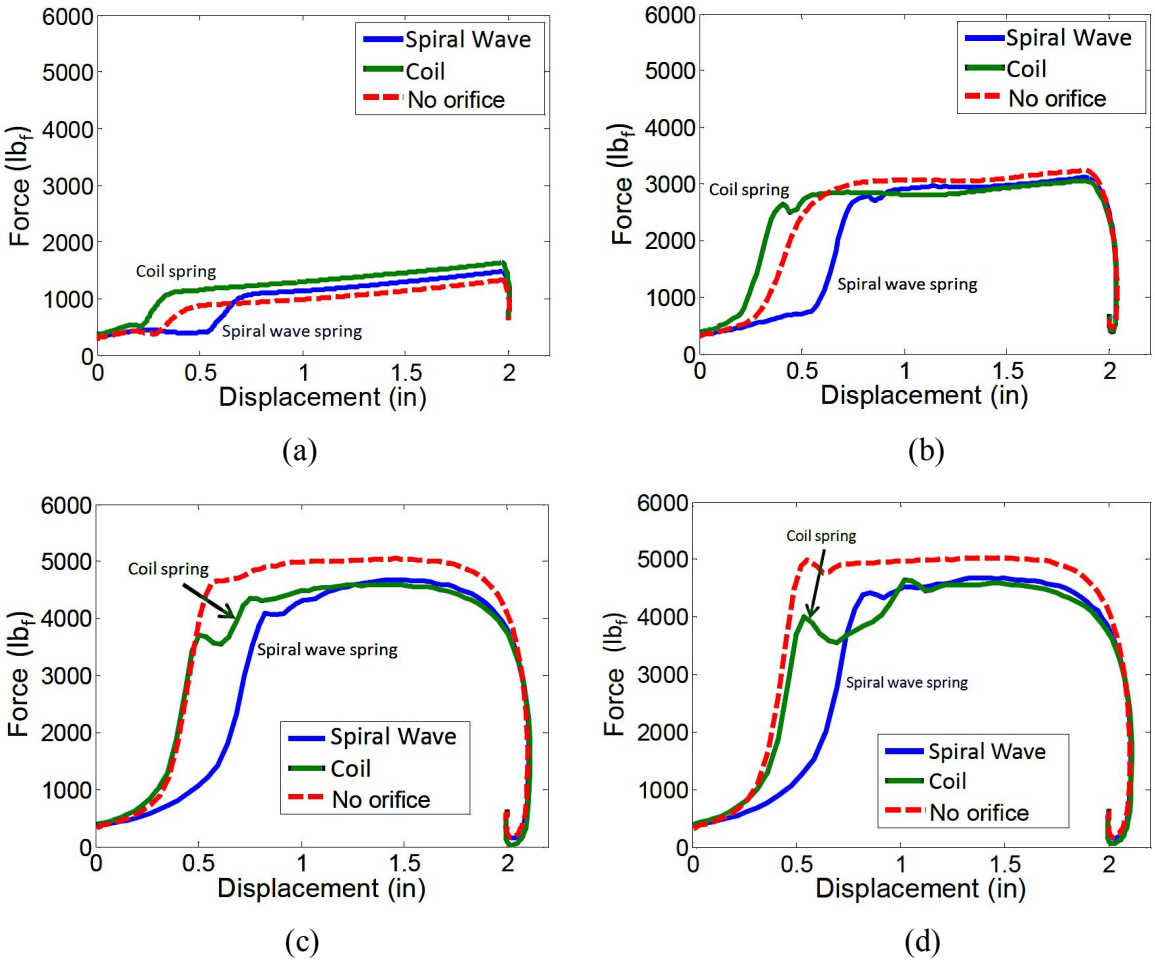

Figure 4.24. Comparison of the damper force performance with magnetic field off of the spiral wave and coil spring-based MR landing dampers cases to the "No orifice" case. In these tests, a dummy bobbin was used instead of the electromagnetic coil winding (a) constant velocity of 0.1 m/s (0.33 ft/s), (b) constant velocity of 0.4 m/s (1.31 ft/s), (c) constant velocity of 1.2 m/s (3.94 ft/s), and (d) constant velocity of 1.6 m/s (5.25 ft/s)

Table 4.1. Design parameters for electromagnetic analysis of the MR valve in the landing gear damper

Maximum Current (in Amperes)	3.50
Number of coils	3.00
Number of turns per coil	189
Center orifice diameter (mm / inches)	9.40 / 0.37
Annular gap thickness (mm / inches)	0.79 / 0.03
Coil active length, L_c (mm / inches)	8.38 / 0.30
MR valve active length, L_a (mm / inches)	11.18 / 0.50

Table 4.2. Properties and dimensions of customized spiral wave and coil springs

Spiral Wave Spring		**Coil Spring**	
Minimum I.D. (mm / inches)	26.213 / 1.032	Minimum I.D. (mm / inches)	30.050 / 1.183
Maximum O.D. (mm / inches)	33.02 / 1.30	Maximum O.D. (mm / inches)	33.020 / 1.300
Spring rate (N/mm / lb_f/in)	10.47 / 59.80	Spring rate (N/mm / lb_f/in)	8.32 / 47.5
Working height @ 288.24-352.3 N / 64.8-79.2 lb_f (mm / inches)	50.80 / 2.00	Solid height @ 404.34 / 90.9 lb_f (mm / inches)	14.880 / 0.586
Working height @ 376.76 N / 84.7 lb_f (mm / inches)	1.788 / 45.420	No. of coils (active / inactive)	3 / 2
Free height (mm / inches)	2.914 / 74.02	Free height (mm / inches)	63.50 / 2.50

CHAPTER 5: Analysis of Spring-Assisted Adaptive Magnetorheological Landing Gear Dampers with a Control Algorithm

5.1 Introduction and Overview

A single stage flow-mode type magnetorheological (MR) landing gear damper was designed to attain a desired peak stroking load of 4000 lb_f over a desired equivalent sink rate range of 6 - 26 ft/s. This represents a considerable increase in the energy attenuation requirement over the entire sink rate range and almost 54% increase from the related previous work by Choi *et al.*, (2012) where the sink rate range was from 6-12 ft/s. To achieve this increase in the high-end of the sink rate range, a spring-based passive (or relief) valve MR landing gear damper was developed. The MR valve was designed to semi-actively control the peak stroking load over the 6-12 ft/s sink rate range, whereas the relief valve was designed to passively control the peak stroking load over the 12-26 ft/s sink rate range.

In prior study (Choi *et al.*, 2012), the authors conducted the design and test of an adaptive landing gear system, incorporated with MR fluids, that was capable of automatically adapting its load-stroke profile to protect the aircraft and its occupants over a wider range of aircraft gross weights and sink rates (6-12 ft/s) than conventional hydraulic landing gear dampers. The authors used two force feedback control algorithms, which were the bang-bang current control and the continuous current control to achieve the desired constant peak stroking load control objective. The controlled stroking loads achieved using these two force feedback control algorithms were experimentally evaluated using a damper test setup over the desired sink rate range.

This current work intends to expand the high end of the sink rate range, so that the peak stroking load can be held constant for sink rates ranging from 6-26 ft/s hence extending the high end of the speed range from 12 ft/s (from prior work) to 26 ft/s. This can be achieved through the use of an adaptive landing gear system. The main purpose of an adaptive landing gear system is to adapt the load stroke profile in response to payload and sink rate variations of a helicopter. However, there are important challenges to successfully design and implement an adaptive landing gear system (Choi *et al.*, 2012). First, the time interval of the landing shock pulse during hard landing events is typically 50-200 ms in duration. In order to successfully control the load-stroke profile over this short period of time, landing gear dampers must be able to adjust their stroking load faster than the duration of the shock pulse occurring during the landing event. In addition, the adaptive landing gear system must be compact and lightweight and satisfy the performance design targets. Finally, the stroking load must be able to adjust automatically in accordance with control algorithms based on real-time measurements of sink rate and crash severity. The fact that landing loads depend on the helicopter payload and sink rate, as well as ground conditions and helicopter attitude, there is a large variation in the landing load pulse within which the stroking load of the landing gear damper must be controlled. In order to mitigate shock, landing gear devices used in the landing gear systems must be able to adapt in real-time to these changes in landing events, and such adaptive capabilities cannot be achieved using only passive landing gear dampers with a single condition (single payload mass and excitation level), a set load stroke profiles, or manually adjustable load stroke profiles. Consequently, the objective of this current effort is to maintain a constant stroking load of 4000 lb_f over an extended equivalent sink rate range (6-26 ft/s) while taking into account the same challenges encountered in prior studies. In order to meet these challenges as well as the objective

of this work, a spring-based passive (or relief) valve MR landing gear system that has a constant cracking pressure, was proposed in this study.

The motivation behind this current work stems from different aspects of adaptive MR landing gear systems. MR application to adaptive landing gear systems has been investigated by several research groups (Choi *et al.*, 2012; Choi and Wereley, 2003; Mikulowski and Holnicki-Szulc, 2007; Batterbee *et al.*, 2007a; Batterbee *et al.*, 2007b; Lin *et al.*, 2009; Mikulowski and LeLetty, 2008) referred in Chapter 1. It is important to note that all these studies previously mentioned about adaptive MR landing gear systems were designed and tested with scaled-down stroking loads intended for laboratory testing.

Studies to suppress the fuselage vibration for improving the ride quality and safety of aircraft have also been explored. Lin *et al*. (2009) developed a control algorithm using fuzzy proportional-integral-derivative (PID) hybrid control for adaptive capability to nonlinear system variations. The fuzzy PID hybrid control algorithm could effectively reduce the fuselage acceleration when compared to passive control and PID control. Mikulowski and Holnicki-Szulc (2007) proposed a closed loop feedback control algorithm to recognize the impact energy based on the initial velocity and mass of the falling structure (velocity sensor), determine the optimal acceleration value for the adaptive impact absorber, and execute the control signal in the closed loop during the process (acceleration sensor feedback). Their closed loop feedback control algorithm was successfully implemented to maintain the optimal acceleration level with reference to the identified impact energy and the stroke of the adaptive absorber. A flow mode type MR landing gear damper was proposed for a lightweight helicopter skid landing gear system, which was designed, at full-scale and maintained a desired stroking load of 4000 lb_f over a desired sink rate range of 6-12 ft/s (Choi *et al.*, 2012). Two force feedback control algorithms

(the bang-bang current control and the continuous current control) were proposed to maintain the stroking load of the MR landing gear damper constant over the desired sink rate range of 6-12 ft/s. These control algorithms were experimentally evaluated by using the single damper drop test setup. The performance of the MR landing gear damper was experimentally validated over the desired sink rate range under the iron-bird drop testing stand which is equipped with four MR landing gear dampers and uses a skid landing gear.

In this follow-on effort, a full-scale, flow-mode type MR valve landing gear damper, coupled with a spring-assisted passive valve that has a constant cracking pressure, was developed to increase the high end of the sink rate range from 12 ft/s, from prior study (Choi *et al.*, 2012), to 26 ft/s while maintain a peak stroking force of 4000 lb_f over a desired sink rate ranging from 6-26 ft/s. Two different springs were used (a conventional coil spring and a spiral wave spring) for the analysis. To verify that the spring-assisted passive valve worked properly, a servo-hydraulic testing system (MTS 810) was used by applying a damper piston velocity with the hydraulic exciter of the MTS machine to the MR landing gear damper (Chapter 4). Single damper drop tests were conducted at the University of Maryland, College Park to experimentally measure the stroking load of the MR landing gear damper coupled with the passive valve over equivalent sink rates up to about 18 ft/s. The total drop mass was 430 lbs. In order to maintain the peak stroking load of the MR landing gear damper constant over the desired range of sink rates of 6-26 ft/s, a bang-bang current control algorithm was formulated using a force feedback signal. This control algorithm was experimentally evaluated using the single damper drop test setup. To experimentally measure the stroking load of the MR landing gear damper with the spring-assisted passive valve over higher desired equivalent sink rates up to 26 ft/s, single damper drop tests (with a total drop mass of 1283 lbs) were conducted at Boeing Structures Test

Laboratory in Mesa, Arizona. Finally, a ballasted frame called iron-bird, which emulated the lightweight helicopter with a complete skid landing gear system and incorporated four MR landing gear dampers that were each coupled with a spring-based passive valve, was drop tested at Boeing as well (with a total drop mass of 2627 lbs). The bang-bang current control algorithm was also used in the iron-bird drop test to regulate the damper force of the MR landing gear dampers over the desired sink rate range of 6-26 ft/s.

5.2 MR and Passive Valve Functions of the Landing Gear Damper

The schematic diagram of the MR and passive (or relief) valves of the MR landing gear damper used in this study is presented in Figure 4.4 of Chapter 4. In this figure, the MR valve has one annular single flow path, one center orifice contributing to the spring-assisted relief valve, three layers of magnetic coil windings, a spring, and a seal. The spring in the relief valve is pre-compressed; therefore, it does not open until the MR valve force develops to a desired stroking load of 4000 lb_f. The working principle of the MR valve is that, by activating the magnetic field input inside the MR valve, the desired stroking load is produced at an equivalent sink rate of 6 ft/s. At higher equivalent sink rates of about 11 or 12 ft/s, the MR valve is turned off and works as a passive valve to maintain the desired stroking load at 4000 lb_f. At this point, the spring compresses, and the seal opens for the center orifice to work as an additional fluid path. As a result, the damper force reduces because the MR fluid pressure in the center orifice drops.

5.3 Single Damper Drop Test of the MR Landing Gear Damper with a Spring-Based Passive Valve

5.3.1 Single Damper Drop Test with a Drop Mass of 430 lbs

5.3.1.1 Setup and Instrumentation

In order to experimentally evaluate the damper force of the MR landing gear damper with a spring-assisted passive valve at higher sink rates, single-drop damper tests were conducted, first at the University of Maryland, College Park. The experimental test setup stand was constructed, as shown in Figure 5.1. In this first drop testing experiment, the drop mass was chosen to be 430 lbs, and starting from a given drop height, the drop mass fell freely along four guiding rods. To prevent metal-to-metal impact, a rubber stack was placed on a strike plate attached to the damper shaft. A single landing gear damper having an MR valve coupled with a coil spring-assisted relief valve and a single landing gear damper having an MR valve coupled with a spiral wave spring were drop tested. Several tests and revisions of the relief valve to decrease its flow resistance by increasing the diameter of the center orifice were conducted.

5.3.1.2 Test Results

In order to decrease the pressure resistance of the center orifice, the diameter size of the center orifice was revised a few times. In the revisions, the diameter of the center orifice was increased from 0.300 in or 7.62 mm (from the original design in Chapter 4) to 0.375 in or 9.525 mm, as shown in figure 5.2.

Figure 5.3 (a) represents the damper force characteristics of the MR landing gear damper with the coil relief valve versus the equivalent sink rate, and Figure 5.3 (b) is the maximum damper displacement. In this case, the initial gas pressure was 200 psi inside the damper, and the MR fluid amount was 690 grams. As shown in Figure 5.3 (a), the coil relief valve MR landing

gear damper shows that the maximum operating sink rate range is from 9.5-14 ft/s. This indicates that the coil-based landing gear damper performance satisfies neither the low speed nor the high speed design targets of maintaining a peak stroking force of 4000 lb_f over the desired 6-26 ft/s sink rate range. Figure 5.4 (a) illustrates the maximum damper force of the MR landing gear damper with the spiral wave relief valve versus the equivalent sink rate. The initial gas pressure was also 200 psi, and the MR fluid amount was 665 grams inside the damper. As shown in Figure 5.4 (a), the spiral wave spring-based relief valve works well at this tuned gas pressure and MR fluid amount. The achievable maximum equivalent sink rate range that can maintain the desired damper force level of 4000 lb_f is from 6 ft/s to about 16 ft/s. The high speed design target is not satisfied due to the limited damper stroke available, as shown in figure 5.4 (b). Within a force error bound of ±1000 lb_f, the maximum achievable equivalent sink rate range is from 6 ft/s to 18 ft/s. The equivalent sink rate, $V_{eq,sink}$, was determined by the following equation:

$$V_{eq,sink} = 2.7\sqrt{2gh_{drop}} \quad [5.1]$$

Here, g is the gravitational acceleration, and h_{drop} is the initial drop height. A factor of 2.7 was used to account for the kinematic relationship between the connection points of the installed MR landing gear damper to the fuselage and the landing skid.

The best performance of the single-drop test was obtained from the spiral wave spring-based MR landing gear damper, and the low speed design target is satisfied in this case. The spiral wave spring based relief valve landing gear damper force better performance over that of the coil relief valve case is due to the spiral wave spring more stable transient motion than the coil spring because of the axisymmetric shape of the spiral wave spring.

5.3.2 *Single Damper Drop Test with a Drop Mass of 1287 lbs*

Single MR landing gear damper drop tests were also conducted at the Boeing Structures Test Laboratory. Three different landing gear dampers were tested: (1) a landing gear damper having only an MR valve without a relief valve (baseline MR landing gear damper), (2) a landing gear damper having an MR valve coupled with a coil spring-assisted relief valve, and (3) a landing gear damper having an MR valve coupled with a spiral wave spring-assisted relief valve. The ballasted drop mass was 1283 lbs for all cases.

Figure 5.5 shows the maximum achievable equivalent sink rate of the MR landing gear dampers. As seen in this figure, the baseline MR landing gear damper achieved the desired damper force of 4000 lb_f up to the equivalent sink rate of 10 ft/s, but the MR landing gear dampers with the spiral wave and coil spring-based relief valves maintained the desired damper force up to a higher equivalent sink rate of 18 ft/s. This increase in the maximum achievable equivalent sink rate implies that the spiral wave and coil spring-based relief valves operated aptly. If a force error bound of ±1000 lb_f is specified, then the maximum achievable equivalent sink rate of the baseline can be increased from 12 ft/s to 22 ft/s by using either the spiral wave or coil spring-relief valves. However, the performance at lower equivalent sink rates of the MR landing gear damper with the spiral wave spring-based relief valve was better than that of the coil spring-based relief valve.

5.3.3 *Force Feedback Control: Bang-Bang Current Control Algorithm*

At higher sink rates, the MR valve of the landing gear damper is turned off, and only the passive valve is in effect; hence, the damping is dominated by passive viscous damping, which is proportional to velocity squared. In order to reduce harsh loads transmitted to the helicopter fuselage and the passengers, the stroking load must be maintained at or close to the desired

stroking load design threshold of 4000 lb_f. In this study, in order to maintain the peak stroking load of the MR landing gear damper constant over the desired sink rate range of 6-26 ft/s, a bang-bang current control algorithm formulated as in Figure 5.6 using a force feedback signal was used.

In the bang-bang current control algorithm, the damper force was measured using a load cell, and the control current input was determined by the force error between the desired force and the measured damper force. For the bang-bang current control algorithm, the control current input is given by the following equation:

$$i = \begin{cases} 4A, if\ (\epsilon F_d - F) > 0 \\ 0A, if\ (\epsilon F_d - F) \leq 0 \end{cases} \quad [5.2]$$

Here, ϵ is the control gain of the bang-bang control. F_d is the desired damper force and was set to 4000 lb_f. F is the actual measured damper force. Additional details of the control algorithm are discussed by (Choi *et al.*, 2012). Figure 5.7 presents the controlled damper force of the MR landing gear dampers with the spiral wave and coil spring-based relief valves versus the equivalent sink rate under the bang-bang current control. In this case, the spiral wave and coil spring-based valves produced the same maximum achievable equivalent sink rate of 18 ft/s. However, compared to the coil spring case, the spiral wave spring case shows better controlled damper force performance at relatively low sink rate range of 14 ft/s or below. Figure 5.8 illustrates the control gain of the bang-bang current control algorithm. As seen in this figure, the spiral wave spring-based relief valve case shows slightly more control sensitivity to the control gain compared to the coil spring-based relief valve case.

5.3.4 *Iron-Bird Drop Test with a Drop Mass of 2627 lbs*

To assess control performance of the MR landing gear systems, further testing of the iron-bird setup was conducted. The ballasted drop mass was 2627 lbs. Four MR landing gear dampers with spiral wave spring-assisted relief valves were incorporated (Figure 5.9) into the iron-bird drop test setup, as shown in Figure 5.10. The assembled spiral wave spring-based MR landing gear dampers were initially pressurized at 200 psi of nitrogen gas and were filled with 665 grams of MR fluid (MRF-132DG from Lord Corporation). In order to verify that all four assembled spiral wave spring-assisted MR landing gear dampers had a similar performance and prior to incorporating them in the iron-bird apparatus, single damper drop tests were conducted on each damper at the University of Maryland, as shown in Figure 5.11. This figure illustrates that all four assembled MR landing gear dampers show a similar damper force performance as it follows a similar trend as the best selected spiral wave spring-based MR landing gear damper single damper drop test performance. After these single damper drop tests were conducted, all four dampers were safely setup on the iron-bird drop test apparatus (Figure 5.10), and a front view of a basic representation of the iron-bird setup is presented in Figure 5.12 with the iron-bird position before impacting the ground, Figure 5.12 (a), and after impact, Figure 5.12 (b). In Figure 5.10, the Aft 1 and Aft 2 represent the rear left and right MR landing gear dampers, respectively. The Fwd 1 and Fwd 2 represent the front left and right MR landing gear dampers, respectively. The center of gravity (C.G.) of the drop mass was evenly balanced, so the ground could impact the four MR landing gear dampers equally during the drop test. At each damper top position, tri-axial load cells were installed to measure the actual damper force of the MR landing gear dampers in three axes. For damper force evaluation and damper force control purpose, only axial damper forces were used. At C.G. of the drop mass, an accelerometer was installed to

measure the drop acceleration. The damper stoppers were installed to prevent the MR landing gear dampers from exceeding the maximum damper stroke of 3.25 inches.

Figure 5.13 illustrates the maximum damper force at constant current input versus the maximum sink rate obtained from the iron-bird drop MR landing gear damper tests and the previous single damper drop tests conducted. In this case, the constant current inputs of 0 A and 4 A were chosen. In addition, the iron-bird drop testing at constant current input was conducted up to a sink rate of only 10 ft/s in order to reduce the risk of the testing fixture experiencing a failure. As shown in this figure, the iron-bird drop test results of MR landing gear dampers at constant current inputs are similar to the results of the single damper drop tests. Hence, single damper drop testing is a good method of estimating the damper force performance of the MR landing gear damper when compared to the iron-bird drop testing with constant current input cases.

5.3.4.1 Bang-Bang Current Control Algorithm for the Iron-Bird Drop Test

The bang-bang current control algorithm was used to regulate the damper force of the MR landing gear dampers over the desired sink rate range of 6-26 ft/s. In the bang-bang current control algorithm, the damper forces were measured using each load cell installed at each damper top position, and the control current inputs applied to each MR landing gear damper were individually determined by each force error between the desired force and the measured damper forces. For the bang-bang current control algorithm, the control current inputs, i_m, applied to the MR landing gear dampers at each damper position are given by:

$$i_m = \begin{cases} 4A, if\ (\varepsilon F_d - F_m) > 0 \\ 0A, if\ (\varepsilon F_d - F_m) \leq 0 \end{cases} \quad [5.3]$$

Here, m = Fwd 1, Fwd 2, Aft 1, Aft 2. The desired damper force, F_d, was again chosen to be 4000 lb_f. F_m is the actual damper force measured from the load cells at each damper top position. In this case, the drop mass sink rate was used. The block diagram of the bang-bang current control algorithm for the iron-bird drop test is presented in Figure 5.14.

Maximum damper forces measured at each damper top location averaged the maximum damper force. Figure 5.15 illustrates the maximum damper force under the bang-bang current control input versus the maximum sink rate obtained from the iron-bird drop tests using the MR landing gear dampers with a spiral wave spring-based relief valve. In this case, the iron-bird drop testing was conducted up to a sink rate of 26 ft/s. As shown in this figure, the bang-bang current control can maintain the MR landing gear damper force at the desired 4000 lb_f over a wide sink rate range. If the error bound is ±1000 lb_f, which represents a reasonable safety margin, the bang-bang current control can achieve the desired damper force up to the sink rate of 22 ft/s.

Figure 5.16 represents the control gain of the bang-bang current control used in the single damper drop and iron-bird drop tests. As seen in this figure, the control gain decreases as the sink rate increases. In the iron-bird drop case, the control gain is continuously changed until a sink rate of 16 ft/s. But, the control gain of the single damper drop test case is discontinuously varied.

5.4 Conclusions

In this effort, a full-scale, flow-mode type magnetorheological (MR) landing gear damper coupled with a spring-assisted passive (or relief) valve was designed, fabricated, and tested in order to expand the high end of the sink rate range from 12 ft/s (from the previous effort by Choi *et al.*, 2012) to 26 ft/s while maintaining a stroking load of 4000 lb_f over a desired sink rate range of 6-26 ft/s. The MR valve of the landing gear damper was designed using a Bingham-plastic

type damper model incorporating minor viscous loss factors, which are proportional to velocity squared. The spring-assisted relief valve of the landing gear damper was modeled by a single-degree-of-freedom mass-spring-damper lumped model, which predicted the force behavior of the relief valve of the MR landing gear damper to satisfy the desired stroking load of 4000 lb_f over the sink rate range of 12-26 ft/s.

From the laboratory tests, it was experimentally investigated that a desired stroking load of 4000 lb_f was held over a desired equivalent sink rate range of 6 -26 ft/s.

A single damper drop test setup was built to evaluate stroking loads of the MR landing gear damper for sink rates higher than 6 ft/s for a drop mass of 430 lbs first, then 1283 lbs. A force feedback control algorithm (bang-bang current control) was also developed. Using this force feedback controller, the stroking load was successfully regulated to maintain a constant stroking load of 4000 lb_f over a 6-18 ft/s equivalent sink rate range. Considering a force error bound of ±1000 lb_f, the maximum achievable equivalent sink rate range could be increased to 6-22 ft/s by using either the spiral wave or coil spring-relief valves. The spiral wave spring-relief valve performed better than the coil spring-relief valve at lower sink rate range, due to the spiral wave spring's axisymmetric shape around the center axis. For further iron-bird drop damper testing, the spiral wave srping-relief valve was chosen.

From a full-scale iron-bird drop testing (with a total drop mass of 2627 lbs), it was experimentally demonstrated that the MR landing gear dampers with a spiral wave spring-based relief valve could control the stroking load over a wider range of sink rates.

The bang-bang current control algorithm successfully regulated the stroking load at 4000 lb_f over a sink rate range of 6-16 ft/s in these iron-bird tests. If a force error bound of ±1000 lb_f was taken into account, the control was superior over a sink rate range of 6-22 ft/s, which by far

exceeds the sink rate range of the previous study (which was 6-12 ft/s). The single damper drop testing method was a good damper force estimation procedure as it showed similar testing results compared to the iron-bird testing, which emulated a full-scale lightweight helicopter.

References

Batterbee, D.C., Sims, N.D., Stanway, R., and Wolejsza, Z., (2007a) Magnetorheological landing gear: 1. A design methodology. *Smart Materials and Structures*, 16: 2429-2440. DOI: 10.1088/0964-1726/16/6/046.

Batterbee, D.C., Sims, N.D., Stanway, R., and Rennison, M., (2007b) Magnetorheological landing gear: 2. Validation using experimental data. *Smart Materials and Structures*, 16: 2441-2452. DOI: 10.1088/0964-1726/16/6/047.

Choi, Y.-T., and Wereley, N.M., (2003) Vibration control of a landing gear system featuring ER/MR fluids. *AIAA Journal*, 40(3): 432–439. DOI: 10.2514/2.3138.

Choi, Y.-T., Robinson, R., Hu, W., Wereley, N.M., Birchette, T.S., and Bolukbasi, A.O., (2012) Analysis and control of a magnetorheological landing gear system for a helicopter. Proceedings of the American Helicopter Society 68th Annual Forum & Technology Display, Fort Worth, TX, USA.

Lin, L.H., Yong, C., Qi, H., and Jian, L., (2009) Fuzzy PID control for landing gear based on magnetorheological (MR) damper. International Conference on Apperceiving Computing and Intelligence Analysis (ICACIA), 22-25. DOI: 10.1109/ICACIA.2009.5361162.

Mikulowski, G.M., and Holnicki-Szulc, J., (2007) Adaptive landing gear concept- feedback control validation. *Smart Materials and Structures*, 16: 2146-2158. DOI: 10.1088/0964-1726/16/6/017.

Mikulowski, G.M., and LeLetty, R., (2008) Advanced landing gears for improved impact absorption. Proceedings of the 11th International Conference on New Actuators, 363-366, Bremen, Germany.

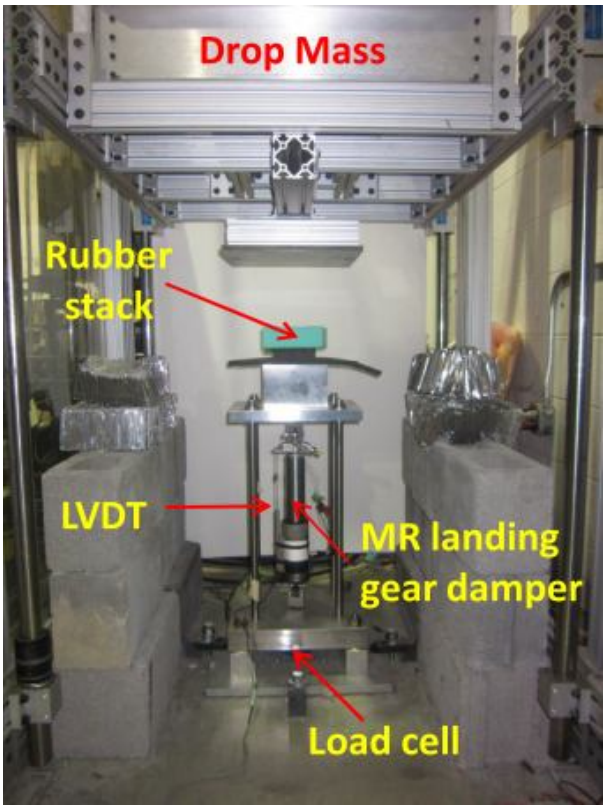

Figure 5.1. Single MR landing gear damper drop test setup at the University of Maryland

MR: magnetorheological

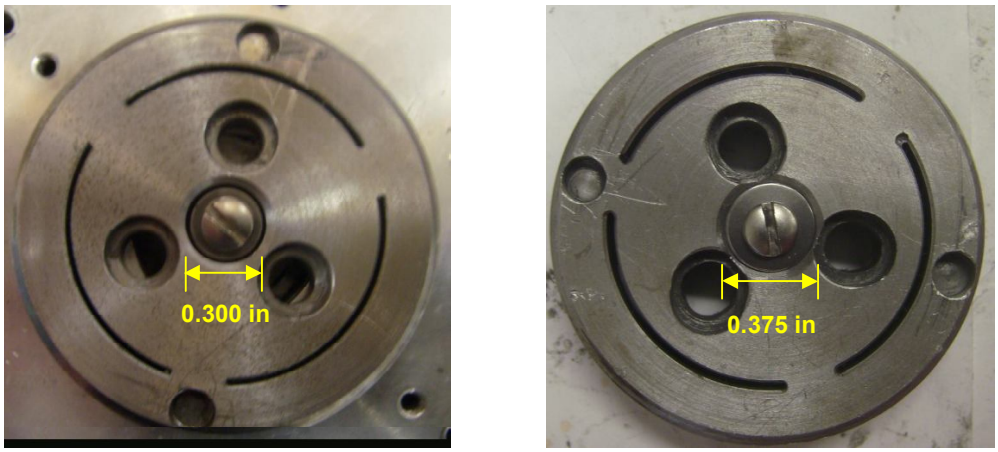

(a) (b)

Figure 5.2. Revison of the center orifice of the relief valve (a) original center orifice diameter: 0.300 in; (b) revised center orifice diameter: 0.375 in

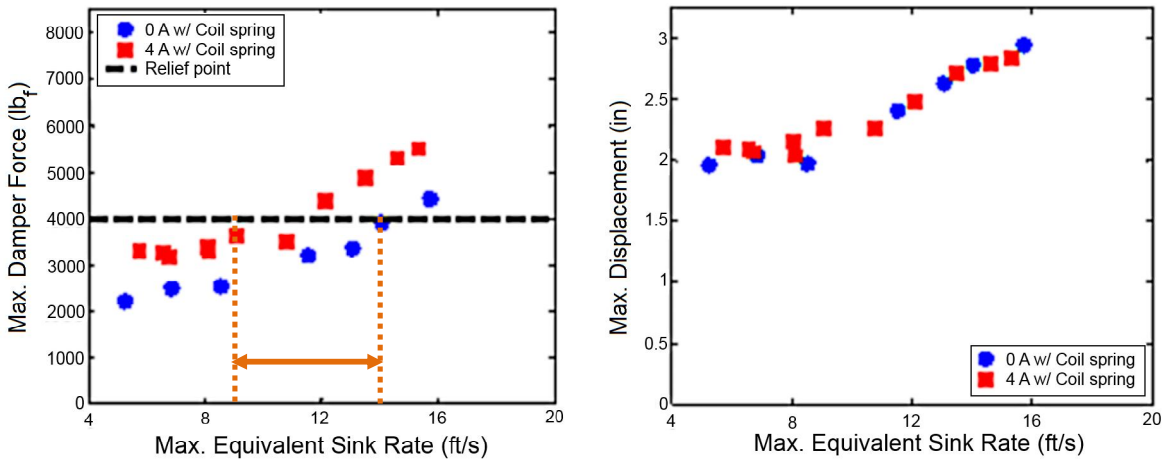

Figure 5.3. Maximum damper force of the MR landing gear damper with (a) coil spring-based MR landing gear damper with initial gas pressure of 200 psi; (b) maximum damper displacement

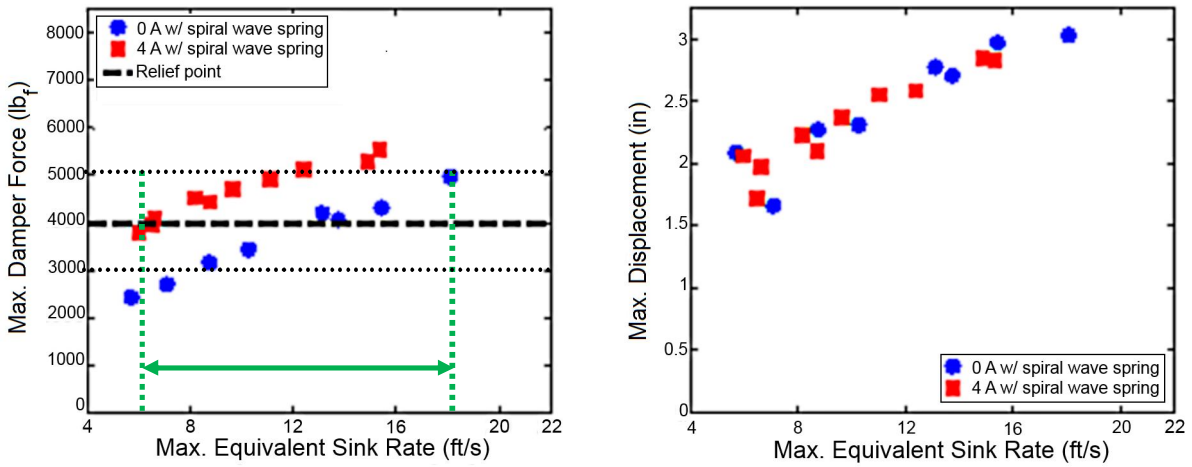

Figure 5.4. Maximum damper force of the MR landing gear damper with (a) spiral wave spring-based MR landing gear damper with initial gas pressure of 200 psi; (b) maximum damper displacement

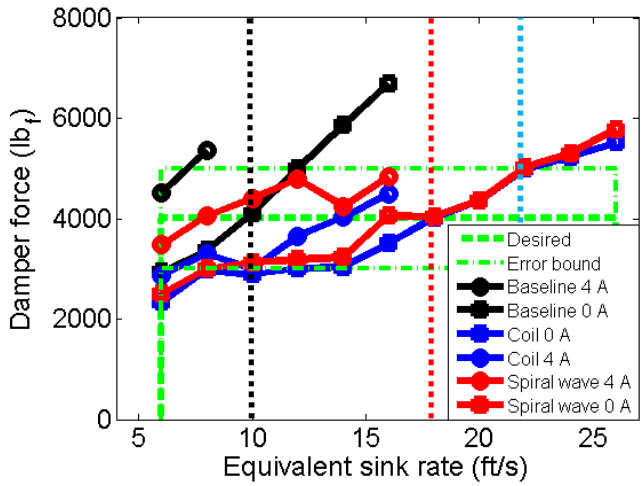

Figure 5.5. Maximum achievable equivalent sink rate of the MR landing gear dampers within a force error bound of ±1000 lb_f (the drop mass was 1283 lbs)

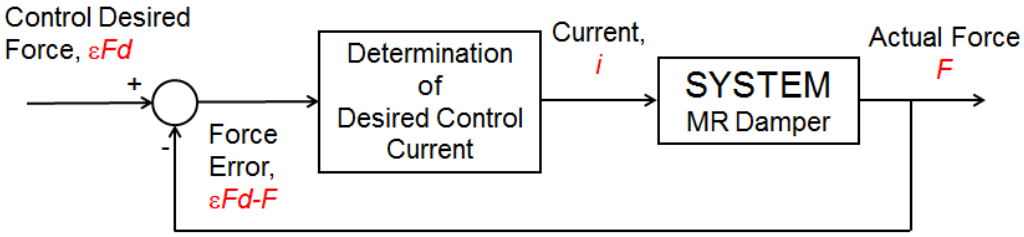

Figure 5.6. Block diagram of the bang-bang current control algorithm used for single MR landing gear damper drop tests

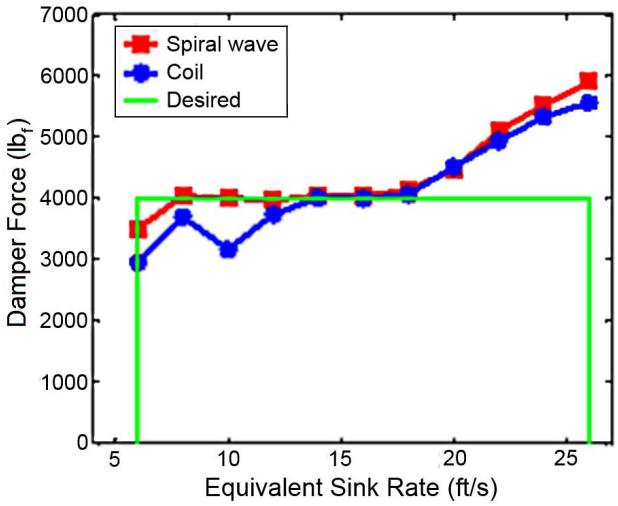

Figure 5.7. Controlled damper force of the MR landing gear dampers with the spiral wave and coil spring-based relief valves versus the equivalent sink rate under the bang-bang current control of the single-drop test device

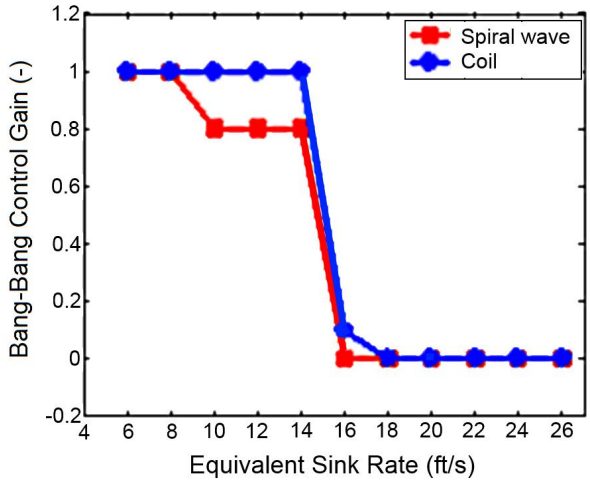

Figure 5.8. Control gain of the bang-bang current control for the single damper drop test

Figure 5.9. Photograph of the four spiral wave spring-based MR landing gear dampers used for the iron-bird drop test

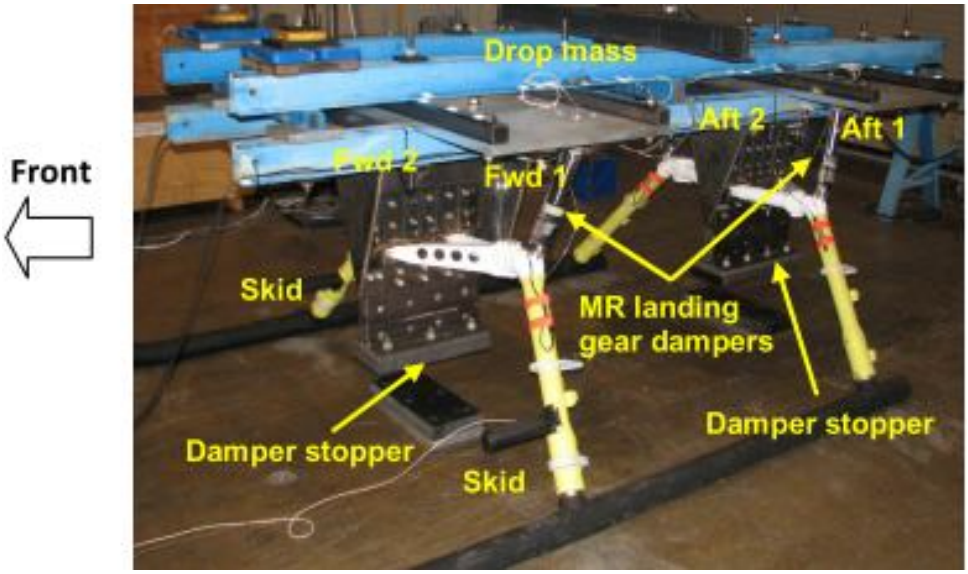

Figure 5.10. Experimental iron-bird drop test setup with four MR landing gear dampers coupled with spiral wave spring-assisted passive (or relief) valves

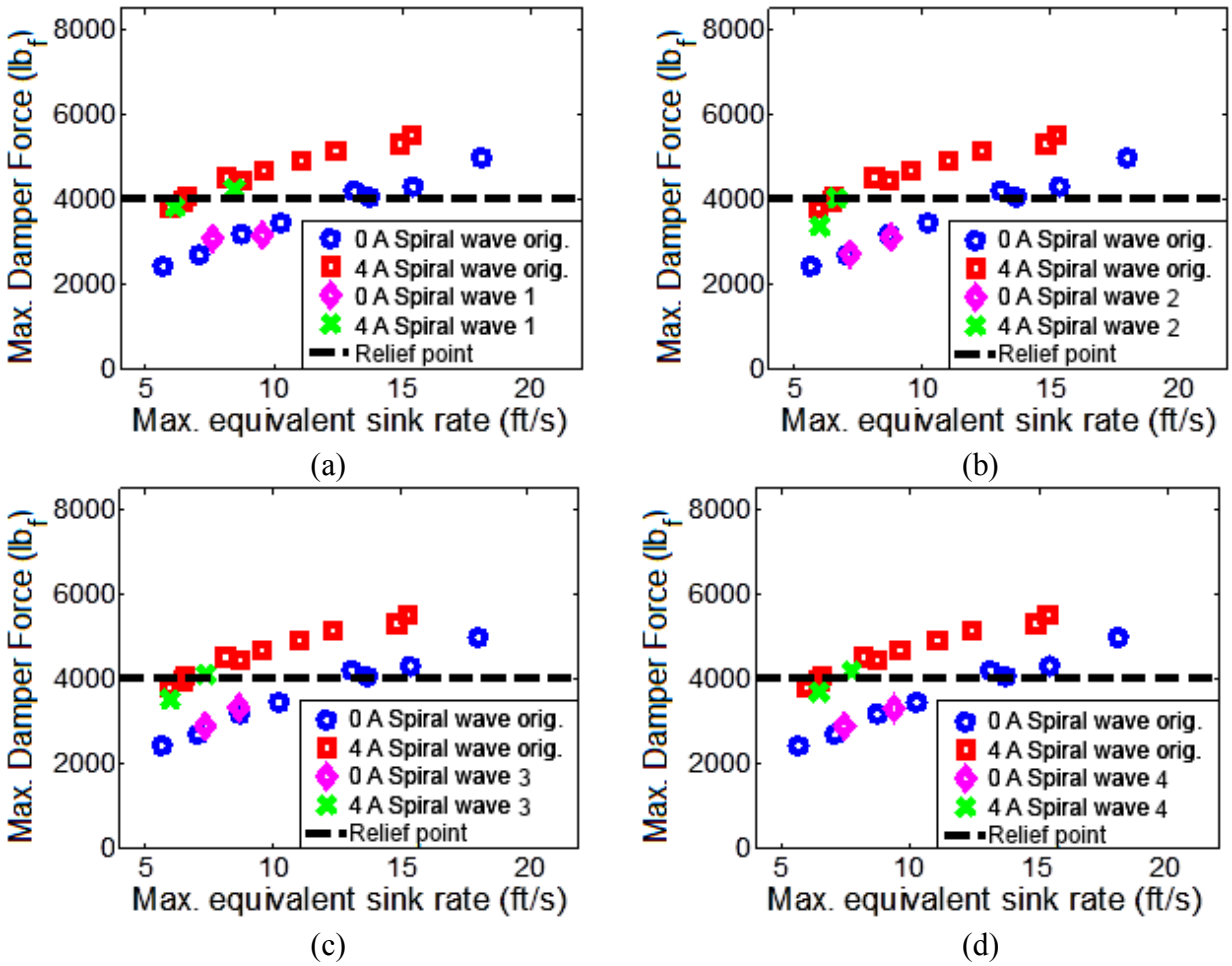

Figure 5.11. Maximum damper force versus maximum equivalent sink rate obtained from the single MR landing gear damper drop tests of all four spiral wave spring-based dampers at the University of Maryland with a drop mass of 430 lbs (a)-(d) are performances of spiral wave spring-based dampers 1 through 4, respectively.

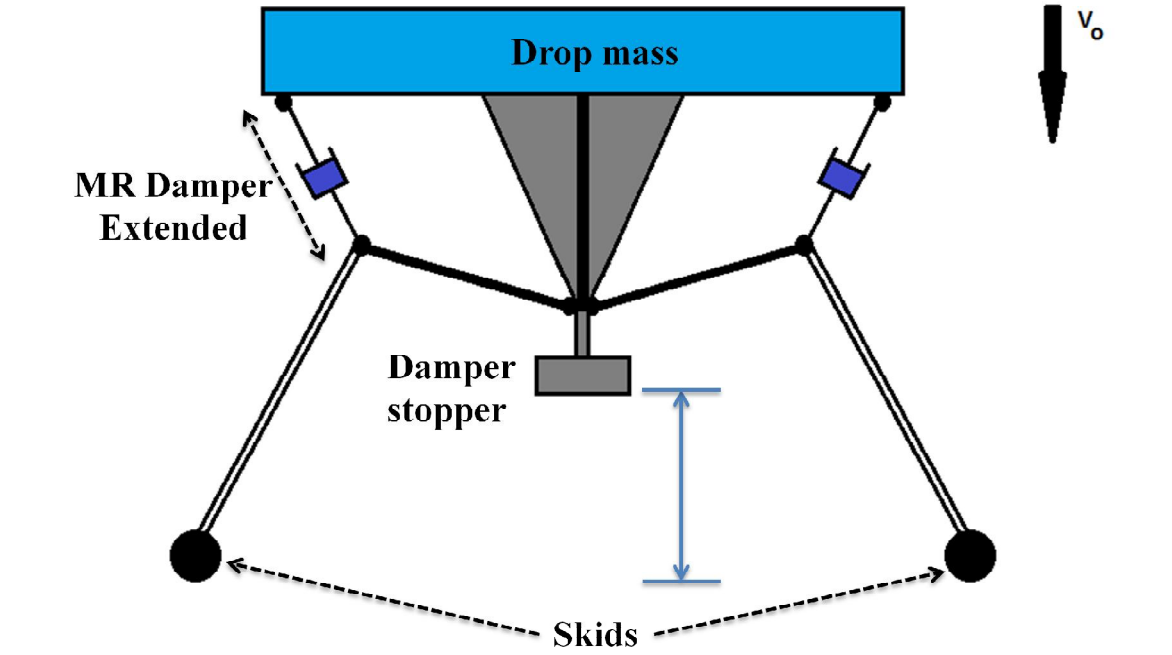

(a)

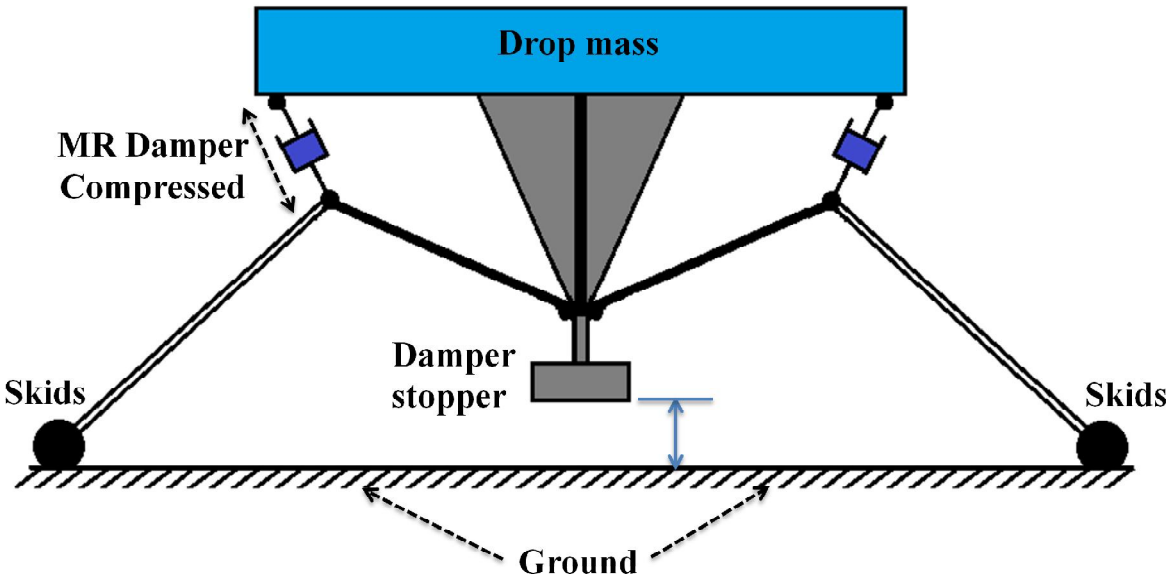

(b)

Figure 5.12. Basic front view representation of the iron-bird drop test setup (a) pre-impact: MR damper is extended; (b) post-impact: MR damper is compressed

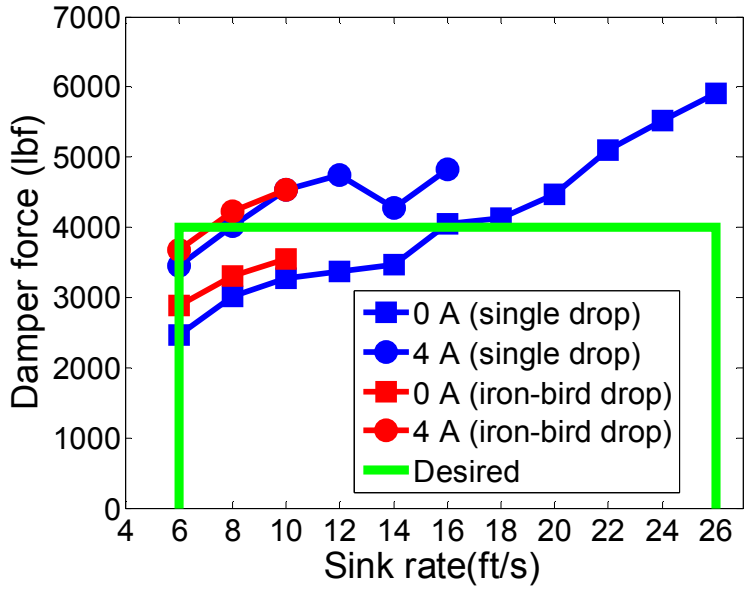

Figure 5.13. Maximum damper force at constant current input versus sink rate obtained from the iron-bird drop tests conducted at Boeing Structures Test Laboratory

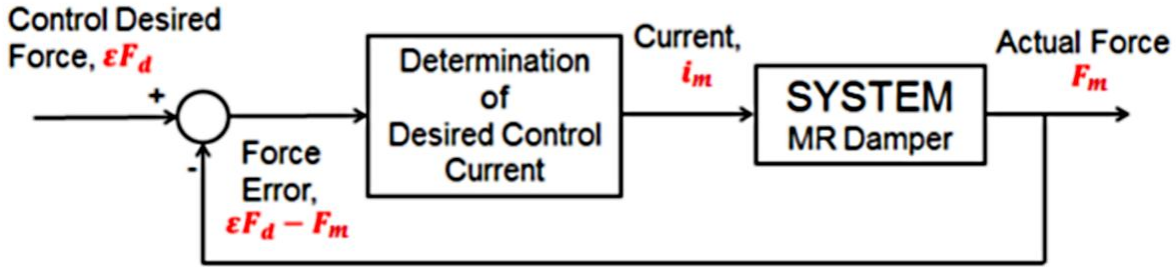

Figure 5.14. Block diagram of the bang-bang current control algorithm used for iron-bird MR landing gear dampers drop tests

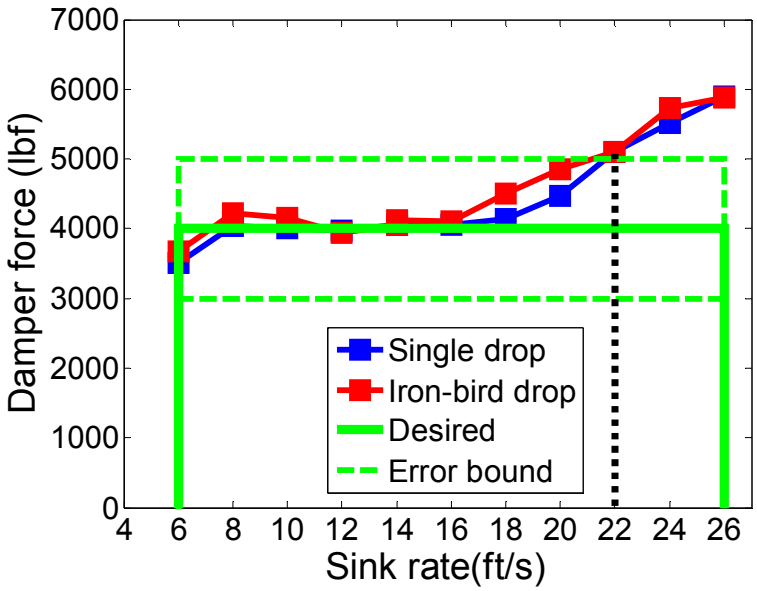

Figure 5.15. Maximum damper force under the bang-bang current control input versus the maximum sink rate obtained from the iron-bird drop tests using the MR landing gear dampers with a spiral wave spring-based relief valve

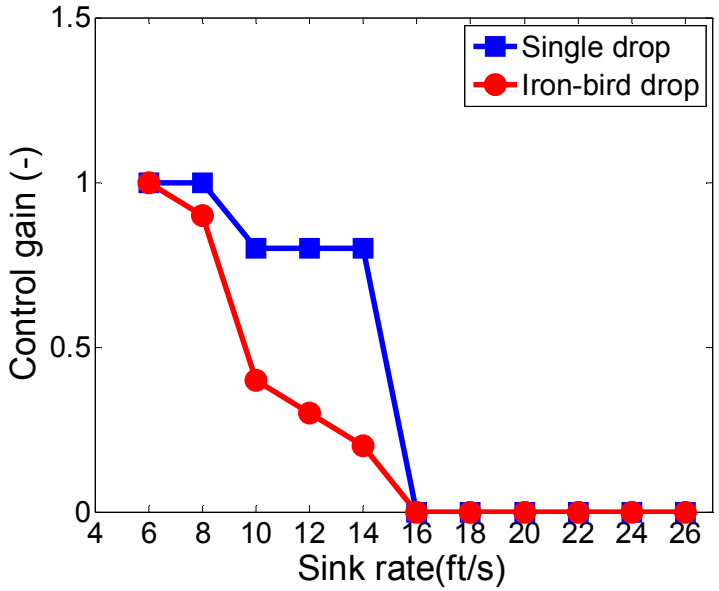

Figure 5.16. Control gain of the bang-bang current control versus sink rate for the single damper and iron-bird drop tests

CHAPTER 6: Nonlinear Modeling of Adaptive Magnetorheological Landing Gear Dampers with a Spring-Assisted Passive Valve under Impact Conditions

6.1 Introduction and Overview

The landing performance of a lightweight helicopter can be improved with adaptive landing gear dampers by continuously adjusting their stroking loads to provide shock mitigation capabilities and accommodate various operating conditions. In prior work, adaptive landing gear dampers have been investigated (Choi *et al.*, 2012; Choi and Wereley, 2003; Mikulowski and Holnicki-Szulc, 2007; Batterbee, *et al.*, 2007a; Batterbee *et al.*, 2007b; Lin *et al.*, 2009; Mikulowski and LeLetty, 2008). Adaptive magnetorheological (MR) landing gear dampers for a lightweight helicopter that maintained a constant peak stroking force of 4000 lb_f across sink rates ranging from 6-12 ft/s (1.8-3.7 m/s) were designed, fabricated and successfully tested (Choi *et al.*, 2012). In this follow-on effort, it was desired to expand the high end of the sink rate range, so that the peak stroking load could be held constant for sink rates ranging from 6-26 ft/s (1.8-7.9 m/s), thereby extending the high end of the speed range from 12 ft/s in the first study to 26 ft/s. A spring-based passive (or relief) valve MR landing gear system that has a constant cracking pressure was proposed for this study. In the prior chapter, we theoretically proposed and analyzed a bang-bang current control algorithm, formulated using a force feedback signal to maintain the peak stroking load of the MR landing gear damper constant over the desired sink rate range of 6-26 ft/s. The analysis was conducted using a single-degree-of-freedom (SDOF) as a modeling approach. Simulation results of the model showed that the stroking load was successfully regulated to maintain a constant stroking load of 4000 lb_f over a 6-18 ft/s equivalent

sink rate range. Considering a force error bound of ±1000 lb_f, the maximum achievable equivalent sink rate range could be increased to 6-22 ft/s by using either the spiral wave or coil spring-relief valves.

This chapter focuses on better understanding the behavior of the MR landing gear damper coupled with a spiral wave spring-assisted passive valve operating over the range of 6 -26 ft/s. Two models are examined in this study. The first one (model #1) is a nonlinear Bingham-Plastic (BP) type damper model incorporating the pressure drop due to the spring-assisted relief valve seal's opening, the MR valve minor loss factors, Darcy friction and viscous forces, which are proportional to the velocity squared. The second model (model #2) is a modified version of the first model as it considers, in addition to the pressure drop due to the relief valve seal's opening, the pressure drop across the center orifice of the relief valve to better account for the damper force behavior at higher speeds. This model includes minor loss factors, Darcy friction and viscous forces across the MR valve and the center orifice of the relief valve. In addition, the gas pressure inside the MR damper is considered; hence, the total force of the MR landing gear damper with a spiral wave spring-assisted relief valve includes the gas force.

These models were experimentally validated using single damper drop test data obtained from the drop tower facility at Boeing Structures Test Laboratory in Mesa, Arizona for nominal drop speeds of up to 26 ft/s / 2.7 (shaft velocity of 2.9 m/s). The dividing factor of 2.7 accounts for the kinematic relationship between the connection points of the MR landing gear damper to the fuselage and the landing skid as explained in chapter 5 section 5.3.1.2.

6.2 MR Valve Coupled with a Spring-Assisted Relief Valve

A full-scale, flow-mode type MR valve landing gear damper coupled with a spring-assisted passive valve that has a constant cracking pressure was developed to expand the high

end of the sink rate range from 12 ft/s, from prior work (Choi *et al.*, 2012), to 26 ft/s while maintaining a stroking load of 4000 lb_f over a desired sink rate range of 6-26 ft/s. The MR valve as designed to semi-actively control the peak stroking load over the 6-12 ft/s sink rate range, while the passive valve was designed to passively control the stroking load over the 12-26 ft/s sink rate range. The MR valve of the landing gear damper was designed using a nonlinear analytical Bingham-Plastic (BP) type damper model considering the field dependent behavior of MR fluids and nonlinear viscous loss factors that are dependent on velocity squared. The passive valve was designed based on a computer simulation related to spring dynamic equations of motion, which estimated the force behavior of the passive valve of the MR landing gear damper to meet the desired stroking load of 4000 lb_f over the desired sink rates of 12-26 ft/s. A spring-based passive valve MR landing gear damper was designed using the MR damper analysis then constructed. Two different springs were used (a conventional coil spring and a spiral wave spring) for the analysis. Based on better testing results obtained from the spiral wave spring-based MR landing gear damper, the spiral wave spring was selected for further testing of the MR landing gear damper in the iron-bird drop test apparatus at the Boeing Structures Test Laboratory in Mesa, Az.

6.3 Nonlinear Bingham Plastic-Type Modeling with Viscous Effects and Minor Losses in the Landing Gear Damper MR Valve Only (Model #1)

A hydraulic model of the MR and passive relief valves of the landing gear damper is presented in Figure 6.1. The routinely used Bingham-plastic (BP) model, which assumes a laminar flow range for all involved MR landing gear damper piston velocities, was extended to a nonlinear (turbulent) flow range, which is induced from high speed impact loadings. The MR

landing gear damper total force, F_t, in the BP-type nonlinear model incorporating turbulent flows is given by:

$$F_t = A_p \Delta P \quad [6.1]$$

Here, A_p is the effective piston area of the MR landing gear damper, and ΔP is the pressure drop across the valves.

6.3.1 Passive Relief Valve Closed

Relevant equations of the spring-assisted relief valve are revisited from Chapter 4. When the passive valve is closed, the seal closes the center orifice of the spring-assisted relief valve. Hence, the MR fluid passes only through the MR valve as shown in Figure 6.1 (a). The following equations then apply:

$$\Delta P = \Delta P_{mr} \quad [6.2]$$

$$\Delta P_{relief} = \infty \quad [6.3]$$

$$Q_p = A_p V_p = Q_{mr} \quad [6.4]$$

$$Q_{relief} = 0 \quad [6.5]$$

ΔP_{mr} is the pressure drop through the MR valve, and ΔP_{relief} is the pressure drop across the relief valve. Q_p is the total flow rate passing through the piston, and V_p is the piston velocity. Q_{mr} is the flow rate passing through the MR valve, and Q_{relief} is the flow rate passing through the relief valve. Here, the pressure drop through the MR valve, ΔP_{mr}, is derived from the BP-type nonlinear damper model incorporating minor loss factors, which are proportional to velocity squared, and the equation is given as follows:

$$\Delta P_{mr} = \left[nf \frac{\rho(L_a + L_c)}{4d_1} \left(\frac{Q_{mr}}{A_{mr}}\right)^2 + \frac{\rho\left(K_{entry} + K_{exit}\right)}{2} \left(\frac{Q_{mr}}{A_{mr}}\right)^2 \right] + \frac{2nL_a\tau_y}{d_1} \quad [6.6]$$

Here, ρ is the density of the MR fluid, L_a is the active MR valve length associated with one magnetic coil winding, and L_c is the length of one magnetic coil winding. A_{mr} is the flow area of the MR valve; n is the number of magnetic coil windings, and d_1 is the gap diameter of the MR valve. In Equation 6.6, there are minor losses due to the MR fluid flowing through an entrance and exit of the MR valve gap, which causes a sudden contraction and expansion of the flow. These minor losses represent additional energy dissipation in the flow, which generates additional pressure drop across the MR valve. Prior experimental work by Mao *et al.* (2013) demonstrated that minor losses are significant in flow behavior, especially at high piston velocities. K_{entry} and K_{exit} in Equation 6.6, are the minor loss factors in the MR valve associated with sudden entrance and exit effects, respectively. In this study, it was assumed that $K_{entry} = 0.7$ and $K_{exit} = 0.5$ (White, 1986; Idel'chik, 1994; Franzini and Finnemore, 1997; Spurk and Aksel, 2008).

The Darcy friction factor, f, is a piecewise continuous function of the Reynolds number, Re, and detailed equations are given in the reference by Choi, Yoo, and Wereley (2005b). In the laminar flow range, the Darcy friction factor is computed as:

$$f = \frac{96}{Re}, if\ Re \leq 2300 \qquad [6.7]$$

The Reynolds number is defined as follows:

$$Re = \frac{\rho V D_h}{\eta} \qquad [6.8]$$

V is the average velocity of the flow passing through the MR valve gap, and η is the MR fluid viscosity. It is important to note that the critical Reynolds number is chosen to be 2300 to ensure a laminar flow range for all $Re < 2300$ (Spurk and Aksel, 2008). To render the analysis simpler in this study, the MR valve annular flow path was approximated as a rectangular duct. Hence, the

hydraulic diameter, D_h, for a rectangular duct is obtained from (White, 1986, Franzini and Finnemore, 1997) the following equation:

$$D_h = 2d_1 \quad [6.9]$$

In the turbulent flow range, the Darcy friction factor is computed as:

$$\frac{1}{f^{0.5}} \approx 1.8\log_{10}\left[\left(\frac{\varepsilon}{3.7D_h}\right)^{1.11} + \frac{6.9}{4000}\right], \text{if } Re > 4000 \quad [6.10]$$

Here, ε, is the average wall roughness in the MR valve gap and is assumed to be 0.006 mm in this study to represent a smooth condition. Since there is no defined equation to calculate the friction factor, f, in the transition flow case from laminar to turbulent ($2300 < Re \leq 4000$), the convex combination (Slotine and Li, 1991) was used to compute the Darcy friction factor in this transitional region as follows:

$$f = (1-\alpha)\frac{96}{Re} + \alpha\frac{1}{\left\{1.8\log_{10}\left[\left(\frac{\varepsilon}{3.7D_h}\right)^{1.11} + \frac{6.9}{4000}\right]\right\}^2}, \text{if } 2300 < Re \leq 4000 \quad [6.11]$$

Here, the parameter, α, is expressed as:

$$\alpha = \frac{Re - 2300}{4000 - 2300} \quad [6.12]$$

Finally, in Equation 6.6, τ_y is the MR fluid yield stress (Wereley and Pang, 1998; Mao *et al.*, 2005).

6.3.2 Passive Relief Valve Open

When the relief valve is open, the seal opens the center orifice of the relief valve, which allows the MR fluid to pass through the MR valve as well as the center orifice. As a result, the damper force decreases because the MR fluid pressure in the center orifice drops; hence, the following equations apply:

$$\Delta P = \Delta P_{mr} = \Delta P_{relief} \quad [6.13]$$

$$Q_p = Q_{mr} + Q_{relief} \quad [6.14]$$

The pressure drop of the relief valve, ΔP_{relief}, is determined by the pressure drop due to the seal's opening as follows (Merritt, 1967; Choi *et al.*, 2005b):

$$\Delta P_{relief} = \frac{\rho Q_{relief}^2}{2\left(A_{open} C_d\right)^2} \quad [6.15]$$

It is important to note in this first model that Equation 6.15 is held under the assumption that the diameter of the center orifice is sufficiently large that its pressure drop is negligibly smaller than the pressure drop due to the valve being open. Here, the discharge coefficient, C_d, is given by:

$$C_d = \frac{C_v C_c}{\sqrt{1 - C_c^2 \left(\frac{A_{open}}{A_p}\right)^2}} \quad [6.16]$$

where C_v is the velocity coefficient (C_v = 1), and C_c is the contraction coefficient (C_c = 0.611) (Merritt, 1967). In addition, A_{open} is the flow area of the opened relief valve orifice, and is calculated by:

$$A_{open} = \pi d_o x \quad [6.17]$$

where d_o is the center orifice diameter and x is the displacement of the seal.

6.3.2.1 Single-Degree-of-Freedom Mass Spring Damper Lumped Model

Using a single DOF mass-spring-damper lumped model shown in Figure 6.2, the displacement of the seal was calculated by numerically solving the following equation

$$M\ddot{x} + c\dot{x} + kx = F_t \left(\frac{A_{relief}}{A_p}\right) - F_{s0} \quad [6.18]$$

where

$$F_{s0} = \left(\frac{A_{relief}}{A_p}\right) 4000\ lb_f \quad [6.19]$$

Here, M is the mass of the seal, and c is the damping of the spring, k is the stiffness of the spring, and A_{relief} is the cross-sectional area of the center orifice.

6.3.2.2 Calculation of Flow Rates

The flows at each path depend on the pressure drop, and the fluid resistances are nonlinear functions of flow rates. The flow rates Q_{mr} and Q_{relief} are not directly determined from the total flow rate, Q_p. Therefore, a numerical iteration method (Choi *et al.*, 2005b) was used to calculate each flow rate. First, the iteration method begins with guessing the initial flow rates as follows:

$$Q_{mr}^{-} = \frac{Q_p}{2} \text{ and } Q_{relief}^{-} = \frac{Q_p}{2} \quad [6.20]$$

Using Eq. 6.6 with initial flow rates Q_{mr}^{-} and Q_{relief}^{-}, the new flow rate, Q_{relief}^{+} is computed as follows:

$$Q_{relief}^{+} = \left| A_{open} C_d \sqrt{\frac{2\Delta P_{mr}|_{Q_{mr}=Q_{mr}^{-}}}{\rho}} \right| \quad [6.21]$$

Where $\Delta P_{mr}|_{Q_{mr}=Q_{mr}^{-}}$ is obtained by replacing Q_{mr} with Q_{mr}^{-} in Eq. 6.6. Then, it is necessary to calculate the error of the estimated total flow rate as follows:

$$\left|\left(Q_{relief}^{+} + Q_{mr}^{-}\right) - Q_p\right| \leq \gamma \quad [6.22]$$

Here, γ is the predefined error. If the error of the estimated total flow rate is not smaller than the predefined error, then the new initial flow rate, Q_{mr}^{+}, of the MR valve needs to be increased or decrease by:

$$Q_{mr}^{+} = (1 \pm \delta) Q_{mr}^{-} \quad [6.23]$$

Here, δ is the convergence rate of the estimation to the flow rate.

6.3.3 *Design of the Spring-Assisted Passive Valve of the MR Landing Gear Damper*

The predicted damper force of the MR landing gear damper with the spring-based passive valve was estimated to meet the desired stroking load of 4000 lb_f over the desired sink rate range of 6 to 26 ft/s using equations 6.1 to 6.23. Figure 6.3 represents the predicted damper force versus sink rate. For each case, a half-sine function was theoretically calculated to simulate the piston velocity of the MR landing gear damper as shown in Figure 6.4. The maximum sink rate of this particular case is 26 ft/s (7.9 m/s). A spring stiffness of $k = 50\ lb_f/in$ (8.75 N/mm) was chosen. As illustrated in Figure 6.3, the damper force (F_{ON}) generated by the activating the MR valve can theoretically meet the desired stroking load of 4000 lb_f at the low sink rate of 6 ft/s. Then, at higher sink rate, the MR landing gear damper theoretically meets the desired stroking load by turning the MR valve off and releasing additional MR fluid by cracking the pressure when the center orifice relief valve opens up.

6.4 Single Damper Drop Tests

In order to experimentally evaluate the force of the MR landing gear damper with the passive relief valve at higher sink rates and emulate impact conditions, single damper drop tests were conducted using a drop tower facility at the Boeing Structures Test Laboratory in Mesa, Arizona. One set of tests was conducted using a landing gear damper having an MR valve only (baseline), and another set of tests was conducted using a landing gear damper having an MR valve coupled with a spiral wave spring-assisted relief valve. These two tests are considered for the analysis in this chapter. The dampers were pressurized at 200 psi, and the ballasted drop mass was 1283 lbs. The equivalent sink rate, $V_{eq.sink}$, was determined by the following equation:

$$V_{eq.sink} = 2.7\sqrt{2gh_{drop}} \qquad [6.24]$$

Here, g is the gravitational acceleration, and h_{drop} is the initial drop height. A factor of 2.7 was used to emulate the kinematic correlation between the skid of a helicopter and the location of the installed MR landing gear damper.

Data from the load cell and the LVDT (Linear Variable Differential Transformer) were recorded with a sampling rate of 1 kHz. The LVDT data were differentiated by the data acquisition system to produce the velocity data. A second-order low-pass Butterworth filter with a 100 Hz cutoff frequency was used to filter the recorded load cell data for force evaluation and the LVDT data for damper stroke and velocity evaluations of the MR landing gear damper with spring-assisted relief valve.

6.5 Drop Test Results and Predicted Results from Model #1

The predicted damper piston velocity in equation 6.25 and illustrated in Figure 6.4 was utilized to estimate velocity time histories from the drop test:

$$V_p(t) = V_{p0} \sin\left(\frac{\pi t}{t_d}\right) \qquad [6.25]$$

Here, V_{po} is the initial impact velocity obtained from the initial condition, and t_d is the duration of the impact event. Filtered sample test data are shown in Figures 6.5 through 6.7. As illustrated in Figure 6.8, the predicted velocity response was plotted versus the actual velocity data, it is important to note that the impact of 6 ft/s (1.83 m/s) occurred at 50 ms. Other velocity peaks observed before 50 ms from the actual data are noise related. The modeled velocity predicts the actual velocity time history well.

The predicted MR landing gear damper force time histories of were obtained from the nonlinear BP-type model (model #1) and plotted versus the actual transient force responses. Figures 6.9 (a) and (b) show the experimental force results of the baseline damper at a nominal

speed of 6 ft/s for the field-OFF and the field-ON cases plotted versus the predicted force time responses. The predicted damper force response from model #1 (nonlinear BP-type model with viscous effects and minor losses in the MR valve gap) tends to under predict the damper force for the field-OFF case. The maximum damper force is well captured for the field-ON case in Figure 6.9 (b); however, the modeled force does not seem to capture the effect of a time delay occurring in the actual experimental force data. In Figures 6.10 (a) and (b), the predicted force response tends to slightly under predict the MR landing gear damper experimental field-OFF force during the impact period at 6 ft/s. For the field-ON case, as the model tends to slightly over predict the total damper force time history, it does not emulate the time delay occurring in the actual filtered test data similarly to the baseline damper field-ON case. At a sink rate of 16 ft/s (4.9 m/s) in Figures 6.11 (a) and (b), the nonlinear model #1 predicts well the maximum damper force response for the field-OFF case; however, for the field-ON case, the model under predicts the maximum damper force. At higher sink rates of 22 and 26 ft/s (6.7 m/s and 7.9 m/s, respectively) in Figures 6.12 (a) and (b), the model does not capture higher forces, and it estimates a peak force of about 4500 lb_f (20,017 N) for the spiral wave spring-based damper force while the actual peak force is around 5000 lb_f (22,241 N) for 22 ft/s and 6000 lb_f and (26,689 N) for 26 ft/s. The BP-type model #1 significantly under predicts the peak damper force by about 25% at a sink rate of 26 ft/s.

6.6 Nonlinear Bingham Plastic-Type Modeling with Viscous Effects and Minor Losses in the MR and Relief Valves (Model #2)

6.6.1 Pressure Drop across the Center Orifice of the Relief Valve

In the previous model #1, it was assumed that the center orifice diameter, d_o, of the MR landing gear damper relief valve was sufficiently large that the pressure drop across the center

orifice was negligibly smaller than the pressure drop due to the seal's opening. The first model simulated results showed that higher forces were not well captured. Hence, in this second model, the assumption is reconsidered. The pressure drop across the relief valve, ΔP_{relief}, is now produced from the pressure drop due to the seal's opening as well as the viscous and minor loss effects in the center orifice as shown in Figure 6.13. Hence, Equation 6.15 is modified as follows:

$$\Delta P_{relief} = \frac{\rho Q_{relief}^2}{2(A_{open}C_d)^2} + f_{or}\frac{\rho L_o}{2d_o}\left(\frac{Q_{relief}}{A_{relief}}\right)^2 + \frac{\rho(K_{en.or} + K_{ex.or})}{2}\left(\frac{Q_{relief}}{A_{relief}}\right)^2 \quad [6.26]$$

In Equation 6.26, L_o is the center orifice length, and f_{or} is the Darcy friction factor considered from the center orifice, which satisfies Equations 6.7 to 6.12; however, in Equation 6.9, the hydraulic diameter is replaced with d_o, the diameter of the center orifice of the passive valve:

$$D_h = d_o \quad [6.27]$$

Minor losses due to the MR fluid flowing through the entrance and exit of the center orifice of the relief valve cause a sudden contraction and expansion of the flow. These minor losses represent additional energy dissipation in the flow, which generates additional pressure drop across the center orifice of the relief valve. $K_{en.or}$ and $K_{ex.or}$ in Equation 6.26, are the minor loss factors in the center orifice of the relief valve associated with sudden entrance and exit effects, respectively. In this study, it was assumed that $K_{en.or} = 0.7$ and $K_{ex.or} = 1$ (Merritt, 1967). The total minor loss factor is expressed in Equation 6.28:

$$K_{tot.or} = K_{en.or} + K_{ex.or} \quad [6.28]$$

In order to facilitate flow rates calculation, Equation 6.26 is expressed in the following form:

$$\Delta P_{relief} = \frac{\rho Q_{relief}^2}{2d_o}\left\{\frac{d_o A_{relief}^2 + [f_{or}L_o + d_o(K_{tot.or})](A_{open}C_d)^2}{(A_{open}A_{relief}C_d)^2}\right\} \quad [6.29]$$

6.6.1.1 Calculation of Flow Rates

As the flow at each path depends on the pressure drop and fluid resistances are nonlinear functions of flow rates, the flow rates Q_{mr} and Q_{relief} are calculated through a numerical iteration method (Choi *et al.*, 2005b). The iteration method starts with estimating the initial flow rates as in equation 6.20, then using equation 6.6 with initial flow rates Q_{mr}^{-} and Q_{relief}^{-}. The new flow rate, Q_{relief}^{+} is subsequently computed as follows:

$$Q_{relief}^{+} = \left| A_{open} A_{relief} C_d \sqrt{\frac{2d_o}{\rho}} \left\{ \frac{\Delta P_{mr}|_{Q_{mr}=Q_{mr}^{-}}}{d_o A_{relief}^2 + \left[f_{or} L_o + d_o (K_{tot.or}) \left(A_{open} C_d \right)^2 \right]} \right\} \right| \qquad [6.30]$$

$\Delta P_{mr}|_{Q_{mr}=Q_{mr}^{-}}$ is obtained from replacing Q_{mr} in Equation 6.6 with Q_{mr}^{-}. It is essential to calculate the error of the estimated total flow rate as in equation 6.22, and if the error of the estimated total flow rate is not smaller than the predefined error, γ, then the new initial flow rate, Q_{mr}^{+}, of the MR valve needs to be increased or decreased by equation 6.23.

6.6.2 Time Constant

In order to emulate time delay in the damper yield force (field-dependent damper force) for practical application, the pressure drop associated with the MR fluid yield stress is assumed to pass through a low-pass filter as follows:

$$\dot{\widetilde{\Delta P}}_{MRF} = \frac{\Delta P_{MRF}}{\tau_s} - \frac{\widetilde{\Delta P}_{MRF}}{\tau_s} \qquad [6.31]$$

Here, $\widetilde{\Delta P}_{MRF}$ is the emulated pressure drop associated with the MR fluid yield stress, and τ_s is the time constant of the MR damper. In table 6.1, key parameters used in this study for the spiral wave spring-based MR landing gear damper are specified. Time constants of MR dampers are usually dependent on the MR fluid viscosity and density as well as the geometry of the MR valve

(Choi and Wereley, 2002), and are in the range of 5-10 ms. The pressure drop associated with the MR fluid yield stress is defined in the following equation:

$$\Delta P_{MRF} = \frac{2nL_a\tau_y}{d_1} \quad [6.32]$$

The pressure drop associated with the MR fluid yield stress, ΔP_{MRF}, was substituted by $\widetilde{\Delta P}_{MRF}$ in Equation 6.6, which in turn, affects the simulated response of the total damper force, F_t, in Equation 6.18.

6.6.3 Theoretical Analysis of the Gas Pressure

From the first set of single damper drop tests conducted at the University of Maryland, College Park, the initial gas pressure of the MR damper was increased to 200 psi to handle impact loadings of sink rates higher than 12 ft/s (3.7 m/s). Thus, for the set of tests conducted at the Boeing Structures Test Laboratory in Mesa, Arizona, initial gas pressure effect on the spring force was theoretically calculated. In order to simplify the analysis, the fully extended MR landing gear damper with the spring-assisted relief valve was divided into two control volumes that indicated the volume chambers where the gas pressure had an effect, as shown in Figure 6.14. By applying Boyle's law (Mao *et al*., 2013) to chamber # 2, assuming isothermal conditions, the spring force, F_{sp}, due to the gas pressure of the MR landing gear damper can be determined by the following equation:

$$F_{sp} = A_p P_i \left(\frac{V_{2i}}{V_{2i} - A_p S}\right) \quad [6.33]$$

Here, P_i is the initial gas pressure inside the MR damper and V_{2i} is the initial gas volume:

$$V_{2i} = A_p l_2 \quad [6.34]$$

where $l_2 = 4.86e^{-4}m$.

Here, l_2 is the length of chamber #2. In Equation 6.33, S is the MR damper piston stroke, which is the same as the damper piston displacement, y_p, in Figure 6.14. The damper stroke, S, is in the range of 0 to 8.26 cm (0 to 3.25 inches) and is estimated by integrating piston velocity, V_p, in Equation 6.35:

$$S(t) = V_{p0}\frac{t_d}{\pi}\left[1 - \cos\left(\frac{\pi t}{t_d}\right)\right] \quad [6.35]$$

Moreover, the piston area, A_p, is expressed as:

$$A_p = \frac{\pi D_p^2}{4} \quad [6.36]$$

where $D_p = 5.36e^{-2}\ m$ (or $2.11\ in$).

Using a single DOF mass-spring-damper lumped model, the displacement of the seal was calculated by numerically solving equation 6.18 with the following equation for the total damper force, F_t, shown below:

$$F_t = A_p\Delta P + F_{sp} \quad [6.37]$$

6.7 Drop Test Results and Predicted Results from Model #2

The actual force responses from the drop tests were plotted versus the predicted force time histories using the modified nonlinear BP-type model with the viscous effects and minor losses across the MR and passive relief valves, in addition to the gas force (model #2). Utilizing the predicted piston velocity, Figures 6.15 (a) and (b) show that model #2 estimates the maximum damper force well (within 1% for the field-OFF case and 7.2% for the field-ON case) for the baseline MR landing gear damper. Figures 6.16 (a) and (b) show that model #2 tends to slightly over estimate the MR landing gear damper field-OFF-and-ON forces during the impact period at 6 ft/s for the spiral wave spring-assisted MR landing gear damper. For the field-ON case, as the model tends to slightly over predict the total damper force time history, it also

emulates the time delay occurring in the actual experimental data. At the end of the impact, the predicted results in Figures 6.15-6.18 all account for the gas force, which make the damper force decrease slowly then level off as the end of the landing event approaches. At a sink rate of 16 ft/s, model #2 tends to over predict the maximum force time history for the field-OFF case in Figure 6.17 (a) but captures the maximum damper force response very well for the field-ON case in Figure 6.17 (b). At higher sink rates of 22 ft/s (6.7 m/s) in Figure 6.18 (a) and 26 ft/s (7.9 m/s) in Figure 6.18 (b), model #2 captures higher forces very well (within 7%). The model #2 predicts the actual results better than model #1.

6.8 Conclusions

This chapter focused on the effectiveness of two nonlinear models to predict the performance of MR landing gear dampers over sink rates ranging from low (6 ft/s or 1.8 m/s) to high speed (26 ft/s or 7.9 m/s) impact conditions.

Two models were investigated using the drop test data conducted at the Boeing Structures Test Laboratory in Mesa, Arizona of both MR landing gear dampers with an MR valve only (baseline) and with a spiral wave spring-assisted passive valve. The first model was a nonlinear Bingham-Plastic (BP)-type flow model incorporating viscous effects and minor loss factors only across the MR valve of the landing gear damper (model #1). The second model was a modified version of the nonlinear BP-type flow model, incorporating viscous effects and minor loss factors across both the MR and passive relief valves of the landing gear damper (model #2); also, a force was included in the analysis that accounted for the gas pressure in the gas over oil oleo configuration used here.

On the one hand, results demonstrated that model #1 could not accurately predict the baseline and spiral wave spring-assisted passive valve MR landing gear dampers force behavior

for the field-OFF case, but the model was able to predict the maximum damper force behavior for the field-ON case at a low sink rate of 6 ft/s. Further impact speeds examination showed that model #1 could not adequately predict higher forces at sink rates higher than 16 ft/s as the model under predicted the damper force by about 25% at high sink rate of 26 ft/s. In addition, model #1 was not accounting for the time delay occurring in the actual experimental data for the field dependent damper force behavior and the effect of the gas force.

On the other hand, model #2 was more useful than model #1 as it captured the baseline and spiral wave spring-assisted MR landing gear dampers force histories from the drop test data more accurately. The second model (model #2) accounted for the time delay occurring in actual data as well as the gas force. The model accurately described the MR landing gear dampers force responses at sink rates ranging from 6 ft/s to 26 ft/s for the Field-OFF and ON cases while capturing the maximum damper forces at higher impact speeds of 26 ft/s within 7% for the field-OFF case. Model #2 predicted the landing gear damper behavior more accurately than model #1 because model #2 reconsidered the assumption held by model #1 that the diameter of the center orifice was big enough, so that its pressure drop is negligibly smaller than the pressure drop due to the seal's opening. Model #2 considered and included the pressure drop across the passive relief valve center orifice in addition to the pressure drop across the MR valve, which allowed for a better prediction of high-speed forces.

References

Batterbee, D.C., Sims, N.D., Stanway, R., and Wolejsza, Z., (2007a) Magnetorheological landing gear: 1. A design methodology. *Smart Materials and Structures*, 16: 2429-2440. DOI: 10.1088/0964-1726/16/6/046.

Batterbee, D.C., Sims, N.D., Stanway, R., and Rennison, M., (2007b) Magnetorheological landing gear: 2. Validation using experimental data. *Smart Materials and Structures*, 16: 2441-2452. DOI: 10.1088/0964-1726/16/6/047.

Choi, Y.-T., and Wereley, N.M., (2002) Comparative analysis of the time response of electrorheological and magnetorheological dampers using nondimensional parameters. *Journal of Intelligent Material Systems and Structures*, 13(7/8): 443-451. DOI: 10.1106/104538902028557.

Choi, Y.-T., and Wereley, N.M., (2003) Vibration control of a landing gear system featuring ER/MR fluids. *AIAA Journal*, 40(3): 432–439. DOI: 10.2514/2.3138.

Choi, Y.-T., Yoo, J.H., and Wereley, N.M., (2005b) Double adjustable magnetorheological dampers for a gun recoil system. International Mechanical Engineering Congress and Exposition (IMECE), Orlando, FL, USA.

Choi, Y.-T., Robinson, R., Hu, W., Wereley, N.M., Birchette, T.S., and Bolukbasi, A.O., (2012) Analysis and control of a magnetorheological landing gear system for a helicopter. Proceedings of the American Helicopter Society 68th Annual Forum & Technology Display, Fort Worth, TX, USA.

Franzini, J.B., and Finnemore, E.J., (1997) *Fluid Mechanics with Engineering Applications*, McGraw Hill.

Idel'chik, I.E., (1994) *Handbook of Hydraulic Resistance,* 3rd Edition, CRC Press, FL, USA.

Lin, L.H., Yong, C., Qi, H., and Jian, L., (2009) Fuzzy PID control for landing gear based on magnetorheological (MR) damper. International Conference on Apperceiving Computing and Intelligence Analysis (ICACIA), 22-25. DOI: 10.1109/ICACIA.2009.5361162.

Mao, M., Choi, Y.-T., and Wereley, N.M., (2005) Effective design strategy for a magnetorheological damper using a nonlinear flow model. Proceedings of SPIE, 5760: 446-455. DOI: 10.1117/12.601061.

Mao, M., Hu, W., Wereley, N.M., Browne, A.L., Ulicny, J.C., and Nancy, J., (2013) A nonlinear analytical model for magnetorheological energy absorbers under impact conditions. *Journal of Intelligent Material Systems and Structures*, 22(115015): 1-12. DOI: 10.1088/0964-1726/22/11/115015.

Merritt, H.E., (1967) *Hydraulic Control Systems*. John Wiley & Sons, New York, USA.

Mikulowski, G.M., and Holnicki-Szulc, J., (2007) Adaptive landing gear concept- feedback control validation. *Smart Materials and Structures*, 16: 2146-2158. DOI: 10.1088/0964-1726/16/6/017.

Mikulowski, G.M., and LeLetty, R., (2008) Advanced landing gears for improved impact absorption. Proceedings of the 11th International Conference on New Actuators, 363-366, Bremen, Germany.

Slotine, J.J.E., and Li, W., (1991) *Applied Nonlinear Control*. New Jersey, Prentice-Hall, 283-284.

Spurk, J.H., and Aksel, N., (2008) *Fluid Mechanics*, 2nd Edition. Springer-Verlag, Berlin Germany. DOI 10.1007/978-3-540-73537-3.

Wereley, N.M., and Pang, L., (1998) Nondimensional analysis of semi-active electro- and magneto-rheological dampers using parallel plate models. *Smart Materials and Structures*, 7: 732-743. DOI: 10.1088/0964-1726/7/5/015.

White, F.M., (1986) *Fluid Mechanics*, 2nd Edition, McGraw-Hill, Ohio, USA.

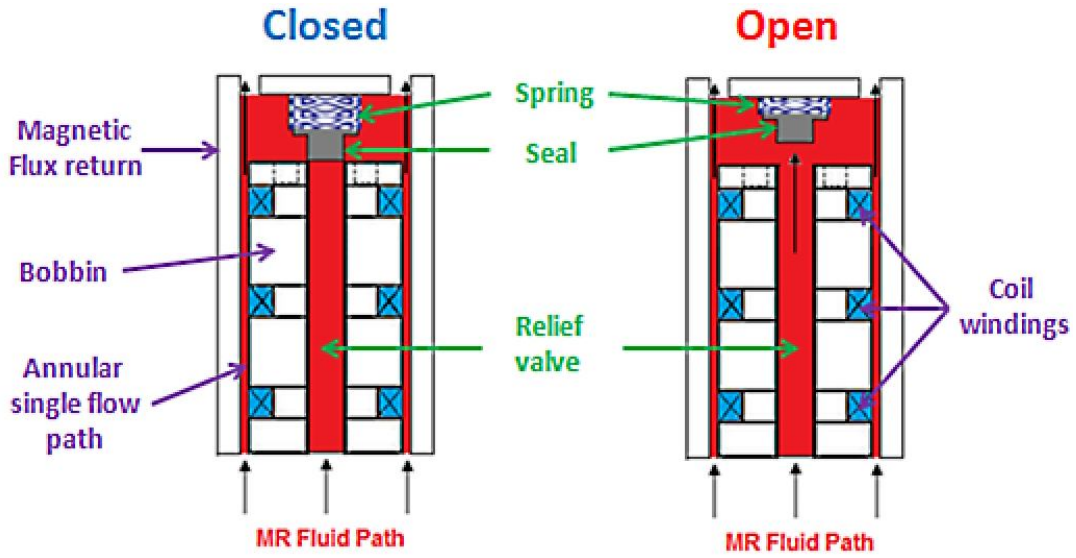

(a) (b)

Figure 6.1. Schematic and cross-sectional view of the MR valve coupled with a spring-assisted passive (or relief) valve in the landing gear damper for a lightweight helicopter; (a) passive valve closed and (b) passive valve open

MR: Magnetorheological

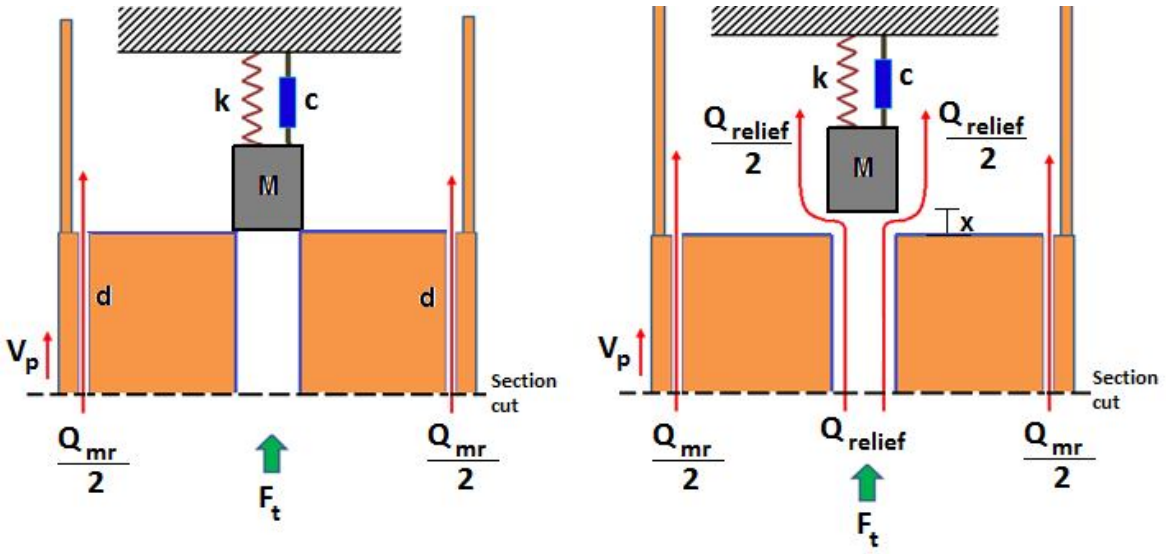

(a) (b)

Figure 6.2. Hydraulic model of the MR and passive valves of the MR landing gear damper: (a) Relief valve is closed and the MRF only flows through the MR valve; (b) Relief valve is open and the MRF flows through two paths: the MR valve and the center orifice relief valve

MRF: Magnetorheological fluid

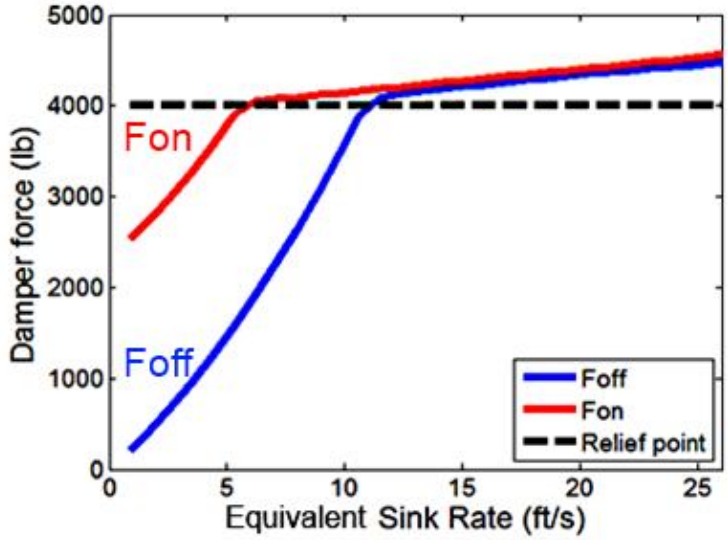

Figure 6.3. Predicted damper force of the relief valve of the MR landing gear damper versus sink rate with a desired spring stiffness of 50 lb_f/in (8.76 kN/m)

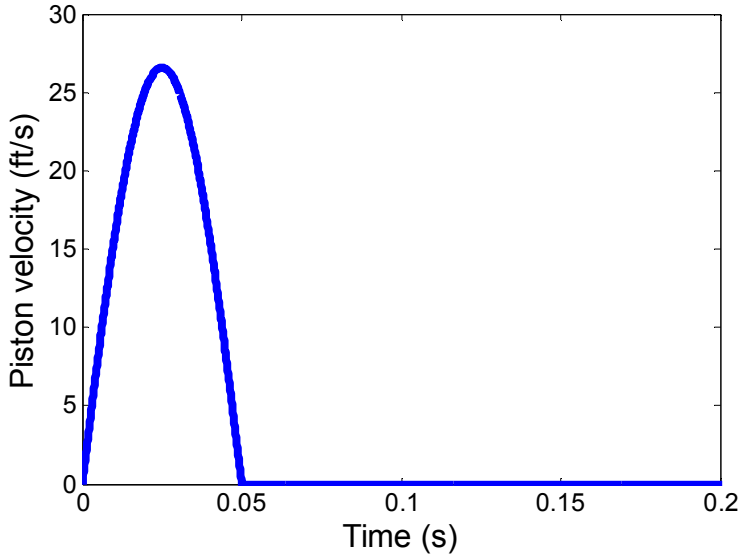

Figure 6.4. A half-sine predicted piston velocity for a 50 ms event duration at a nominal speed of 26 ft/s (7.9 m/s)

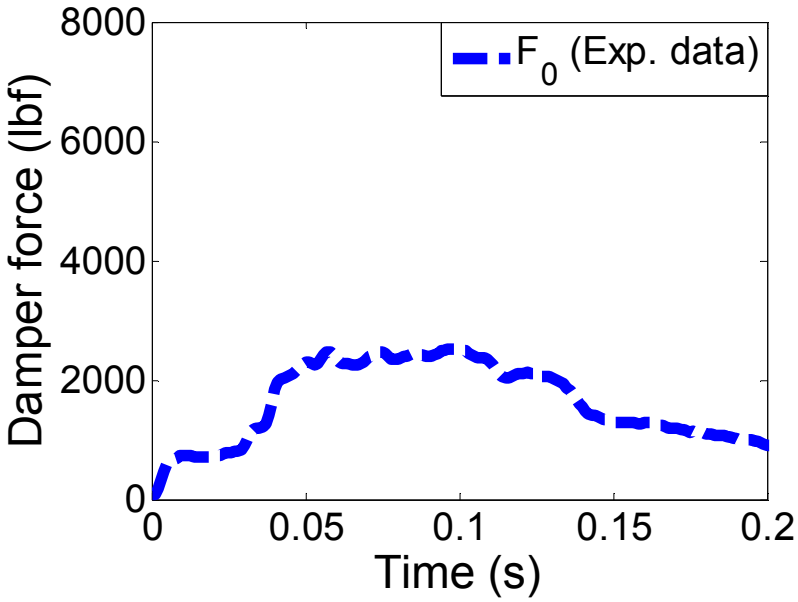

Figure 6.5. Transient impact force response at a nominal drop speed of 6 ft/s (1.8 m/s)

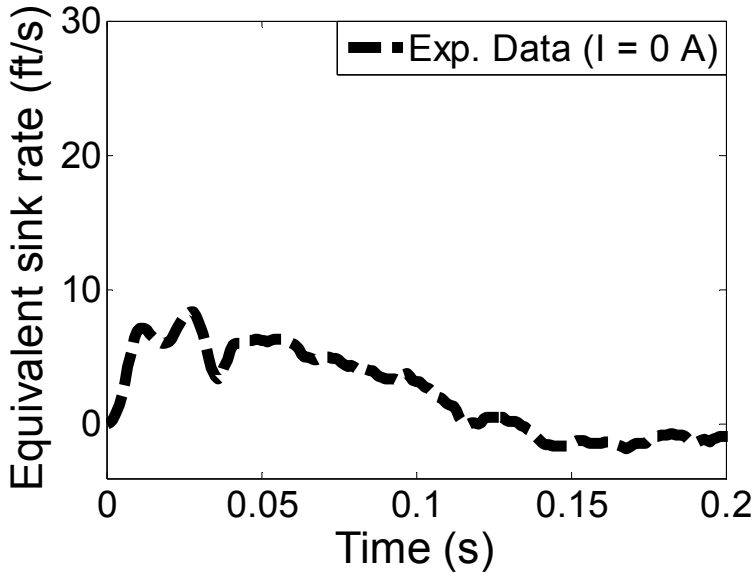

Figure 6.6. Transient piston velocity response at a nominal drop speed of 6 ft/s (1.8 m/s)

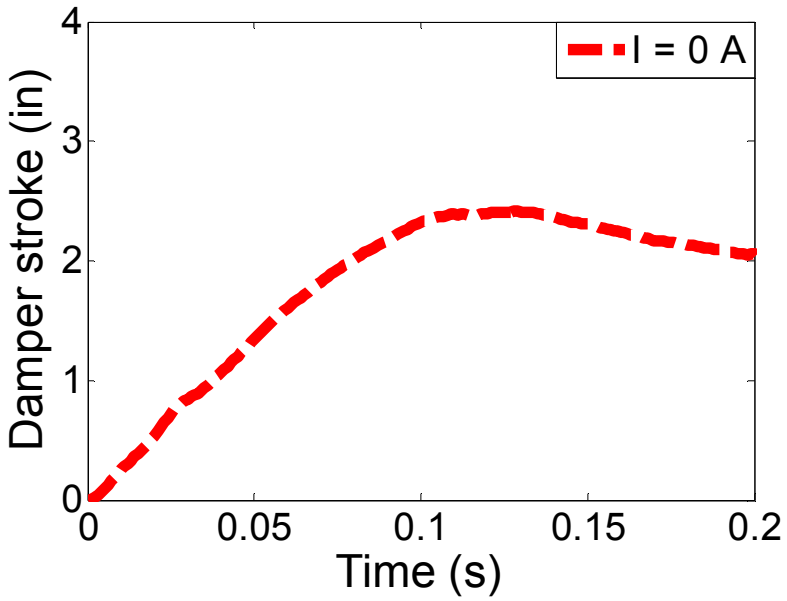

Figure 6.7. Transient piston displacement response measured with an LVDT at a nominal drop speed of 6 ft/s (1.8 m/s)

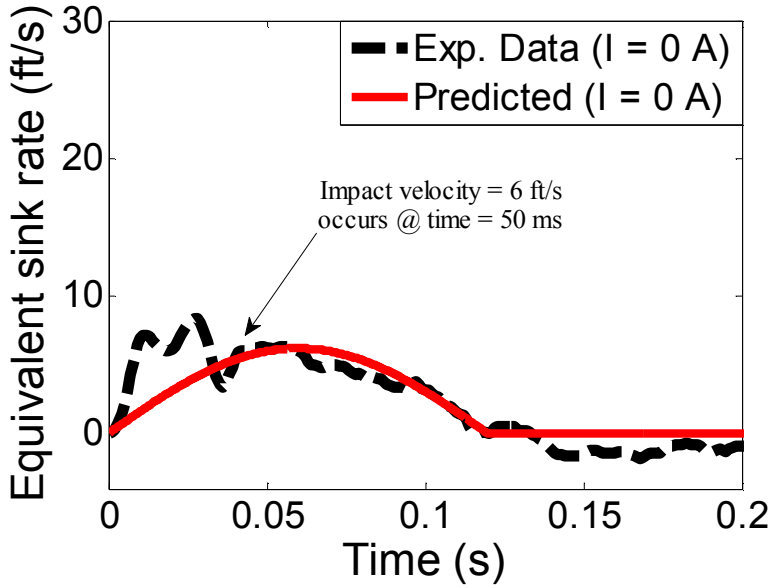

Figure 6.8. Predicted velocity time histories versus filtered experimental velocity data

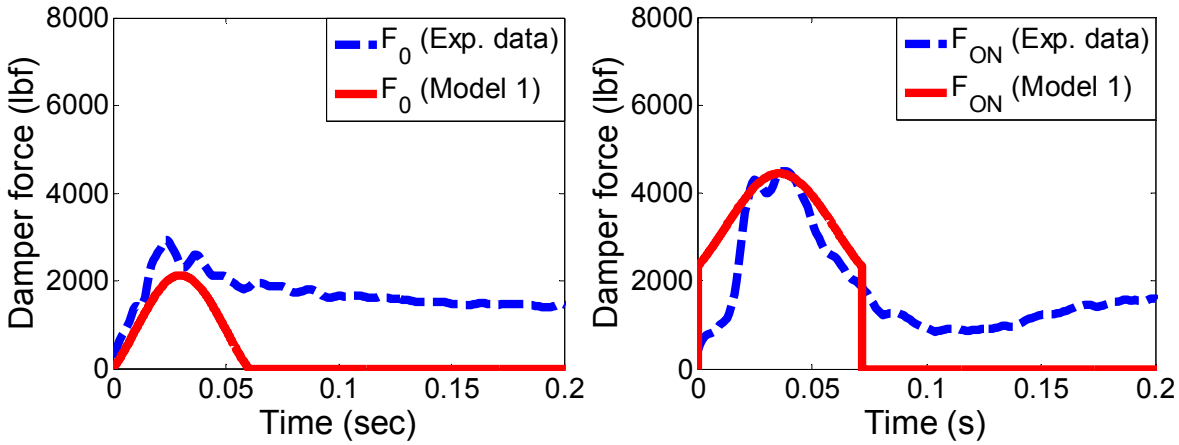

Figure 6.9. Transient force responses of the baseline MR landing gear damper (equipped with an MR valve only) versus time at a nominal drop speed of 6 ft/s versus simulated results from model #1. Cases: (a) field-OFF; (b) field-ON

Model #1: nonlinear Bingham Plastic (BP)-type model with viscous effects and minor losses in the MR valve gap

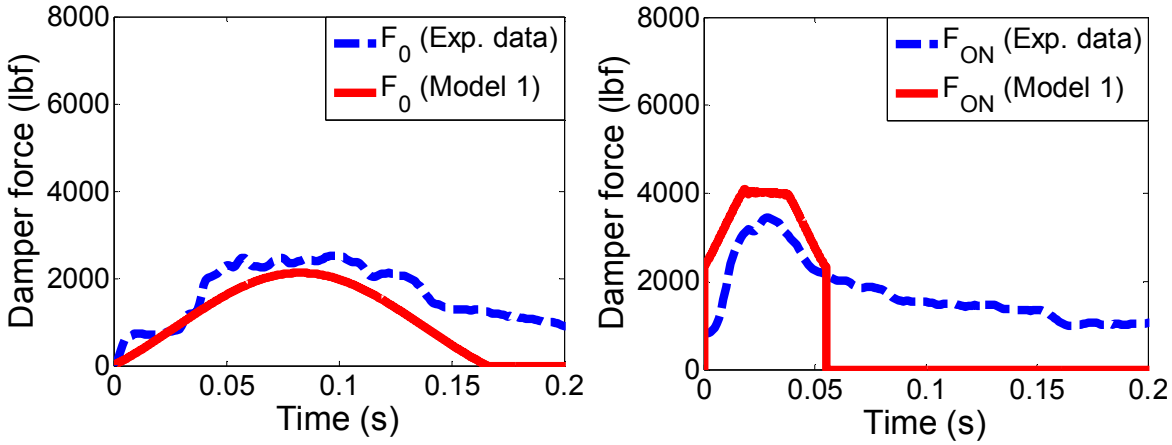

Figure 6.10. Transient force responses of the spiral wave-assisted MR landing gear damper (equipped with an MR valve and a passive valve) versus time at a nominal drop speed of 6ft/s versus simulated results of model #1. Cases: (a) field-OFF; (b) field-ON

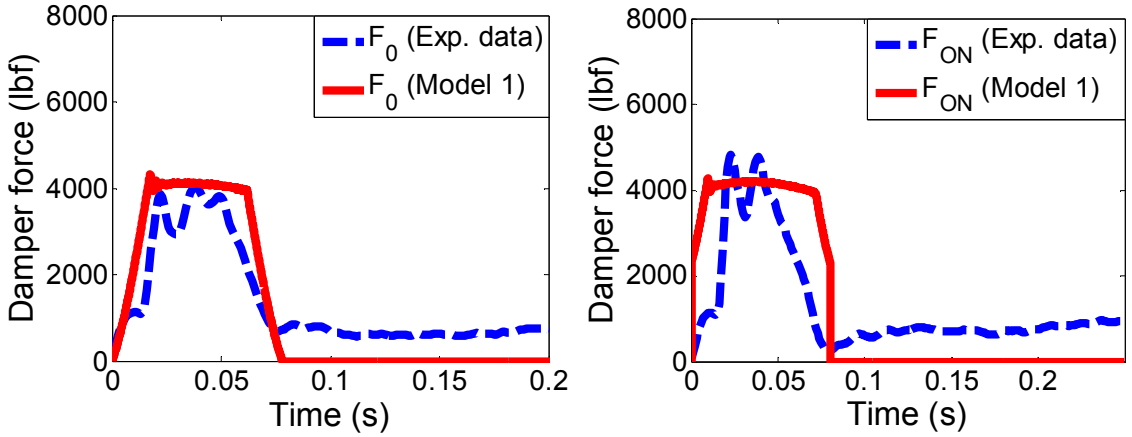

(a) (b)

Figure 6.11. Transient force responses of the spiral wave-assisted MR landing gear damper (equipped with an MR valve and a passive valve) versus time at a nominal drop speed of 16ft/s versus simulated results of model #1. Cases: (a) field-OFF; (b) field-ON

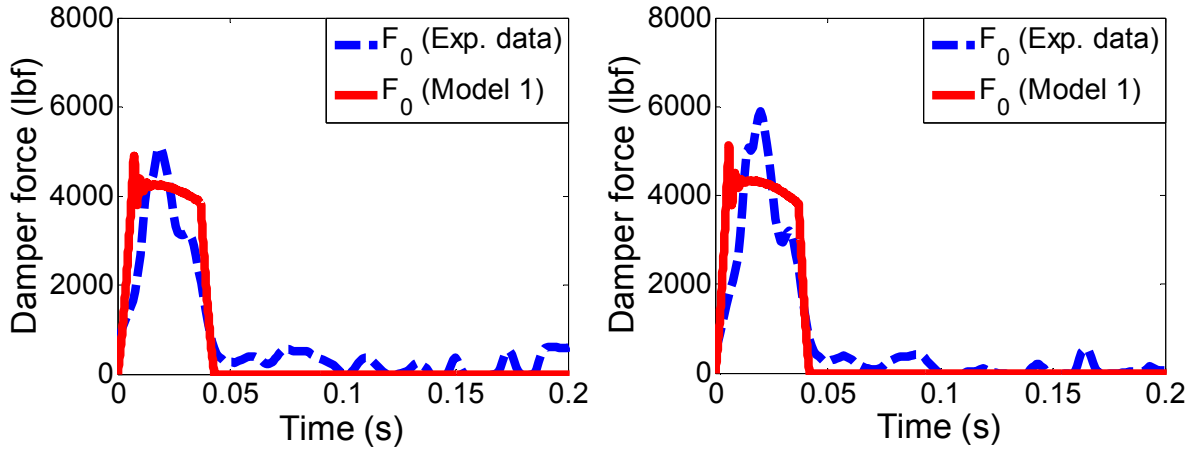

(a) (b)

Figure 6.12. Transient force responses of the spiral wave-assisted MR landing gear damper (equipped with an MR valve and a passive valve) versus time at a nominal drop speed of (a) field-OFF case at 22 ft/s and (b) field-OFF case at 26 ft/s versus simulated results of model #1

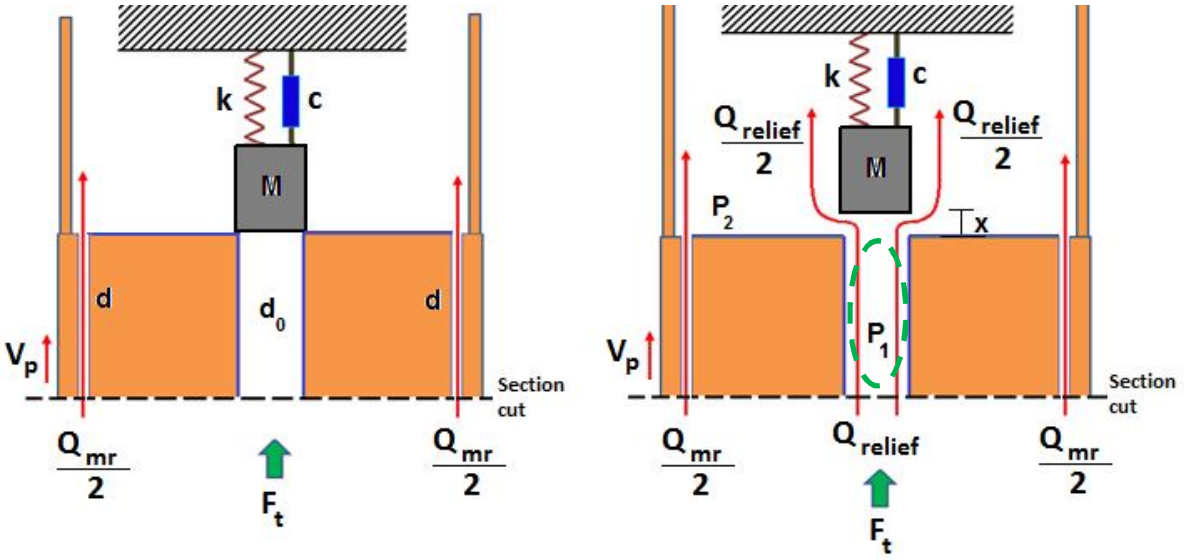

Figure 6.13. Hydraulic model of the MR and passive valves of the MR landing gear damper: (a) relief valve is closed; (b) relief valve is open and the pressure P_1 across the center orifice is considered

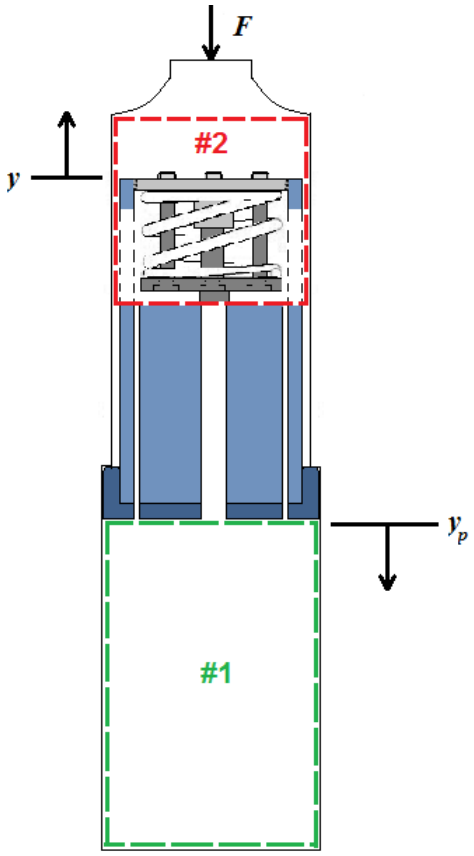

Figure 6.14. Schematic of the control volumes where the gas force has an effect in the MR landing gear damper with spiral wave spring-assisted relief valve

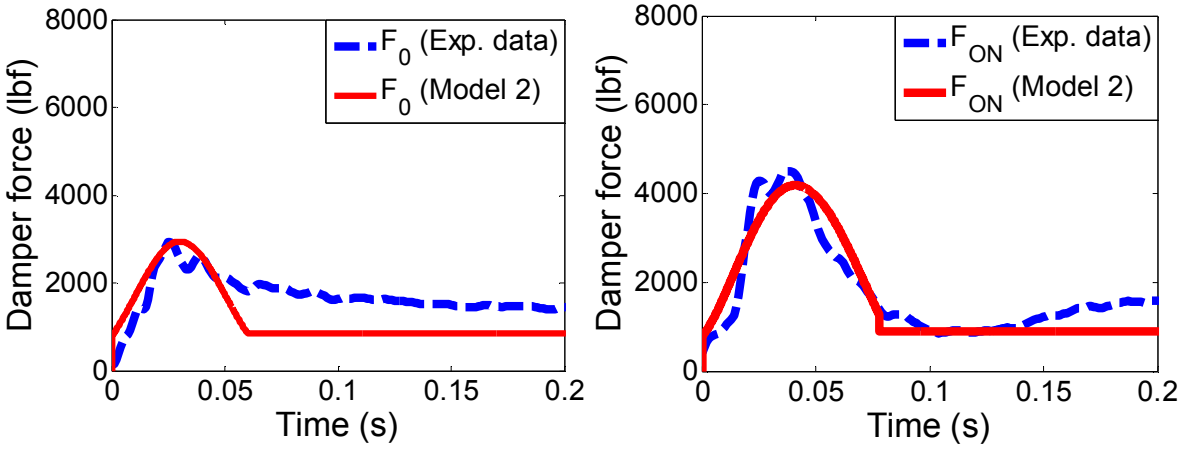

(a) (b)

Figure 6.15. Transient force responses of the baseline MR landing gear damper (equipped with an MR valve only) versus time at a nominal drop speed of 6 ft/s versus simulated results from model #2. Cases: (a) field-OFF; (b) field-ON

Model #2: modified nonlinear Bingham Plastic (BP)-type model with viscous effects and minor losses in the MR valve gap and the center orifice relief valve + gas force

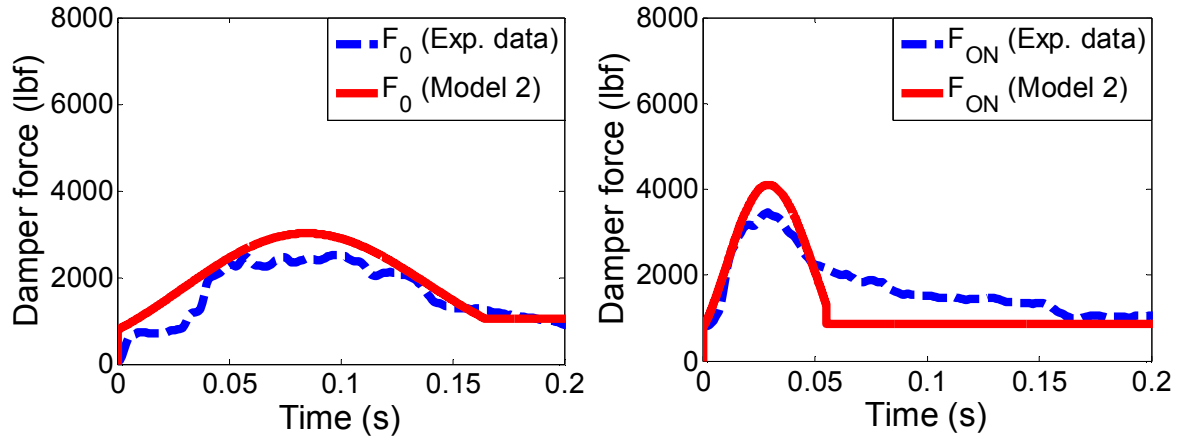

(a) (b)

Figure 6.16. Transient force responses of the spiral wave-assisted MR landing gear damper (equipped with an MR valve and a passive valve) versus time at a nominal drop speed of 6ft/s versus simulated results of model #2. Cases: (a) field-OFF; (b) field-ON

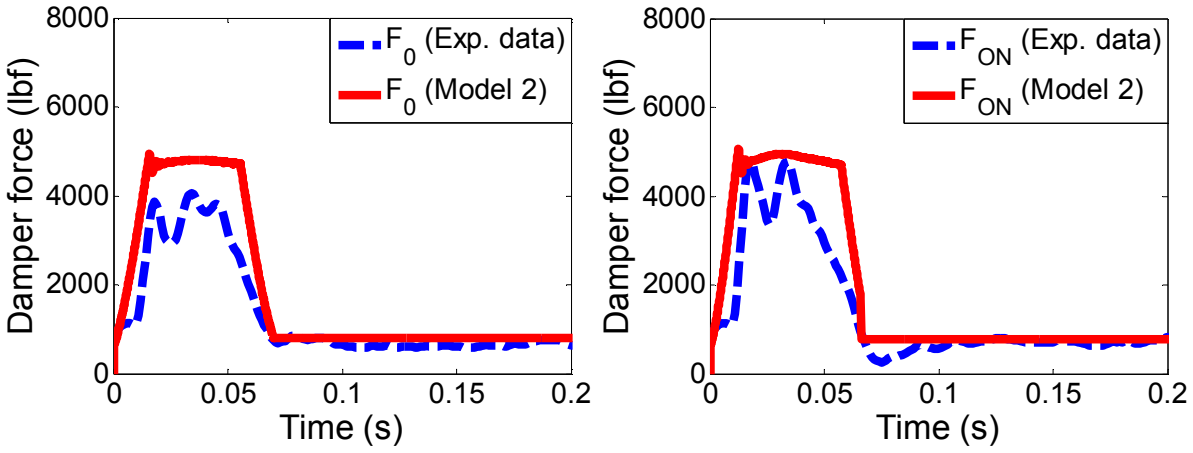

(a) (b)

Figure 6.17. Transient force responses of the spiral wave-assisted MR landing gear damper (equipped with an MR valve and a passive valve) versus time at a nominal drop speed of 16 ft/s versus simulated results of model #2. Cases: (a) Field-OFF; (b) field-ON

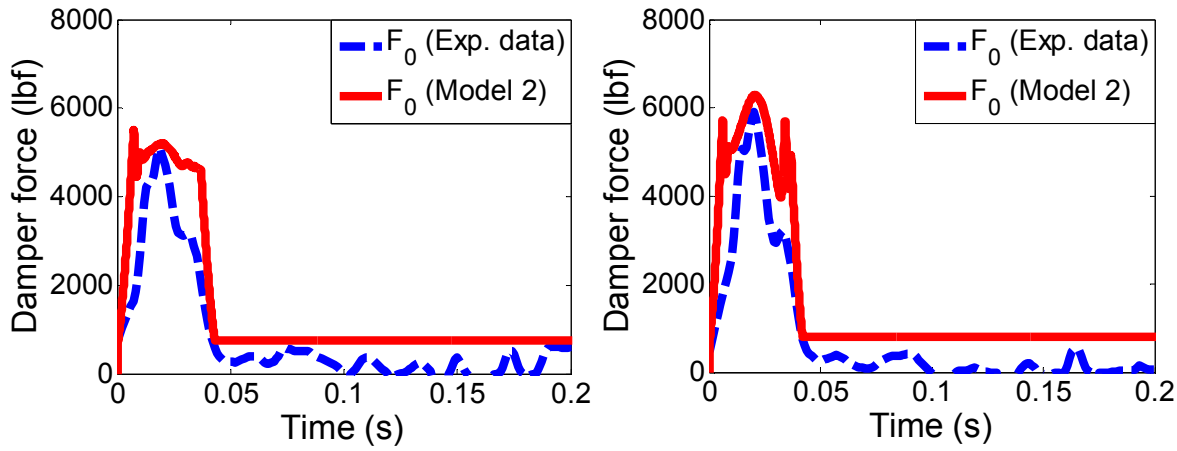

(a) (b)

Figure 6.18. Transient force responses of the spiral wave-assisted MR landing gear damper (equipped with an MR valve and a passive valve) versus time at a nominal drop speed of (a) field-OFF case at 22 ft/s and (b) field-OFF case at 26 ft/s versus simulated results of model #2.

Table 6.1.: Key parameters of the MR landing gear damper with a spiral wave spring-based passive valve

Mass of the seal, M in kg (lbs)	0.05 (0.11)
Actual spiral wave spring stiffness, K in kN/m (lb_f/in)	10.47 (59.8)
Damping ratio, ζ	1.8
Time constant, τ in ms	7
Maximum allowable seal displacement in mm (inches)	5.08 (0.2)

CHAPTER 7: Conclusions and Future Work

This chapter summarizes the work conducted in this study. The primary results and research contributions are highlighted and suggestions are made for the extension of this work to future studies.

7.1 Conclusions

Since their introduction, magnetorheological fluids (MRFs) and MRF devices have provided solution to many engineering challenges. Moreover, the large success of MRFs continues to motivate current and future applications. MRF application to landing gear systems have been considered, but studies on the feasibility of utilizing an MRF that comprise important characteristics to preserve in landing gear fluid certification and rotorcraft application have not yet been fully investigated. This research focused on MRFs suitability to be applied to lightweight helicopter landing gear systems by mixing a desired MRF with low off-state viscosity (to keep viscous forces as low as possible at high sink rates), large yield force (for MR device controllability), and stability (easily remixed to prevent fluid stratification leading to poor performance). In addition, this research concentrated on efforts to achieve landing performance challenge to maximize operating sink rate range of a lightweight helicopter by designing, manufacturing, and testing adaptive MR landing gear dampers coupled with a nonconventional spiral wave spring-based passive valve. The main objective of this dissertation was to improve landing gear systems performance of a lightweight helicopter.

7.1.1 Magnetorheological Fluids Study

In the MRF study part of this dissertation, MRFs were synthesized using different carrier hydraulic oils certified for landing gear use, and the feasibility of these MRFs, to see if they

qualify for use in landing gear systems, was assessed. A series of sample MRFs were synthesized for different solid loadings (vol% of iron, Fe, particles) using landing gear hydraulic fluids as the carrier fluids: MIL-H-5606, MIL-PRF-83282, and MIL-PRF-87257. A lecithin surfactant was used to maintain the suspension and to prevent particle agglomeration. These synthesized MRFs were also compared to commercially available MRFs from Lord Corporation with comparable solid loadings.

First, magnetorheological properties were tested as a function of applied field, and the experimental data were characterized using the Bingham Plastic (BP) model. The yield stress and viscosity of the MRF composites, using flow curve data, were identified. The MR landing gear fluid composite compared favorably with a commercial MRF (both containing 26 vol% magnetic particles).

Second, a particle sedimentation study was performed on the MRFs synthesized using an inductance coil-based sedimentation rate monitoring system. Hence, particle dispersion stability was effective, and redispersion showed similar results, even though fluids were left inactive for over a month.

Third, the performance of a linear stroke MR damper, filled with the synthesized MRFs, was characterized using a Nonlinear BiViscous (NBV) model. The NBV model was used to successfully identify the yield force. MR damper behavior was compared to that of the damper including a commercial MRF of the same solid loadings (of 32 vol% particle concentration). The yield forces of the MRFs containing particles in the size range of 6-10 μm Fe particles (32 vol%) compared favorably with that of the commercial MRFs, and measured yield forces of the MR damper with either MRF were within 5% of each other.

Synthetic oil-based MRF (of 32 vol% Fe particles) was utilized in an MR damper and underwent high shear rate drop testing to experimentally verify the tuning nature of the MR device at different impact velocities and magnetic field strengths. Hence, the peak stroking force and energy dissipated by the MR damper strongly depended on the changes in the magnetic field strengths.

Based on this range of tests used to characterize MRFs synthesized using certified landing gear fluids in this study, it was shown that it is feasible to use such hydraulic oils as the carrier fluids in model MRFs to develop landing gear applications. In addition, because the commercially available fluids have comparable performance, the LORD Corp. MRFs were later used in the development of landing gear oleos in this dissertation.

In the continued study of MRFs in this dissertation, the behavior of two MRFs with different compositions was investigated. The first fluid (MRF-37) had 35.7 vol% of iron Fe powder, 4.3 vol% glass beads, and 60 vol% of carrier fluid. The second fluid (MRF-40) had 40 vol% of Fe powder, and 60 vol% of carrier fluid. Based on this study, the following conclusions were made:

- MRF-37 (with glass beads) showed a substantial increase in yield force in the as-mixed fluid damper cycling tests. The yield force more than doubled in the damper tests at high field strengths (here 2 to 3 A in the electromagnet) suggesting that nonmagnetic fillers can substantially increase damper yield force.
- MRF-37 (with passive particles or glass beads) had an off-state viscosity 22% greater than the MRF-40 (no glass beads).
- After subjecting MRF-37 to endurance testing (518,400 cycles of sinusoidal loading at 4 Hz), the yield force enhancement effect was eliminated because the glass beads were

crushed to very small sizes. This further supports the conclusion that the passive particles (glass beads) are the strong contributing factor to the damper yield force enhancement.

- MRF-37 would provide a lower specific gravity fluid with a much higher damper yield force at full field, thereby providing performance improvements for applications where the MR device is intended for single or infrequent use.

7.1.2 Magnetorheological Fluids Devices and Application

In the MR device and application section of this dissertation, an adaptive MR landing gear damper with a spring-assisted passive (relief) valve for a lightweight helicopter was designed to maintain a constant peak stroking force of 4000 lb_f across sink rates ranging from 6-26 ft/s. It was desired to expand the high end of the sink rate range from 12 ft/s from a prior study (Choi *et al.*, 2012) to 26 ft/s, while preserving low speed force levels. To achieve this increase in the high end of the sink rate range, the adaptive landing gear damper developed in this study was equipped with an MR valve that was designed to semi-actively control the peak stroking load over the 6-12 ft/s sink rate range and a spring-assisted passive (or relief) valve that was designed to passively control the stroking load over the 12-26 ft/s sink rate range.

The MR valve was designed using a nonlinear analytical damper model or Bingham-plastic model that depended on the behavior of MR fluids and nonlinear viscous factors. The passive relief valve was designed based on a computer simulation related to spring dynamic equations of motion, which estimated the damper force behavior to meet the desired stroking load of 4000 lb_f over the desired sink rate range of 12-26 ft/s.

A nonlinear analysis based on the pressure drop across the MR valve and the passive relief valve center orifice was conducted to estimate the center orifice diameter range. The optimal diameter of the center orifice was calculated to be 0.3 inches (7.62 mm).

Two different springs were used (a conventional coil spring and a spiral wave spring) for the analysis and construction of the passive valve. Moreover, an electromagnetic analysis of the MR valve in the landing gear damper using the commercial software ANSYS was performed to predict the magnetic field strength in the MR gap while taking into consideration the center orifice diameter selected.

An experimental study using a material testing system (MTS) machine was performed to evaluate the damper force behavior of the spiral wave and coil spring-based MR landing gear dampers to verify that the relief valve operated properly. A dummy bobbin was designed, fabricated, and tested using ramp damper tests due to the speed limitation of the servo-hydraulic testing machine. In these ramp tests, instead of the electromagnetic coil winding that activates the MR valve, the dummy bobbin was used for comparison purposes and to check if the relief valve in the spiral wave and coil spring based MR landing gear dampers worked correctly. Using the MTS machine, the stroking load (or damper force) of the MR landing gear damper coupled with a spring-assisted relief valve was measured for constant velocity inputs to verify that the spring-based relief valve was working appropriately. Three different damper configurations: a dummy bobbin with no relief valve, a bobbin with a spiral wave spring-based relief valve, and a bobbin with a coil spring-based relief valve were tested. At a constant velocity of 5.25 ft/s (1.6 m/s), the no relief valve case showed higher damper force performance (around 5000 lb_f) than the spiral wave and coil spring-based MR landing gear damper cases, which remained around 4400 lb_f. This implies that the spiral wave and coil spring-based relief valves were opening and keeping the stroking load constant, hence the relief valves were working properly. Also, the spiral wave spring-based MR landing gear damper case showed more stable transient behavior, which could be due to the fact that the spiral wave spring was axisymmetric hence well balanced

around its center axis compared to the coil spring. This stable behavior of the spiral wave spring based MR landing gear damper made it more attractive than the coil spring based damper, so that the spiral wave spring was used for the rest of the study.

After verifying that the prototype of the MR landing gear damper worked appropriately, a full-scale, flow-mode type MR landing gear damper coupled with a spring-assisted passive (or relief) valve was designed, fabricated, and drop tested in order to experimentally demonstrate the extension of the high end of the sink rate range from 12 ft/s (from the previous effort by Choi *et al.*, 2012) to 26 ft/s while maintaining a stroking load of 4000 lb_f over a desired sink rate range of 6-26 ft/s.

From the laboratory tests, it was experimentally investigated that a desired stroking load of 4000 lb_f was held over a desired equivalent sink rate range of 6 -26 ft/s.

A single damper drop test apparatus was built to evaluate stroking loads of the MR landing gear damper for sink rates higher than 6 ft/s for a drop mass of 430 lbs first, then 1283 lbs. A force feedback control algorithm (bang-bang current control) was also developed. Using this force feedback controller, the stroking load was successfully regulated to maintain a constant stroking load of 4000 lb_f over a 6-18 ft/s equivalent sink rate range. Considering a force error bound of ±1000 lb_f, the maximum achievable equivalent sink rate range could be increased to 6-22 ft/s by using either the spiral wave or coil spring-relief valves. The spiral wave spring-relief valve performed better than the coil spring-relief valve at lower sink rate range, due to the spiral wave spring's axisymmetric shape around the center axis. For further iron-bird drop damper testing, the spiral wave spring-relief valve was selected.

From a full-scale iron-bird drop testing (with a total drop mass of 2627 lbs), it was experimentally demonstrated that the MR landing gear dampers with a spiral wave spring-based

relief valve could control the stroking load over a wider range of sink rates. The bang-bang current control algorithm successfully regulated the stroking load at 4000 lb_f over a sink rate range of 6-16 ft/s in these iron-bird tests. If a force error bound of ±1000 lb_f was taken into account, the control was superior over a sink rate range of 6-22 ft/s, which by far exceeds the sink rate range of the previous study (which was 6-12 ft/s). The single damper drop testing method was a good damper force estimation procedure as it showed similar testing results compared to the iron-bird testing, which emulated a full-scale lightweight helicopter.

Finally, the effectiveness of two nonlinear models that predicted the performance of MR landing gear dampers over sink rates ranging from low (6 ft/s or 1.8 m/s) to high speed (26 ft/s or 7.9 m/s) impact conditions was considered.

Two models were experimentally investigated using the drop test data at the Boeing Structures Test Laboratory in Mesa, Arizona with two MR landing gear dampers: one with an MR valve only (baseline) and the other with a spiral wave spring-assisted passive valve. The first model was a nonlinear BP-type flow model incorporating viscous effects and minor loss factors only across the MR valve of the landing gear damper (model #1). The second model was a modified version of the nonlinear BP-type flow model, incorporating viscous effects and minor loss factors across both the MR and passive relief valves of the landing gear damper (model #2); also, a gas force was included in the analysis.

On the one hand, results demonstrated that model #1 could not accurately predict the baseline and spiral wave spring-assisted passive valve MR landing gear dampers force behavior for the field-OFF case, but the model was able to predict the maximum damper force behavior for the field-ON case at a low sink rate of 6 ft/s. Further impact speeds examination showed that model #1 could not effectively predict higher forces at sink rates higher than 16 ft/s as the model

under predicted the damper force by about 25% at high sink rate of 26 ft/s. In addition, model #1 was not accounting for the time delay occurring in the actual experimental data for the field dependent damper force behavior and the effect of the gas force.

On the other hand, model #2 was more practical than model #1 as it captured the baseline and spiral wave spring-assisted MR landing gear dampers force histories from the drop test data more precisely. The second model (model #2) accounted for the time delay occurring in actual data as well as the gas force. The model accurately described the MR landing gear dampers force responses at sink rates ranging from 6 ft/s to 26 ft/s for the Field-OFF and ON cases while capturing the maximum damper forces at higher impact speeds (of 26 ft/s) within 7% for the field-OFF case. Model #2 predicted the landing gear damper behavior more accurately than model #1 because model #2 reconsidered the assumption held by model #1 that the diameter of the center orifice was big enough, so that its pressure drop is negligibly smaller than the pressure drop due to the seal's opening. Model #2 actually considered and included the pressure drop across the passive relief valve center orifice in addition to the pressure drop across the MR valve, which allowed for a better prediction of high-speed forces while still predicting low-speed forces accurately.

7.2 Original Contributions

In the MRF investigation of this dissertation, MRFs were developed using certified landing gear hydraulic oils, and it was demonstrated in this study that these fluids are suitable MRFs and applicable to landing gear systems. The synthesized MRFs performance is comparable to commercial MRFs.

The yield force performance of an MRF was doubled by substituting magnetic for passive particles (hollow glass beads). The MRF specific gravity was reduced; however, this

MRF is more for applications where the MR device is used infrequently because of passive particle deterioration over time.

In the MR devices and application segment of this dissertation, a practical MR landing gear system, which combines an MR valve with a spring-assisted passive valve, was developed. The operating sink rate range (from 6-22 ft/s) was maximized while maintaining a peak stroking force of about 4000 lb_f across the desired sink rate range. There was a substantial increase from 12 ft/s (from a previous study directly related to this work by Choi *et al*., 2012) to 22 ft/s. In addition, a model combining an MR valve with a spring-assisted relief valve and a gas reservoir was experimentally validated under impact loads with equivalent sink rates ranging from 6-26 ft/s, which corresponds to piston velocities ranging from 2.2-9.6 ft/s. The model was able to match the peak impact loads.

7.3 Future Work

Throughout the course of this work, several topics, beyond the scope of this current research, were encountered. Additional work remains to be completed before MRFs can be certified for use in helicopter landing gear systems. In what follows, a brief discussion of those topics is provided. While the initial results are promising, further investigation of several key areas of the MRF behavior itself as well as the MR landing gear device that encloses the fluid, is warranted.

MRFs that were synthesized using different carrier hydraulic oils (MIL-H-5606, MIL-PRF-83282, and MIL-PRF-87257) certified for landing gear use, were subjected to a series of tests for characterization purposes in order to assess the feasibility of these MRFs to substantiate their potential qualification for use in landing gear systems. To extend this work to future studies, additional testing is warranted to ensure that the addition of particle solids and

surfactants does not affect key properties of the hydraulic carrier fluids such that operating temperature range and resistance to flammability are preserved in landing gear applications. For instance, the synthesized MRFs could benefit from large range of operating temperature testing in a flow mode damper to ensure that the properties of the synthesized MRF inside the damper are not severely affected due to damping change and self-heating. In addition, high shear (higher than 1000 s^{-1}) and high velocity investigation of the synthesized MRFs can also be useful due to the fact that MRF behavior at high shear is largely governed by the carrier oil; consequently, the carrier fluid can also be evaluated at high shear rates.

In the continued study of MRFs, the substitution of nonmagnetic particles for magnetic CI particles in MRFs was investigated in the context of MR dampers or flow mode devices. Two MRF samples (MRF-40 and MRF-37) were synthesized and a comparative study of their characteristics was conducted to determine the impact of the nonmagnetic glass beads on MRF (yield stress and sedimentation rate) and MR damper (yield force and post-yield damping) performance. Although the results were promising due to the ability to provide a lower specific gravity fluid (MRF-37) with a much higher damper yield force at full field, thereby providing performance improvements for applications where the MR device is intended for single or infrequent use, concerns were raised during the endurance test as particles eroded due to extensive cycling. To expand this work to future studies, and for cases where extensive cycling would be required, more durable passive fillers that are not subject to erosion, as glass beads are, would be more appropriate. Further study (Klingenberg and Ulicny, 2011) is also needed to better describe the underlying physics contributing to the yield force enhancement in the MR damper when using MRF with glass beads.

In the MR device and application section of this dissertation, an adaptive MR landing gear damper with a nonconventional spiral wave spring-assisted passive (relief) valve for a lightweight helicopter was successfully designed, fabricated, and tested. The device was able to maintain a constant peak stroking force of 4000 lb_f across sink rates ranging from 6-22 ft/s using a bang-bang current control algorithm. Although the desired sink rate range was originally 6-26 ft/s, the maximum operating sink rate range achieved in this current study represented a substantial increase from 12 ft/s (from a previous study directly related to this work by Choi *et al*., 2012) to 22 ft/s. This current follow-on effort was considerable; however, the maximum sink rate capability can be revisited for future work. Due to the limited geometry of the existing MD 500 landing gear damper used as the test bed in this study, the maximum sink rate capability was limited as well. A new damper design with an optimized geometry needs to be considered to achieve higher sink rates while maintaining the same constant stroking load throughout the sink rate range.

Bibliography

Aviation Maintenance and Training Manual (2003), Integrated Publishing, Inc. Port Richey, FL. Available at: http//www.tpub.com

Batterbee, D.C., Sims, N.D., Stanway, R., and Wolejsza, Z., (2007a) Magnetorheological landing gear: 1. A design methodology. *Smart Materials and Structures*, 16: 2429-2440. DOI: 10.1088/0964-1726/16/6/046.

Batterbee, D.C., Sims, N.D., Stanway, R., and Rennison, M., (2007b) Magnetorheological landing gear: 2. Validation using experimental data. *Smart Materials and Structures*, 16: 2441-2452. DOI: 10.1088/0964-1726/16/6/047.

Bell, R.C., Miller, E.D., Karli, J.O., Vavreck, A.N., and Zimmerman, D.T., (2007) Influence of particle shape on the properties of magnetorheological fluids. International Journal of Modern Physics B, 21(28-29): 5018-5025. DOI: 101142/S0217979207045979.

Bell, R.C., Karli, J.O., Vavreck, A.N., Zimmerman, D.T., Ngatu, G., and Wereley, N.M., (2008) Magnetorheology of submicron diameter iron microwires dispersed in silicone oil. *Smart Materials and Structures*, 17(015028): 1-6. DOI: 10.1088/0964-1726/17/01/015028.

Bitman L., Choi, Y.-T., Choi, S.B., and Wereley, N.M., (2005) Electrorheological damper analysis using an Eyring-plastic model. *Smart Materials and Structures*, 14(1): 237-246. DOI: 10.1088/0964-1726/17/14/1/024.

Browne, A.L., McCleary, J.D., Namuduri, C.S., and Webb, S.R., (2004) Impact performance of magnetorheological fluids. ASME International Mechanical Engineering Congress and Exposition, Paper No. IMECE 2004-60542.

Carlson, J.D., Sprecher, A.F., and Conrad, H., (1990) Electrorheological fluids. Proceedings of the Second International Conference on ER Fluids, Technomic, Lancaster, Pa.

Carlson, J.D., Catanzarite, D.M., and St. Clair, K.A., (1995) Commercial magneto-rheological fluid device. Lord Corporation, Cary, NC 27511 USA. Proceedings of the 5th International Conference on ER Fluids, MR Fluids and Associated Technology, U. Sheffield, UK, 20-28.

Carlson, J.D., (1999) Magnetorheological Fluid Actuators. Adaptronics and Smart Structures, Editor H. Janocha Springer Berlin, 180-195, ISBN 3-540-61484-2.

Carlson, J.D., and Jolly, M.R., (2000) MR fluid, foam and elastomer devices. *Mechatronics*, 10 (4-5): 555-569. DOI: 10.1016/S0957-4158(99)00064-1.

Carlson, J.D., (2001) What makes a good MR fluid. Proceedings of the 8th International Conference on Electrorheological (ER) and Magnetorheological (MR) Suspensions.

Chaudhuri, A., Wereley, N.M., Kotha, S., Radhakrishnan, R., and Sudarshan, T., (2005) Viscometric characterization of cobalt nanoparticle-based magnetorheological fluids using genetic algorithms. *Journal of Magnetism and Magnetic Materials*, 293: 206–214. DOI: 10.1016/j.jmmm.2005.01.061.

Choi, Y.-T., and Wereley, N.M., (2002) Comparative analysis of the time response of electrorheological and magnetorheological dampers using nondimensional parameters. *Journal of Intelligent Material Systems and Structures*, 13(7/8): 443-451. DOI: 10.1106/104538902028557.

Choi, Y.-T., and Wereley, N.M., (2003) Vibration control of a landing gear system featuring ER/MR fluids. *AIAA Journal*, 40(3): 432–439. DOI: 10.2514/2.3138.

Choi, Y.-T., Wereley, N.M., and Jeon, Y.S., (2005a) Semi-active vibration isolation using magnetorheological isolators. *Journal of Aircraft*, 42(5): 1244-1251. DOI: 10.2514/1.7919.

Choi, Y.-T., Yoo, J.H., and Wereley, N.M., (2005b) Double adjustable magnetorheological dampers for a gun recoil system. International Mechanical Engineering Congress and Exposition (IMECE), Orlando, FL, USA.

Choi, Y.-T., Robinson, R., Hu, W., Wereley, N.M., Birchette, T.S., and Bolukbasi, A.O., (2012) Analysis and control of a magnetorheological landing gear system for a helicopter. Proceedings of the American Helicopter Society 68th Annual Forum & Technology Display, Fort Worth, TX, USA.

Eem, S.H., Jung, H.J., and Koo, J.H., (2011) Application of MR elastomers for improving seismic protection of base-isolated structures. *IEEE Transactions on Magnetics*, 46(6): 2901–2904. DOI: 10.1109/TMAG.2011.2156771.

Facey, W.B., Rosenfeld, N., Choi, Y.T., Wereley, N.M., Choi, S.B., and Chen, P., (2005) Design and testing of a compact magnetorheological damper for high impulsive loads. *International Journal of Modern Physics B*, 19(7-9): 1549-1555. DOI: 10.1142/S0217979205030578.

Fang, F.F., and Choi, H.J., (2008) Noncovalent self-assembly of carbon nanotube wrapped carbonyl iron particles and their magnetorheology. *Journal of Applied Physics*, 103(7): 07A301-1-3. DOI: 10.1063/1.2829019.

Franzini, J.B., and Finnemore, E.J., (1997) *Fluid Mechanics with Engineering Applications*, McGraw Hill.

Gavin, H.P., Hanson, R.D., and Filisko, F.E., (1996) Electrorheological dampers, part I: analysis

and design. *Journal of Applied Mechanics*, 63: 678-82. DOI: 10.1115/1.2823348.

Gonzales, F.D., (2005) Characterizing the behavior of magnetorheological fluids at high velocities and high shear rates. Ph.D Thesis, Mechanical Engineering, Virginia Polytechnic Institute and State University, Virginia.

Hiemenz, G., Hu, W., and Wereley, N.M., (2008) Semi-active magnetorheological helicopter crew seat suspension for vibration isolation. *Journal of Aircraft*, 45(3): 945-953. DOI: 10.2514/1.32736.

Hu, W., and Wereley, N.M., (2003) Nondimensional damping analysis of flow-mode magnetorheological and electrorheological damper. Proceedings of IMECE'03 ASME, International Mechanical Engineering Congress & Exposition, Washington, D.C., USA.

Idel'chik, I.E., (1994) *Handbook of Hydraulic Resistance,* 3rd Edition, CRC Press, FL, USA.

Jiang, W., Cao, Z., Gu, R., Ye, X., Jiang, C., and Gong, X., (2009) A simple route to synthesize $ZnFe_2O_4$ hollow spheres and their magnetorheological characteristics. *Smart Materials and Structures*, 18(12): 125013-1-4. DOI: 10.1088/0964-1726/18/12/125013.

Jolly, M.R., Bender, J.W., and Carlson, J.D., (1998) Properties and applications of commercial magnetorheological fluids. Proceedings of the 5th SPIE Annual International Symposium on Smart Structures and Materials, San Diego, CA.

Kamath, G.M., and Wereley, N.M., (1997) A nonlinear viscoelastic-plastic model for electrorheological fluids, *Smart Materials and Structures*, 6: 351-359. DOI: 10.1088/0964-1726/6/3/012.

Klingenberg, D.J., and Ulicny, J.C., (2011) Enhancing magnetorheology. *International Journal of Modern Physics B*, 25(7): 911-917. DOI: 10.1142/S021797921105847X.

Lee, D.Y., and Wereley, N.M., (1999) Quasi-steady Herschel-Bulkley analysis of electro- and magnetorheological flow mode dampers. *Journal of Intelligent Material Systems and Structures*, 10(10): 761-769. DOI: 10.1106/E3LT-LYN6-KMT2-VJJD.

Lin, L.H., Yong, C., Qi, H., and Jian, L., (2009) Fuzzy PID control for landing gear based on magnetorheological (MR) damper. International Conference on Apperceiving Computing and Intelligence Analysis (ICACIA), 22-25. DOI: 10.1109/ICACIA.2009.5361162.

Lord Corporation, www.lord.com.

Lord Corporation (2014) Dr. Dave's Do-It-Yourself MR Fluid, Designing with MR Fluid, Magnetic Circuit Design, FAQs, www.lord.com.

Mao, M., Choi, Y.-T., and Wereley, N.M., (2005) Effective design strategy for a magnetorheological damper using a nonlinear flow model. Proceedings of SPIE, 5760: 446-455. DOI: 10.1117/12.601061.

Mao, M., Hu, W., Choi, Y.-T., Wereley, N.M., (2007) A magnetorheological damper with bifold valves for shock and vibration mitigation. *Journal of Intelligent Material Systems and Structures*, 18(12): 1227-1232. DOI: 10.1177/1045389X07083131.

Mao, M., Hu, W., Wereley, N.M., Browne, A.L., Ulicny, J.C., and Nancy, J., (2013) A nonlinear analytical model for magnetorheological energy absorbers under impact conditions. *Journal of Intelligent Material Systems and Structures*, 22(115015): 1-12. DOI: 10.1088/0964-1726/22/11/115015.

Merritt, H.E., (1967) *Hydraulic Control Systems*. John Wiley & Sons, New York, USA.

Mid-West Spring and Stamping (2011) retrieved from <http://www.mwspring.com/>.

Mikulowski, G.M., and Holnicki-Szulc, J., (2007) Adaptive landing gear concept- feedback control validation. *Smart Materials and Structures*, 16: 2146-2158. DOI: 10.1088/0964-

1726/16/6/017.

Mikulowski, G.M., and LeLetty, R., (2008) Advanced landing gears for improved impact absorption. Proceedings of the 11th International Conference on New Actuators, 363-366, Bremen, Germany.

Mikułowski, G., Wiszowaty, R., and Holnicki-Szulc, J., (2013) Characterization of a piezoelectric valve for an adaptive pneumatic shock absorber. *Smart Materials and Structures*, 22(125011): 1-12. DOI: 10.1088/0964-1726/22/12/125011.

Ngatu, G.T., and Wereley, N.M., (2007) Viscometric and sedimentation characterization of bidisperse magnetorheological fluids. *IEEE Transactions on Magnetics*, 43(6): 2474–2476. DOI: 10.1109/TMAG.2007.893867.

Padalka, O., Song, H.J., Wereley, N.M., Filer II, J.A., and Bell, R.C., (2010) Stiffness and damping in Fe, Co, and Ni nanowire-based magnetorheological elastomeric composites. *IEEE Transactions on Magnetics*, 46(6): 2275-2277. DOI: 10.1109/TMAG.2010.2044759.

Park, B.J., Song, K.H., and Choi, H.J., (2009) Magnetic carbonyl iron nanoparticle based magnetorheological suspension and its characteristics. *Materials Letters*, 63(15): 1350-1352. DOI: 10.1016/j.matlet.2009.03.013.

Patel, R., (2011) Mechanism of chain formation in nanofluid based MR fluids. *Journal of Magnetism and Magnetic Materials*, 323(10): 1360–1363. DOI: 10.1016/j.jmmm.2010.11.046.

Phulé, P., and Ginder, J., (1998) The materials science of field-responsive fluids. *MRS Bulletin*, 23(8): 19–21. DOI: 10.1557/S0883769400030761.

Phillips, R.W., (1969) Engineering Applications of Fluids with a Variable Yields Stress, Ph.D

Thesis, Mechanical Engineering, University of California, Berkeley.

Poddar, P., Wilson, J.L., Srikanth, H., Yoo, J.H., Wereley, N.M., Kotha, S., Barghouty, L. and Radhakrishnan, R., (2004) Nanocomposite magnetorheological fluids with uniformly dispersed Fe nanoparticles. *Journal of Nanoscience and Nanotechnology*, 4(1-2): 192–196. DOI: 10.1166/ jnn.2004.020.

Powell, L.A., Wereley, N.M., and Ulicny, J.C., (2012) Magnetorheological fluids employing substitution of nonmagnetic for magnetic particles to increase yield stress. *IEEE Transactions on Magnetics*, 48(11): 3764-3767. DOI: 10.1109/TMAG.2012.2202885.

Rabinow, J., (1948) The magnetic fluid clutch. *AIEE Transactions,* 67: 1308-1315.

Rabinow, J., (1951) Magnetic fluid torque and force transmitting device. U.S. Patent 2575360.

Rosenfeld, N., Wereley, N.M., Radakrishnan, R., and Sudarshan, T., (2002) Behavior of magnetorheological fluids utilizing nanopowder iron. *International Journal of Modern Physics B*, 16(17-18): 2392–2398. DOI: 10.1142/S0217979202012414.

Shunta, K., Fumikazu, M., and Katsuhiro, H., (2012) Novel soft actuator using magnetorheological elastomer. *IEEE Transactions on Magnetics*, 48(4): 1649-1652. DOI: 10.1109/TMAG.2011. 2173669.

Slotine, J.J.E., and Li, W., (1991) *Applied nonlinear control*. New Jersey, Prentice-Hall, 283-284.

Smalley Steel Ring Company (2011) retrieved from <http://www.smalley.com>.

Snyder, R.A., Kamath, G.M., and Wereley, N.M., (2001) Characterization and analysis of magnetorheological damper behavior under sinusoidal loading. *AIAA Journal*, 39(7): 1241-1253. DOI: 10.1117/12.384563.

Spencer Jr., B.F., Dyke, S.J., Sain, M.K., and Carlson, J.D. (1997) Phenomenological model for

a magnetorheological damper. *Journal of Engineering Mechanics*, ASCE, 123: 230-52.

Spurk, J.H., and Aksel, N., (2008) Fluid Mechanics, 2nd Edition. Springer-Verlag, Berlin Germany. DOI 10.1007/978-3-540-73537-3.

Stanway, R., Sproston, J.L., and El-Wahed, A.K., (1996) Application of electrorheological fluids in vibration control: a survey. *Smart Materials and Structures*, 5(4): 464–482. DOI: 10.1088/094-1726/5/4/011.

Ulicny, J.C., Snavely, K.S., Golden, M.A., Klingenberg, D.J., (2010) Enhancing magnetorheology with nonmagnetizable particles. *Applied Physics Letters*, 96: 231903-1-3. DOI: 10.1063/1.3431608.

Wahl, A.M., (1963) Mechanical Springs, 2nd Edition, McGraw-Hill, New York, USA.

Wang, X., and Gordaninejad, F., (2001) Dynamic modeling of semi-active ER/MR fluid dampers, damping and isolation. Proceedings of SPIE Conference on Smart Materials and Structures, 4331; 82-91.

White, F.M., (1986) *Fluid Mechanics*, 2nd Edition, McGraw-Hill, Ohio, USA.

Wereley, N.M., and Pang, L., (1998) Nondimensional analysis of semi-active electro- and magneto-rheological dampers using parallel plate models. *Smart Materials and Structures*, 7: 732-743. DOI: 10.1088/0964-1726/7/5/015.

Wereley, N.M., Lindler, J, Rosenfeld, N., Choi, Y.-T., (2004) Biviscous damping behavior in electrorheological shock absorbers. *Smart Materials and Structures*, 13(4): 743-752. DOI: DOI: 10.1088/0964-1726/13/4/012.

Wereley, N.M., Chaudhuri, A., Yoo, J.H., John, S., Kotha, S., Suggs, A., Radhakrishnan, R., Love, B.J., and Sudarshan, T.S., (2006) Bidisperse magnetorheological fluids using Fe

particles at nanometer and micron scale. *Journal of Intelligent Material Systems and Structures*, 17(5): 393-401. DOI: 10.1177/1045389X06056953.

Wereley, N.M., (2008) Nondimensional Herschel-Bulkley analysis of magnetorheological and electrorheological dampers. *Journal of Intelligent Material Systems and Structures*, 19(3): 257-268.

Yang, G.Q., (2001) Large-scale magnetorheological fluid damper for vibration mitigation: modeling, testing and control. Ph.D dissertation, University of Notre Dame.